SRESA's International Journal of

LIFE CYCLE RELIABILITY AND SAFETY ENGINEERING

Vol.5 **Issue No.3** **July–September 2016** **ISSN – 2250 0820**

Special Issue on

ROLE OF HYDROGEOLOGY IN RELIABILITY AND SAFETY OF WASTE MANAGEMENT

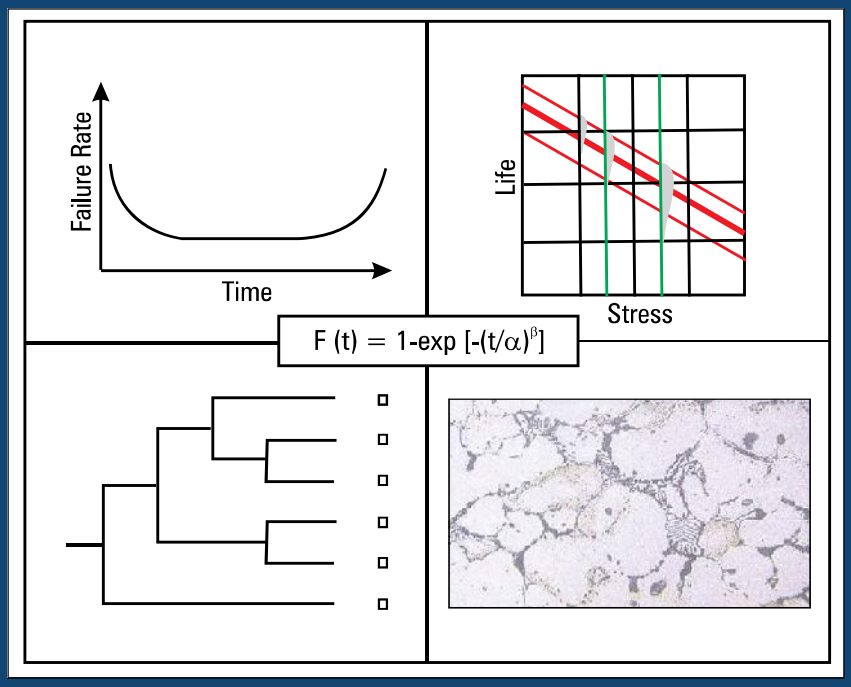

Guest Editor:
Dr. D. Datta

Society for Reliability and Safety
website: http://www.sresa.org.in

SRESA Journal of Life Cycle Reliability and Safety Engineering

Extensive work is being performed world over on assessment of Reliability and Safety for engineering systems in support of decisions. The increasing number of risk-based / risk-informed applications being developed world over is a testimony to the growth of this field. Here, along with probabilistic methods, deterministic methods including Physics-of-Failure based approach is playing an important role. The International Journal of Life Cycle Reliability and Safety Engineering provides a unique medium for researchers and academicians to contribute articles based on their R&D work, applied work and review work, in the area of Reliability, Safety and related fields. Articles based on technology development will also be published as Technical Notes. Review articles on Books published in the subject area of the journal will also form part of the publication.

Society for Reliability and Safety has been actively working for developing means and methods for improving system reliability. Publications of quarterly News Letters and this journal are some of the areas the society is vigorously pursuing for societal benefits. Manuscript in the subject areas can be communicated to the Chief Editors. Manuscript will be reviewed by the experts in the respective area of the work and comments will be communicated to the corresponding author. The reviewed final manuscript will be published and the author will be communicated the publication details. Instruction for preparing the manuscript has been given on inside page of the end cover page of each issue. The rights of publication rest with the Chief-Editors.

SCOPE OF JOURNAL

System Reliability analysis	**Structural Reliability**	**Risk-based applications**
Statistical tools and methods	Remaining life prediction	Technical specification optimization
Probabilistic Safety Assessment	Reliability based design	Risk-informed approach
Quantitative methods	Physics-of-Failure methods	Risk-based ISI
Human factor modeling	Probabilistic Fracture Mechanics	Risk-based maintenance
Common Cause Failure analysis	Passive system reliability	Risk-monitor
Life testing methods	Precursor event analysis	Prognostics & health management
Software reliability	Bayesian modeling	Severe accident management
Uncertainty modeling	Artificial intelligence in risk and reliability modeling	Risk-based Operator support systems
Dynamic reliability models	Design of Experiments	Role of risk-based approach in Regulatory reviews
Sensitivity analysis	Fuzzy approach in risk analysis	Advanced electronic systems reliability modeling
Decision support systems	Cognitive framework	Risk-informed asset management

SRESA AND ITS OBJECTIVES

a) To promote and develop the science of reliability and safety.

b) To encourage research in the area of reliability and safety engineering technology & allied fields.

c) To hold meetings for presentation and discussion of scientific and technical issues related to safety and reliability.

d) To evolve a unified standard code of practice in safety and reliability engineering for assurance of quality based professional engineering services.

e) To publish journals, books, reports and other information, alone or in collaboration with other organizations, and to disseminate information, knowledge and practice of ensuring quality services in the field of Reliability and Safety.

f) To organize reliability and safety engineering courses and / or services for any kind of energy systems like nuclear and thermal power plants, research reactors, other nuclear and radiation facilities, conventional process and chemical industries.

g) To co-operate with government agencies, educational institutions and research oganisations

SRESA's International Journal of

LIFE CYCLE RELIABILITY AND SAFETY ENGINEERING

Vol.5 Issue No.3 July–September 2016 ISSN – 2250 0820

Special Issue on

ROLE OF HYDROGEOLOGY IN RELIABILITY AND SAFETY OF WASTE MANAGEMENT

Guest Editor:

Dr. D. Datta

SOCIETY FOR RELIABILITY AND SAFETY

Typeset & Printed

EBENEZER PRINTING HOUSE
Unit No. 5 & 11, 2nd Floor, Hind Services Industries,
Veer Savarkar Marg,
Dadar (west), Mumbai -28
Tel.: 2446 2632/ 3872
E-mail: outwork@gmail.com

Guest Editorial

This is the special issue of SRESA on the theme "Role of hydrogeology in reliability and safety of waste management". Safety of radioactive waste management ensures the safe disposal of the same in a geological repository. If release of the radionuclide from the geological repository or from the trench where active waste has been dumped after conditioning in the form of a borosilicate glass encapsulated within an over pack canister and if the leach rate is found to be minimal the disposal is said to be safe. In order to assess this condition of safety of the waste disposal facility, reliability based design optimization of the disposal system is essential and in that context, knowledge pertaining to migration of radionuclide through geological repository is desired. Hydrogeology (*hydro-* meaning water, and *-geology* meaning the study of the Earth) is the area of geology that deals with the distribution and movement of groundwater in the soil and rocks of the Earth's crust (commonly in aquifers). The term geohydrology is often used interchangeably. The study of the interaction between groundwater movement and geology can be quite complex. Groundwater does not always flow in the subsurface down-hill following the surface topography; groundwater follows pressure gradients (flow from high pressure to low) often following fractures and conduits in circuitous paths). Overall problems are multiscale multiphysics oriented. With a view to the diversity of this field and its potential application in real issues of the reliability and safety of waste management, this special issue has brought some research articles, depicted below where the basic theme has been discussed.

The first paper of this issue is authored by T.K. Pal, D. Datta and R.K. Bajpai on "Development of Differential Quadrature based Computational Scheme in Cylindrical Geometry and Its application to Simulate Radionuclide Leaching from Radioactive Waste Form". In this paper, authors have presented a new development of a computational tool to solve diffusion equation in cylindrical coordinate. New development is based on differential quadrature which is a tunable numerical fast and efficient numerical solver. Tunable in the sense that time derivative is discretized following forward finite difference scheme, whereas spatial derivatives are taken care by differential quadrature method. DQM based solution is addressed to compute the leaching of radionuclide from radioactive waste form. Results from DQM are compared with analytical or closed form solution and are found in good agreement. Authors have established an empirical model between model parameters and leach rate with the help of multivariable regression analysis method.

The second paper is authored by Sanjeev Kumar Sharma, Varen, S.K. Gupta, Ashis Mallick and D. Datta on "Reliability Based Optimal Design of Water Distribution Network Using Combinatorial Particle Swarm Optimization". In this paper, particle swarm optimization (PSO) method is tuned for a multi-objective combinatorial problem relating to the design of water distribution network. Maximization of network reliability and minimization of cost were considered as the objective functions of the design problem. Imprecise parameters such as consumer satisfaction index is treated as fuzzy to define membership functions corresponding to the excess pressure above the minimum specified head at demand nodes of the network. Usage of EPANET dynamic link library linked with MATLAB was discussed to addressed the combinatorial PSO. Authors have suggested the proposed methodology can be considered as a combinatorial optimization problems for water distribution network.

The third paper addresses the geo-hydrological problems through generalized advection- dispersion equation (GADE). Lattice Boltzmann Method (LBM) and Differential Quadrature Method (DQM) are explored in this paper to obtain the numerical solution of GADE. The time dependent boundary conditions are used. In the LBM based scheme ADE is solved using a D2Q5 lattice model together with single relaxation time (SRT) and Bhatnagar-Gross-Krook (BGK) collision operator. In the DQM based scheme, time derivative is approximated using forward difference and the spatial derivatives using polynomial based DQM. Numerical results are found to be in good agreement when compared with analytical solutions. Stability of both the computational schemes justified their role in solving the initial and boundary value problems of hydro geological category.

The next paper authored by B.K. Sahoo and J.J. Gaware is on "Radon in Ground Water and Soil as a Potential Tracer for Uranium Exploration and Earthquake Precursory Studies". The thrust of this paper is on formulation and modelling of radon transport in soil media and its usefulness for interpretation of measured radon data

with uranium deposit and stress release from earth crust. Authors have derived the corresponding analytical models on the basis of radon transport theory of porous media. Physical processes such as diffusion as well as advection transport, radon emanation and radioactive decay in the soil pore are considered. Authors have pointed out by the analysis of the model solutions that radon monitoring in sub-soil is more reliable for stress release and earthquake precursory studies than deep soil sampling. Further conclusions have been drawn pertaining to radon monitoring in deep soil, preferably in ground water, that monitoring can be applied for detecting the uranium deposit in certain areas. The compensated radon activity is the actual indicator of ^{226}Ra and uranium content in rocks at the vicinity of ground water source. Results of two experimental case studies were also presented to validate the above prediction of model.

The next paper authored by Subrata Bera and A. J. Gaikwad is on "Impact of Linguistic Proposition of Weather Stability in Gaussian Plume Mode". The paper proposes the linguistic formulation of weather stability class required for computation of air concentration while using Gaussian plume model. Traditional technique of using Pasquill-Gifford class, decimal weather class in the scale of 6, has been developed by implementing the proposed formulation. In the decimal weather stability class, weight fraction of composite weather class has also been estimated. The empirical formulae for composite weather class have also been developed and used for dispersion calculation with the help of Gaussian plume model. Interval arithmetic with fuzzy alpha-cut technique has been used to do the necessary computation. Analysis for demonstrating the effect of composite weather stability class on pollutant concentration reduction factor has been presented in this paper.

Guest editor, Dr. D. Datta is very thankful to his all colleagues associated with Society for Reliability and Safety. The guest editor is very thankful to the Chief-editor, Dr. Varde and the managing editor Dr. Manoj. I am very thankful to all the authors who have responded to my invitation, some of them at a short notice, and the publishers who have done a very good job of bringing out this special issue.

Dr. Debabrata Datta

Dr. Debabrata Datta, is presently working in Bhabha Atomic Research Centre (BARC), Mumbai in the capacity of Scientific Officer (H^+) and Head, Radiological Physics & Advisory Division of Health, Safety & Environment Group. His academic excellences are: (i) M. Sc in Nuclear Physics (Kolkata University), (ii) Master of Philosophy (M. Phil) in High Energy Nuclear Physics from SAHA Institute of Nuclear Physics (SINP), Kolkata, (iii) Graduated in the field of **Nuclear Engineering from OCES**, Training School of BARC in 1984-85 and (iv) Doctor of Philosophy (Ph. D) in Computer Science from Mumbai University in 2000.

His proficiency is on software development using soft computing technique. He has developed a large number of software in the field of radiation protection, safety and uncertainty modeling. Three of his developed software had exported to Turkish Atomic Energy on their request. He has contributed in the field of uncertainty modelling of system. He is well recognized internationally for his enormous diverse contribution in statistical analysis of environmental data, fuzzy mathematics, evidence theory, artificial neural network, wavelets and wavelet neural network. He is the recipient of **Eminent Scientist Award, "Millennium Plaques of Honour" from Indian Science Congress Association, in 2010.** He has also **received meritorious awards from National Society of Radiation Physics (NSRP), Association of Medical Physicist's of India (AMPI)**.

He has been honoured as Professor in Physical & Mathematical Sciences in Homi Bhabha National Institute (deemed university of Department of Atomic Energy). He has more than 150 publications in peer reviewed international journals, book chapters, international and national conferences to his credit. He is the author of more than twenty application software and some of them are well validated and acceptable by palisade corp. USA. He is one of the developer and contributor of MATLAB Toolbox. He is a recognized Ph. D guide in Engineering and Sciences disciplines. His research interests are mathematical modelling, statistical analysis of big data, data mining, optimization using evolutionary algorithm, artificial intelligence, bioinformatics, medical informatics, sensitivity and uncertainty modelling of an engineering system. He is the reviewer and editorial board member of many international and National Journals. He is the Life member of many International and National Scientific Organizations.

Life Cycle Reliability and Safety Engineering
Vol.5 Issue 3 (2016) 01-07

Development of Differential Quadrature based Computational Scheme in Cylindrical Geometry and Its application to Simulate Radionuclide Leaching from Radioactive Waste Form

T. K. Pal[1], D. Datta[2], R. K. Bajpai[1]

[1]*Technology Development Division, BARC, Mumbai, India*
[2]*Radiological Physics & Advisory Division, BARC, Mumbai, India*
Email: tkpal@barc.gov.in

Abstract

Differential Quadrature Method (DQM) based computational scheme is developed to solve diffusion equation in cylindrical coordinate. In this scheme, time derivative is approximated using forward difference and the spatial derivatives using polynomial based DQM. This developed scheme is applied to simulate test problem on radionuclide leaching from radioactive waste form. Leach rate is calculated after simulating the leaching process. DQM based results are compared with the analytical solutions and good agreements between the two results are established. The developed tool is used as a numerical tool for computationally intensive calculations, such as regression analysis and correlation analysis etc. Multivariate regression analysis is carried out to establish a linear relationship between leach rate and model parameters e.g., diffusion coefficient, porosity and linear sorption coefficient. Study of correlation analysis carried out in this study shows that diffusion coefficient is positively more correlated with leach rate compared to porosity whereas, K_d is negatively correlated with leach rate.

Keywords: Differential Quadrature, Cylindrical Geometry, Radioactive Waste, Leach rate, regression analysis

1. Introduction

In Indian radioactive wastes management practices for low and intermediate radioactive wastes generated during closed nuclear fuel cycle are being immobilized in various inert matrices such as cement, ceramic, glass etc. after being properly treated with well developed waste treatment practices [1]. These cylindrical waste forms are contained in MS drums, which are being disposed of in suitable geological disposal facility known as Near Surface Disposal facility (NSDF) [1]. Assessment of radiological impact of NSDF is a priory work before getting licenses from regulatory bodies (In India Atomic Energy Regularly Board (AERB) is the licensing authority). In radiological impact assessment, geo-spherical transport equations (Advection-Diffusion-Reaction Equations (ADRE)) are solved using analytical and numerical techniques. Source term modeling is a priori requirement for accurately modeling radionuclide migration from NSDF facility. Two types of source term model are generally considered: dissolution controlled and diffusion controlled leaching. In this work we will be dealing with diffusion controlled leaching of radionuclides from the cylindrical waste-form.

Diffusion process is ubiquitous in the various disciplines of science and engineering. Mathematically diffusion process is modeled using well known Fick's laws. Mathematical form of diffusion process is the well known diffusion equation. Diffusion equations with initial and boundary conditions are generally solved using analytical and various numerical techniques, such as Finite Difference Method (FDM), Finite Element Method (FEM), and Finite Volume Method (FVM) etc. In this work we have attempted to solve the problem using relatively new but well matured numerical technique called Differential Quadrature Method (DQM) [2, 3, 4]. DQM obtains very accurate numerical results by using considerably small number of grid points. Consequently, it requires much less computational effort and memory for storage.

The rest of the paper is organized as follows. Mathematical equations of diffusive leaching of radioactivity and its analytical solution for particular initial and boundary conditions are first introduced in Section 2, then brief description about the DQM is

given in Section 3, Solution of the leaching process using DQM is derived in Section 4. Numerical results and discussion are presented in Section 5 and some conclusions are given in Section 6.

2. Mathematical Models of Diffusive Leaching of Radioactivity

Leaching of radionuclides from the waste-form disposed of in NSDF can be modeled in various ways. Two commonly employed models are: dissolution controlled and diffusion controlled. In diffusion controlled leaching process, radionuclides insides waste-form are in higher concentration compared to that in surrounding pore water in the rock formation. Due to his concentration gradient, radionuclides come out from the waste-form to the pore water in the rock formation. Transport of radionuclides in the waste-form can therefore be modeled as reaction diffusion process with decay term due to radioactive nature of the solute concerned. In this work reaction term which is due sorbtive nature of the materials used in the matrix is modeled as linear isotherm and therefore, reaction diffusion equation converts to a diffusion equation. The rate of change of concentration of radionuclides inside the waste-form can be written as

$$\frac{\partial C(r,t)}{\partial t} = \frac{D_r}{R_d}\frac{\partial^2 C(r,t)}{\partial r^2} + \frac{D_r}{R_d}\frac{1}{r}\frac{\partial C(r,t)}{\partial r} - \lambda C(r,t) \quad (1)$$

where C(r, t) = concentration of radionuclides in waste form (Bq/ml), D_r = radial diffusion coefficient in waste form (cm^2/s), r = radial coordinate inside waste form (cm), λ = radioactive decay constant (s^{-1}), t = time (s), R_d = retardation factor = $\left(1+\frac{\rho}{\theta}K_d\right)$, ρ = bulk density of matrix used (gm/ml), θ = total porosity of the waste form, K_d = distribution coefficient of radionuclide for the matrix used (ml/gm). Eq. (1) is radial diffusion equation with decay term. The diffusion leaching from the top and bottom surfaces is neglected considering thick barriers above and below the waste-form. Initial and boundary conditions for Eq. (1) are

$$C(r,0) = C_0, \quad |r| \le R \quad (2a)$$

$$C(R,t) = 0 \quad t > 0 \quad (2b)$$

$$\left.\frac{\partial C(r,t)}{\partial r}\right|_{r=0} = 0$$

where C_0 = initial concentration of radionuclides in the waste-form (Bq/ml), R = radius of the cylindrical waste-form, Boundary conditions described by Eqs. (2a) and (2b) mean that mass transfer external to the cylinder is so rapid relative to the internal transfer in the cylinder that the surface concentration is maintained at zero for any time greater than zero.

The solution of Eq. (1) subject to the initial and boundary conditions is obtained as [5]

$$C(r,t) = \sum_{n=1}^{\infty} \frac{2C_0}{\alpha_n J_1(\alpha_n)} J_0\left(\frac{\alpha_n r}{R}\right) \times exp\left[-\left(\lambda + \frac{{\alpha_n}^2 D_r}{R_d R^2}\right)t\right] \quad (3)$$

where J_0, J_1 = first kind of Bessel functions of order 0 and 1, respectively, α_n = roots of $J_0(\alpha) = 0$ Eq. (1) gives concentration of radionuclide at various radial distances and at various times. The leach rate ($1/cm^2/s$) of radioactivity can be evaluated using the relation

$$Lr(R,t) = -D_r \left.\frac{\partial C(r,t)}{\partial r}\right|_{r=R} \quad (4)$$

Analytical solution to the Eq. (4) can be written as

$$Lr(R,t) = \sum_{n=1}^{\infty} \frac{2C_0 D_r}{R} exp\left[-\left(\lambda + \frac{{\alpha_n}^2 D_r}{R_d R^2}\right)t\right] \quad (5)$$

The leach rate evaluated using Eq. (5) can be further used in geo-spherical transport modeling.

3. Differential Quadrature Method (DQM)

DQM is numerical technique for solution of differential equations. Historically it was developed as an analogous to numerical integration technique called numerical quadrature. In numerical quadrature, definite integral is approximated as weighted some of integrand values at a group of points in the domain of integration, similarly in DQM, differentiation of a piecewise continuous function is approximated as weighted some of functional values at certain discrete points in the domain of continuity called nodes. Bellman was the pioneer of DQM and he used the technique to solve differential equations [6]. Since then, the technique has gone through various development works [3, 4]. Mathematically DQM can be written as

$$f_x^{(k)}(x_i) = \left.\frac{\partial^k f(x)}{\partial x^k}\right|_{x=x_i} = \sum_{j=1}^{N} A_{ij}^{(k)} f(x_j) \quad (6)$$

$$i = 1, 2, \ldots, N$$

where x_j are the discrete nodes in the domain at which function values are known, $f(x_j)$ are the function values at these nodes, N is the total number of such nodes, and $A_{ij}^{(k)}$ are the weighting coefficients for the order k^{th} derivative of the function, therefore for a N point DQM, $A_{ij}^{(k)}$ are the elements of a N×N matrix.

Weighting coefficients of DQM are not related to any special problem and only depends on the grid spacing. Hence, most demanding task in DQM is to calculate weighting coefficient matrix for a given discrete nodes. Determination of weighting coefficients is carried out using approximation theory where the function under differentiation is first approximated. Based on the procedure of approximating the function, we have various kind of DQM such as, Polynomial DQM (PDQM) where the function is approximated as a polynomial, Fourier Expansion Base DQM (FDQM) where the function is approximated by a Fourier series expansion etc. Shu et al carried out a detailed study on determination of weighting coefficients. [7]. DQM has been used by researcher to solve Advection-Diffusion Equation [8, 9].

4. DQM Solution of Leaching Process

Leaching process as given mathematically in Eq. (1) after approximating time derivative using forward difference and the spatial derivatives using PDQM can be written as Eq. (7)

$$\frac{C(r_i,t+\Delta t)-C(r_i,t)}{\Delta t} = \frac{D_r}{R_d}\left(\sum_{j=1}^{N} A_{ij}^{(2)} C(r_j,t) + \frac{1}{r_i}\sum_{j=1}^{N} A_{ij}^{(1)} C(r_j,t)\right) - \lambda C(r_i,t) \qquad \mathrm{i} = 1, 2, \dots, \mathrm{N}$$

$$C(r_i,t+\Delta t) = (1-\lambda\Delta t)C(r_i,t) + \frac{D_r\,\Delta t}{R_d}\left(\sum_{j=1}^{N} A_{ij}^{(2)} C(r_j,t) + \frac{1}{r_i}\sum_{j=1}^{N} A_{ij}^{(1)} C(r_j,t)\right) \qquad \mathrm{i} = 1, 2, \dots, \mathrm{N} \qquad (7)$$

where Δt is discrete time step, N is the number of sampling grid points along radial direction. A^1, A^2 are the weighting coefficient matrices. In matrix form, Eq. (7) can be written as

$$C(r,t+\Delta t) = (1-\lambda\Delta t)C(r,t) + \frac{D_r\,\Delta t}{R_d}\left[A^{(2)}C(r,t) + RA^{(1)}C(r,t)\right]$$

$$C(r,t+\Delta t) = \begin{pmatrix} C(r_1,t+\Delta t) \\ C(r_2,t+\Delta t) \\ \cdot \\ \cdot \\ C(r_N,t+\Delta t) \end{pmatrix}$$

$$C(r,t) = \begin{pmatrix} C(r_1,t) \\ C(r_2,t) \\ \cdot \\ \cdot \\ C(r_N,t) \end{pmatrix}$$

$$A^{(2)} = \begin{pmatrix} A_{11}^{(2)} & A_{12}^{(2)} & \cdot & \cdot & A_{1N}^{(2)} \\ A_{21}^{(2)} & A_{22}^{(2)} & \cdot & \cdot & A_{2N}^{(2)} \\ \vdots & \vdots & \cdot & \cdot & \cdot \\ A_{N1}^{(2)} & A_{N1}^{(2)} & \cdot & \cdot & A_{NN}^{(2)} \end{pmatrix}$$

$$A^{(1)} = \begin{pmatrix} A_{11}^{(1)} & A_{12}^{(1)} & \cdot & \cdot & A_{1N}^{(1)} \\ A_{21}^{(1)} & A_{22}^{(1)} & \cdot & \cdot & A_{2N}^{(1)} \\ \vdots & \vdots & \cdot & \cdot & \cdot \\ A_{N1}^{(1)} & A_{N1}^{(1)} & \cdot & \cdot & A_{NN}^{(1)} \end{pmatrix}$$

$$R = \begin{pmatrix} \frac{1}{r_1} & 0 & \cdot & \cdot & 0 \\ 0 & \frac{1}{r_2} & \cdot & \cdot & 0 \\ \cdot & \cdot & \cdot & \cdot & \cdot \\ \cdot & \cdot & \cdot & \cdot & \cdot \\ 0 & 0 & \cdot & \cdot & \frac{1}{r_N} \end{pmatrix}$$

where $r_1, r_2, \dots, r_N$ are the radial coordinates of the discrete nodes. In the DQM computational algorithm, initial condition given in Eq. (2a) is implemented explicitly by initializing the problem with an array of concentration as given in Eq. (8a)

$$\begin{pmatrix} C(r_1,0) \\ C(r_2,0) \\ \cdot \\ \cdot \\ C(r_N,0) \end{pmatrix} = \begin{pmatrix} C_0 \\ C_0 \\ \cdot \\ \cdot \\ C_0 \end{pmatrix} \qquad (8)$$

Implementation of boundary condition in Eq. (2b) modifies the Eq. (7) to the Eq. (9)

$$C(r_i,t+\Delta t) = (1-\lambda\Delta t)C(r_i,t) + \frac{D_r\,\Delta t}{R_d}\left(\sum_{j=1}^{N-1} A_{ij}^{(2)} C(r_j,t) + \frac{1}{r_i}\sum_{j=1}^{N-1} A_{ij}^{(1)} C(r_j,t)\right) \qquad \mathrm{i} = 1, 2, \dots, \mathrm{N}-1 \qquad (9)$$

To implement boundary condition given in Eq. (2c), we need to solve following equation which calculate concentration at the center of the cylindrical waste-form.

$$\sum_{j=1}^{N-1} A_{1j}^{(1)} C(r_j, t) = 0$$

$$C(r_1, t) = -\sum_{j=2}^{N-1} A_{1j}^{(1)} C(r_j, t) \quad (10)$$

Implementation of this boundary condition modifies Eq. (9) as

$$C(r_i, t+\Delta t) = (1-\lambda\Delta t) C(r_i, t) + \frac{D_r\,\Delta t}{R_d}\left(\sum_{j=2}^{N-1} A_{ij}^{(2)} C(r_j, t) + \frac{1}{r_i}\sum_{j=2}^{N-1} A_{ij}^{(1)} C(r_j, t)\right)$$
$$\mathrm{i} = 2, 3, \ldots, \mathrm{N}-1 \quad (11)$$

Eq. (10) and (11) are the working equations for the simulation of the leaching process. Elements of the weighting matrixes are calculated using polynomial approach known as PDQM. This approach is also known as Quan and Chang's approach (Quan and Chang 1998a, 1998b, Shu 2000). In this approach, weighting coefficients are written as

$$A_{ij}^{(1)} = \frac{L(x_i)}{(x_i - x_j) L(x_j)}, \quad A_{ii}^{(1)} = -\sum_{j=1}^{N} A_{ij}^{(1)} \quad i \neq j$$

$$A_{ij}^{(2)} = 2A_{ij}^{(1)}\left(A_{ii}^{(1)} - \frac{1}{(x_i - x_j)}\right)$$

$$A_{ii}^{(2)} = -\sum_{j=1}^{N} A_{ij}^{(2)} \quad i \neq j$$

where $L(x_i) = \prod_{j=1}^{N}(x_i - x_j)$, $i \neq j$ is the first derivative of polynomial function of degree N. The locations of grid points can be taken at uniform intervals or non uniform interval. Previous studies reveal that non-uniform mesh from the roots of orthogonal polynomials of functions can greatly enhance the accuracy of the quadrature solution in comparison to uniform mesh. Non-uniform grid points using Chebyshev-Gauss-Lobatto (CGL) grid points can be written as

$$r_i = \frac{1}{2}\left(1 - cos\frac{i-1}{N-1}\pi\right) \quad i = 1, 2, \ldots, N$$

Uniform grid points can be written as

$$r_i = i * \frac{R}{N-1} \quad i = 0, 1, 2, \quad \ldots N-1$$

Leach rate was estimated after calculating concentration profile in the waste form. DQM solution of leach rate as given in Eq. (4) can be written as

$$Lr(R, t) = -D_r \sum_{j=1}^{N} A_{Nj}^{(1)} C(r_j, t) \quad (12)$$

where $C(r_j, t)$ are obtained after solving Eq. (11).

5. Results and Discussions

The leaching process is simulated for a particular radionuclide, ^{137}Cs, which is supposed to be the major radionuclide in cementitious nuclear waste form. The parameters used in the simulation are given in the Table 1.

Table 1: Input data used in simulation

Parameter	Value
C_0(Bq/ml)	1.0
Half Life(y)	30.1
D(cm^2/s)	1.8x10^{-6}
ρ (gm/ml)	1.3
θ	0.15
K_d(ml/gm)	30.0
R(cm)	100.0

Dependency of DQM results on number of grid points is established through estimating error in L_2 norm, provided in Eq. (12) for specific time level.

$$L_2 = \left(\frac{1}{N}\sum_{j=1}^{N}\left|C_j^{(exact)} - C_j^{(numerical)}\right|^2\right)^{\frac{1}{2}} \quad (12)$$

L_2 errors for uniform and non uniform grid points are estimated for different total number of grid points. The results thus obtained are shown in a tabular form in Table 2. It can be observed from the table that L_2 error for non uniform grid are smaller that uniform grid. The results also depict that using DQM we can obtain highly accurate results for very less number of grid points therefore; accelerating the computation speed. Radial concentration profile of ^{137}Cs in the waste form is shown in the Fig. 1 at 10 years time. Fig. 1 shows that DQM based concentration profile exactly matches with analytical solution based concentration

profile. Radial profiles of concentration are shown in Fig. 1 for 10 years, 30 years and 100 years. The nature of the concentration profile shown in Fig 1 shows that well inside the waste form concentration of ^{137}Cs is uniform whereas at the surface the concentration drops sharply and forms a layer, which is called diffusion layer in electrochemistry.

Table 2: L2 error of concentration for different total number of grid points

Number of grid points	L_2	
	Non-uniform Grid	Uniform Grid
10	4.205E-03	9.499E-03
15	1.627E-03	5.554E-03
20	7.188E-04	4.409E-03
25	2.074E-04	1.527E-03
30	5.099E-05	1.799E-03
35	2.550E-05	3.391E-03
40	2.424E-05	2.204E-03
45	2.433E-05	1.913E-03
50	2.434E-05	5.262E-03

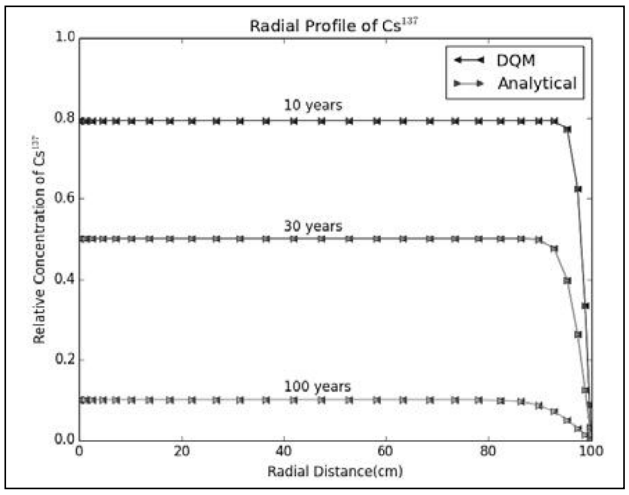

Fig 1: Radial Profile of Concentration of ^{137}Cs inside the waste form: Comparisons between DQM and Analytical Solution

Leach rates are calculated using 30 grid points at various time intervals and compared with analytical solution. The comparison is given in Table 3. Graphical plot of leach rate is shown in Fig. 2. The result shows that DQM based leach rate exactly matches with analytical results. The result also implies that leach rate gradually decreases with time and becomes almost zero after 300 years i.e. after 10 half lives of ^{137}Cs.

Table 3: Leach rate calculation using various total number of grid points

Sr. No.	Time (year)	Leach Rate($cm^{-2}s^{-1}$)	
		DQM	Analytical
1	1	2.0388E-06	2.0953E-06
2	2	1.4570E-06	1.3839E-06
3	5	8.5991 E-07	8.6108 E-07
4	10	5.3982 E-07	5.4106 E-07
5	20	3.0153 E-07	3.0143 E-07
6	30	1.9473 E-07	1.9469 E-07
7	60	6.8342 E-08	6.8338 E-08
8	100	2.0869 E-08	2.0867 E-08
9	300	1.1659 E-10	1.1656 E-08
10	1000	5.9582E-18	5.9536E-18

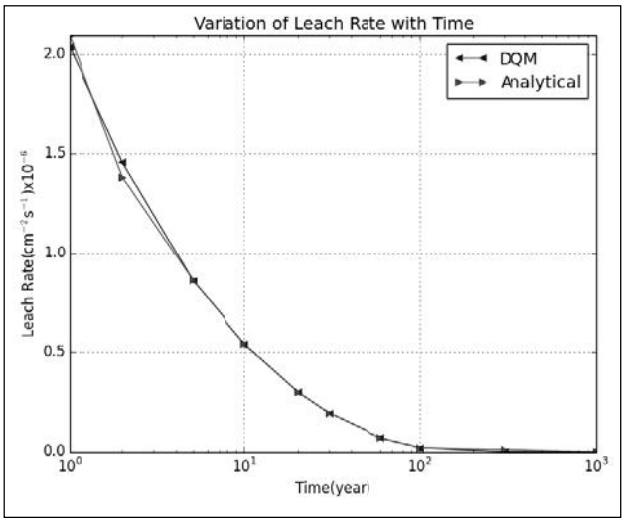

Fig 2: Comparison of Leach Rate calculated using DQM and Analytical Method at various Times

A multivariate linear regression analysis is carried out to establish a linear relation between leach rate and input parameters such as diffusion coefficient, porosity and distribution coefficient. A total of 100 leach rate values are estimated from 100 sampling values of each input parameter. In the sampling method, random input parameters are chosen considering various distributions of input parameters. In this study, values of diffusion coefficient and porosity are taken as uniformly distributed whereas, values of K_d are taken as log-uniform distribution. The various distributions and their characteristics are given in the Table 4. The linear regression model for leach rate is taken as:

$$Lr = \beta_0 + \beta_1 D + \beta_2 \theta + \beta_3 K_d \quad (13a)$$

In matrix form Eq. (13) can be written as

$$M_{Lr} = M_P\, M_\beta \tag{13b}$$

$$M_{Lr} = \begin{pmatrix} Lr_1 \\ Lr_2 \\ \vdots \\ \vdots \\ Lr_N \end{pmatrix}, \quad M_\beta = \begin{pmatrix} \beta_0 \\ \beta_1 \\ \beta_2 \\ \beta_3 \end{pmatrix}$$

$$M_P = \begin{pmatrix} 1 & D^1 & \theta^1 & K_d^1 \\ 1 & D^2 & \theta^2 & K_d^2 \\ \vdots & \vdots & \vdots & \vdots \\ \vdots & \vdots & \vdots & \vdots \\ 1 & D^N & \theta^N & K_d^N \end{pmatrix}$$

where M_{Lr} is the N dimensional column matrix of leach rate calculated from input data, N is the sampling number, which is 100 for this simulation, M_P is a N×4 matrix of input data, M_β is a 4th dimensional column matrix of regression model parameters. From Eq. (13b), matrix M_β can be calculated as

$$M_\beta = \left(M_P{}^T M_P\right)^{-1} M_P{}^T M_{Lr} \tag{13c}$$

Estimation of using 100 sampling data of input parameters is carried out and the result in the form of a matrix is given in Eq. (13d).

Table 4: Various distributions of input parameters

Parameters	Distribution	Minimum value	Maximum value
D (cm^2s^{-1})	Uniform	1.2×10^{-6}	2.4×10^{-6}
θ	Uniform	0.10	0.20
K_d (ml/gm)	Log-uniform	Log(20.0)	Log(40.0)

$$M_\beta = \begin{pmatrix} +3.74128070\mathrm{E}-10 \\ +2.14975800\mathrm{E}-04 \\ +2.54434553\mathrm{E}-09 \\ -1.31768897\mathrm{E}-11 \end{pmatrix} \tag{13d}$$

Therefore, leach rate can be written as,

$$Lr = 3.74128\times10^{-10} + 2.149758\times10^{-4}D + 2.54434553\times10^{-9}\theta - 1.31768897\times10^{-9}K_d$$

The goodness of the linear fit is estimated by calculating R-squared (R^2) value, which is mathematically written as

$$R^2 = \frac{\sum_{i=1}^{N}\left(L_R^i - \langle L_R\rangle\right)^2}{\sum_{i=1}^{N}\left(L_r^i - \langle L_r\rangle\right)^2} = \frac{Var(L_R)}{Var(L_r)}$$

where L_R^i is the i[th] value of leach rate calculated from fitted model, which is a linear model for this study, L_r^i is the i[th] value of leach rate calculated from analytical model, $\langle x\rangle$ implies averaged over x, $Var(x)$ is variance of the data set x. The value of obtained from the linear fit is 0.99, which is close to one and therefore, the fitted model can be taken as good model.

Correlation analysis is carried out to measure influence of various parameters on the leach rate. The correlation coefficients between leach rate and input parameters such as diffusion coefficient, porosity and distribution coefficient are calculated using Eq. (14). Various correlation coefficients obtained from the simulation run are shown in Table 5..

$$r = \frac{N\sum_{i=1}^{N}(x_i y_i) - \left(\sum_{i=1}^{N} x_i\right)\left(\sum_{i=1}^{N} y_i\right)}{\sqrt{\left[N\left(\sum_{i=1}^{N} x_i^2\right) - \left(\sum_{i=1}^{N} x_i\right)^2\right]\left[N\left(\sum_{i=1}^{N} y_i^2\right) - \left(\sum_{i=1}^{N} y_i\right)^2\right]}} \tag{14}$$

where N is the total sampling points. The variables x is leach rate data and y is a single parameter (D, θ, K_d).

Table 5: Correlation coefficient matrix

	Leach Rate ($cm^{-2}s^{-1}$)	D (cm^2s^{-1})	θ	K_d (mlg^{-1})
Leach Rate ($cm^{-2}s^{-1}$)	1.0	0.5816	0.4994	-0.5949
D (cm^2s^{-1})	0.5816	1.0	0.0	0.0
θ	0.4994	0.0	1.0	0.0
K_d (mlg^{-1})	-0.5949	0.0	0.0	1.0

The correlation matrix shows that diffusion coefficient is positively more correlated with leach rate compared to porosity whereas, K_d is negatively correlated with leach rate. Hence, we can interpret in this way that more the value of K_d, less is the leach rate and smaller the leach rate, smaller will be the diffusion. Indirectly, higher the value of K_d, lower the value of D. Considering various input parameters as independent parameters (random sampling), correlation coefficients between parameters are taken as zero.

6. Conclusions

Table 2 of L_2 error shows that, numerical simulation carried out using very few non-uniform grid points

deliver very good results. This property of DQM makes it computationally efficient. Therefore, DQM can readily be used as numerical tool for computationally intensive calculations, such as regression analysis and correlation analysis studied in this paper, uncertainty analysis etc.

The time dependent leach rates calculated at various time using DQM method show good agreement with analytical results and such time dependent leach rate data instead of one particular leach rate data should be used in the source term modeling for safety analysis of NSDF. The linear leach rate equation given in Eq. (13e) and the correlation analysis shows that, leach rate is proportional to diffusion coefficient and porosity of the waste form and inversely proportional to distribution coefficient. Hence, the desire properties of the waste form are lower value of diffusion coefficient and porosity and higher value of distribution coefficient.

References

1. Raj K., Prasad K.K., Bansal N.K., "Radioactive waste management practices in India", Nuclear Engineering and Design, Vol 36, No. 7–8, pp. 914–930, 2006.
2. Bert C.W., Malik M., "Differential quadrature method in computational mechanics: a review", Applied Mechanics Reviews, Vol 49, No. 1, pp. 1–27, 1996.
3. Shu C., "Differential Quadrature and Its Application in Engineering", Springer, Berlin 2000.
4. Zong Z., Zhang Y., "Advanced differential quadrature methods", CRC Press, New York 2009.
5. Nair, R.N., Krishnamoorthy, T.M., "Near-field and far-field migration of radionuclides from a shallow land burial facility", Nuclear Technology, Vol 114, No. 2, pp. 235-244, 1996.
6. Bellman R., Casti J., "Differential quadrature and long-term integration", Journal of Mathematical Analysis and Applications, Vol 34, No. 2, pp. 235-238, 1971.
7. Shu C., Xue H., "Explicit computation of weighting coefficients in the harmonic differential quadrature", Journal of Sound and Vibration, Vol 204, No. 3, pp. 549-555, 1997.
8. Kaya B., "Solution of the advection-diffusion equation using the Differential Quadrature Method", KSCE Journal of Civil Engineering, Vol 14, No. 1, pp. 69-75, 2010.
9. Aswin V.S., Awasthi A., Anu C., "A Comparative Study of Numerical Schemes for Convection-diffusion Equation", Procedia Engineering, Vol 127, pp. 621-627, 2015.

Life Cycle Reliability and Safety Engineering
Vol.5 Issue 3 (2016) 08-15

Reliability Based Optimal Design of Water Distribution Network Using Combinatorial Particle Swarm Optimization

Sanjeev Kumar Sharma[1], Varen[2], S. K. Gupta[3], Ashis Mallick[4], D. Datta[5]

[1]*Dept. of Mechanical Engineering, Indian School of Mines Dhanbad*
[2]*Dept. of Operational Research, Hindu College, University of Delhi, New Delhi,*
[3]*Dept. of Civil Engineering, Indian Institute of Technology (B.H.U.), Varanasi,*
[4]*Dept. of Mechanical Engineering, Indian School of Mines Dhanbad*
[5]*Health Physics Division, Bhabha Atomic Research Centre, Mumbai, India,*
E-mail: sksharma.me@gmail.com

Abstract

Particle Swarm Optimization (PSO) method suitable for continuous domain variables is tuned for a multi-objective combinatorial problem relating to the design of water distribution network. Maximization of network reliability and minimization of cost were considered as the objective functions of the design problem. Consumer satisfaction index being a vaguely defined linguistic parameter was treated as fuzzy to define membership functions corresponding to the excess pressure above the minimum specified head at demand nodes of the network. EPANET dynamic link library was linked with MATLAB to implement the combinatorial PSO for solving Hanoi network problem reported in the literature. The results were found to surpass or compete well with those of other researchers. Hence, the proposed methodology is suggested for solving combinatorial optimization problems, including the design of water distribution networks.

Keywords- water distribution network; combinatorial particle swarm optimization; reliability; fuzzy logic; cost.

1. Introduction

Design of water distribution network constitutes a multi-objective optimization problem. It involves determination of pipe link diameters with an additional focus on minimization of cost, energy losses, risk of pipe failure, nodal pressure deviation from the minimum specified, and maximization of resilience and/or reliability [1-2]. As the proportion of expenses incurred on water distribution network is high and is about 70% or even more [3-4] of the total outlay, designers normally concentrate on minimization of the network cost for obtaining required water quantity and pressure at demand nodes while applying the mass and energy conservation laws. Giustolisi et al. [5] considered uncertainties associated with nodal demands and pipe roughness to minimize the network cost and maximize the hydraulic reliability of the water distribution network. Ekinci and Konak [6] gave least cost designs of water distribution networks based on the minimization of energy losses. Kwon and Lee [7] analyzed reliability of pipe networks under transient condition using probability concept. Based on the satisfaction relating to nodal demands and failure of system components, Tung [8] gave six techniques for evaluating the reliability of water distribution networks. Revelli and Ridolfi [9] applied fuzzy optimization scheme while incorporating uncertainties in pipe roughness, nodal demands, and pressure heads. Xu and Goulter [10] and Bhave and Gupta [11] incorporated fuzzy nodal demands in optimal design of water distribution networks using linear programming. Avi and Uri [12] proposed a method for including reliability in optimal design of water distribution networks by laying focus on failure of system components and nodal demands. Avi [13] presented a methodology considering connectivity of source and demand nodes in assessment of reliability of water supply scheme. The need of introducing reliability in design of water distribution networks, in fact, emanates from uncertainties in consumer demand, nodal pressure, fire flow requirements, pipe roughness, and pipe failures etc. Extensive research using various measures of reliability for water distribution system under failure condition of components or demand variation has been carried out but none of the measures find universal acceptance.

Table 1: Link lengths and nodal demands of Hanoi network

Link index	Link lengths	Node index	Demands
1	100	1	-19940
2	1350	2	890
3	900	3	850
4	1150	4	130
5	1450	5	725
6	450	6	1005
7	850	7	1350
8	850	8	550
9	800	9	525
10	950	10	525
11	1200	11	500
12	3500	12	560
13	800	13	940
14	500	14	615
15	550	15	280
16	2730	16	310
17	1750	17	865
18	800	18	1345
19	400	19	60
20	2200	20	1275
21	1500	21	930
22	500	22	485
23	2650	23	1045
24	1230	24	820
25	1300	25	170
26	850	26	900
27	300	27	370
28	750	28	290
29	1500	29	360
30	2000	30	360
31	1600	31	105
32	150	32	805
33	860		
34	950		

This happens because of lack of consensus on the use of a single measure that can effectively address effect of all parameters, which govern performance of the system. Further, the design of water distribution networks falls in category of large combinatorial optimization problems [14], therefore, various optimization methods have been tested for the design of water distribution networks but universally acceptable method is yet to be finalized [15].

Table 2 The best solution obtained out of ten simulation runs for Hanoi network

Link index	Link Diameter	Flow velocity	Discharge
1	40	6.83	19940.00
2	40	6.53	19050.00
3	40	2.30	6710.68
4	40	2.25	6580.68
5	40	2.01	5855.68
6	30	2.95	4850.68
7	40	1.20	3500.68
8	40	1.01	2950.68
9	30	1.48	2425.68
10	30	1.22	2000.00
11	30	0.91	1500.00
12	24	0.89	940.00
13	20	0.14	99.32
14	20	0.98	714.32
15	30	0.61	994.32
16	30	1.34	2204.96
17	30	1.87	3069.96
18	30	2.69	4414.96
19	40	1.53	4474.96
20	40	2.40	7014.36
21	30	0.86	1415.00
22	24	0.46	485.00
23	40	1.48	4324.36
24	30	1.12	1838.12
25	20	1.40	1018.12
26	24	0.35	369.36
27	16	1.14	530.64
28	24	0.86	900.64
29	24	1.37	1441.24
30	30	0.70	1151.24
31	24	0.75	791.24
32	30	0.26	431.24
33	20	0.45	326.24
34	20	0.66	478.76

Maximization of reliability as a single measure of optimization yields an uneconomical system, therefore, the present study involves cost minimization along with the reliability measure used by Chandramouli [4] to address the issue of nodal outflow quantity and corresponding excess residual pressures above the minimum specified at nodes to maximize the network reliability index of a water distribution network. The excess residual pressures available at the demand

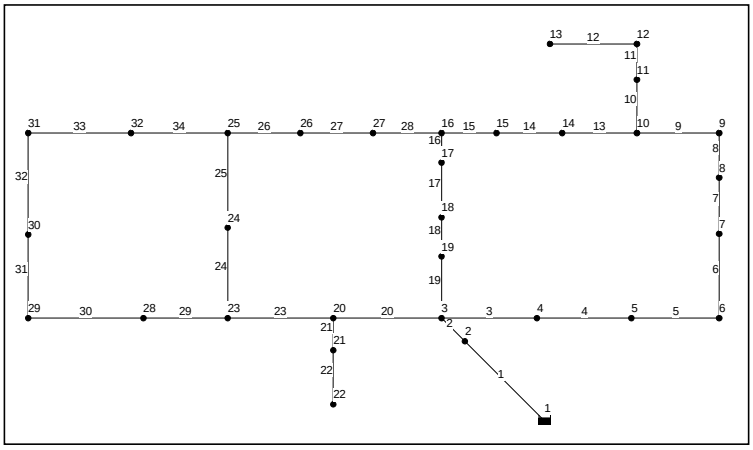

Figure 1 Hanoi water distribution network: 3-loop benchmark problem (Node and link identification numbers are shown)

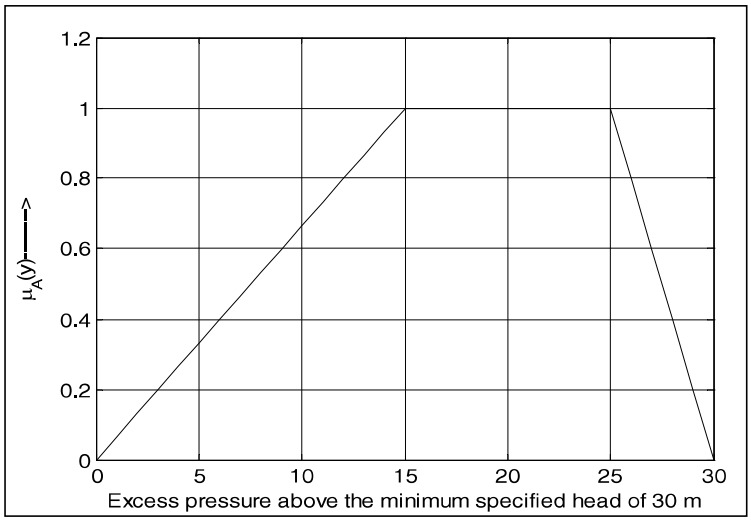

Figure 2 Trapezoidal membership function applied for the consumer satisfaction index

nodes were adopted as fuzzy in accordance with Chandramouli [4] to define trapezoidal membership function for comparison of the results.

Particle swarm optimization method that recently attracted a significant attention of researchers in spite of its sole applicability to real-valued problems has already been applied for combinatorial problems by truncating the real-valued solution to integer but it incurred truncation error and created difficulty in convergence of solutions [16]. Another way of applying PSO to combinatorial optimization problems is to map the discrete search space to a continuous domain and then to demap the result after the analysis. Such a mapping can be made simple by using rounded values but this method is infeasible when values of scaled variables range between zero to one (0-1). Thus, the present study introduces a variation of PSO to design a reliability based water distribution network for the minimum cost. PSO and EPANET tool kit in MATLAB environment are integrated to develop a code for optimal design of water distribution network.

2. Test Problem

Hanoi water distribution network [17-19] comprising 31 demand nodes, 34 pipe links and a single reservoir is shown in Fig. 1. Link lengths and nodal demands are presented in Table 1. Reduced level (RL) of each demand node, minimum specified pressure head, and reservoir elevation of the source node are 0.0, 30.0 and 100.0m, respectively. The Hazen William roughness coefficient for the network is adopted as130.

3. Fuzzy Logic: Concept and Application

Fuzzy logic relies on the fuzzy set theory developed by Lofti A. Zadeh in 1965 [20]. Ever since its inception, fuzzy logic acquired prominence in dealing with imprecision and vagueness in linguistic variables [21] that are commonly observed during verbal human interactions. People employ words rather than numbers to describe the values of variables, for example, delay of a construction process may be described as 'slightly late', 'late' or 'very late'; or quality of a product as low, average, or good etc. These imprecisely known variables are treated as fuzzy to define their intermediate grade of belongingness involving membership functions. Revelli and Ridolfi [9], Bhave and Gupta [11], Ross [22], Kaufmann, and Gupta [23], and Gupta and Bhave [24] have already introduced fuzzy concept in pipeline network design problems.

Fuzzy set theory provides a subset 'A' of the universe of discourse 'S', where the transition between full membership and no membership is gradual rather than abrupt. The fuzzy subset 'A' is defined by a membership function $\mu_A(y)$ that maps the degree to which an element y belongs to a fuzzy subset 'A' from domain 'S' to the range (0-1). A membership function in general can be linear, trapezoidal, Gaussian, or some other forms [25]. The resemblance of Gaussian membership function requires distinction from probability function when y is a countable set (or a probability density function when y is continuous). Probability relates to the indecisiveness in outcome

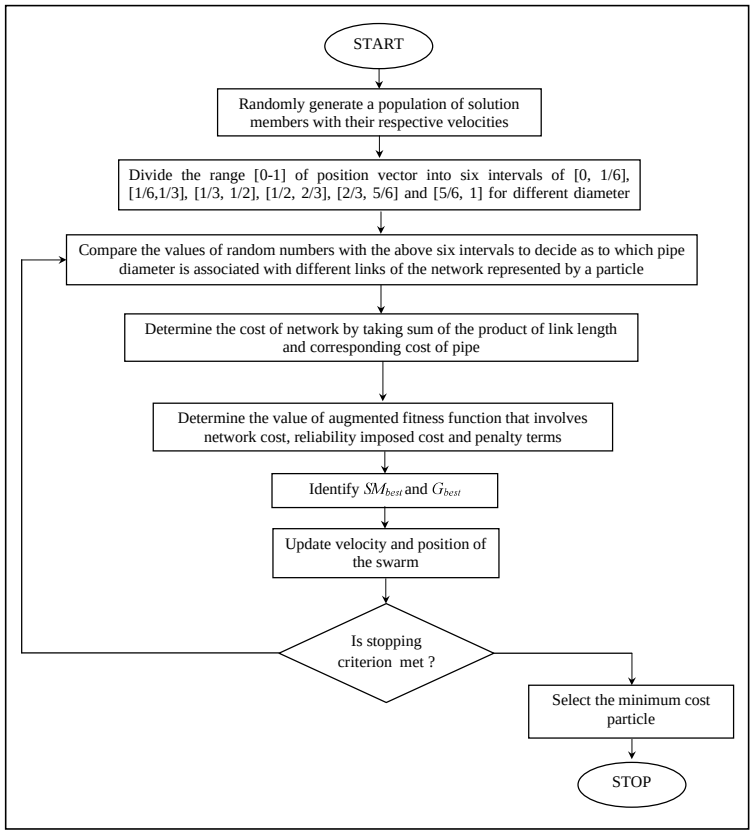

Figure 3 *Flow chart depicting combinatorial Particle Swarm Optimization algorithm as applied to the Hanoi network problem*

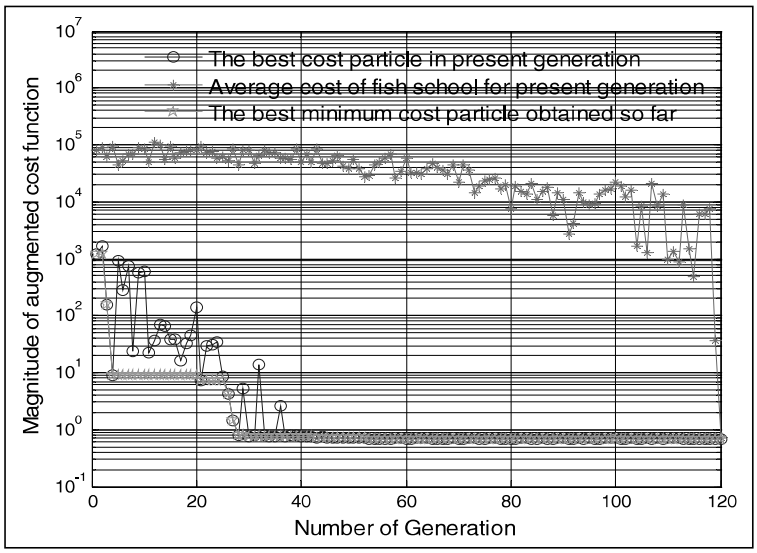

Figure 4 *The convergence characteristics of the average population cost, present generation best, and global best particle obtained so far with iteration number (Network cost = 7.44 million units and NRI = 0.8075)*

of clearly defined and randomly occurring events whereas fuzzy logic is concerned with the ambiguity inherent in the description of the event itself. Thus, fuzziness is expressed in terms of ambiguity rather than uncertainty, and it remains a characteristic of the perception [26].

The universe of discourse S for the present test problem is thus viewed as a set of pressure deviations (+/-) from the minimum specified head at different nodes of the network, whereas, '*A*' is defined as a subset containing pairs of excess pressure-heads above the minimum specified (p_{min} = 30m) and their corresponding membership values. A trapezoidal membership function (see Fig. 2) is adopted to quantify the consumer satisfaction index corresponding to the range of residual pressures at demand nodes. Details of the involved subset and membership functions are:

$$S = \{y \mid y = p_i - p_{\min}\} \tag{1}$$

$$A = \{y, \mu_A(y) \mid \quad 0 \le \mu_A(y) \le 1 \quad for\ y \ge 0\} \tag{2}$$

$$\mu_A(y) = \begin{Bmatrix} y/15 & 0 < y \le 15 \\ 1 & 15 < y \le 25 \\ (30-y)/5 & 25 < y \le 30 \end{Bmatrix} \tag{3}$$

where, p_{min} and p_j represent the minimum specified and available pressure head at node *j*.

4. Network Reliability Index

Reliability is usually defined as the extent to which a device or system serves its intended purpose under given operating conditions over its life time. This way, a water distribution network assumes enviable reliability if it delivers required quantity of water at desirable quality and residual heads to all consumers over its design period. The network reliability index (*NRI*) applied by Chandramouli [4] is therefore adopted. It was defined as ratio of sum of the product of consumer satisfaction levels at excess nodal pressures above the minimum specified ($=p_i - p_{min}$) and nodal demands to the overall demand of the network, and is expressed as:

$$NRI = \frac{\sum_{j=1}^{j=m} SI_j . D_j}{\sum_{j=1}^{j=m} D_j} \quad for\ j = 1, 2 \ldots m = 31 \tag{4}$$

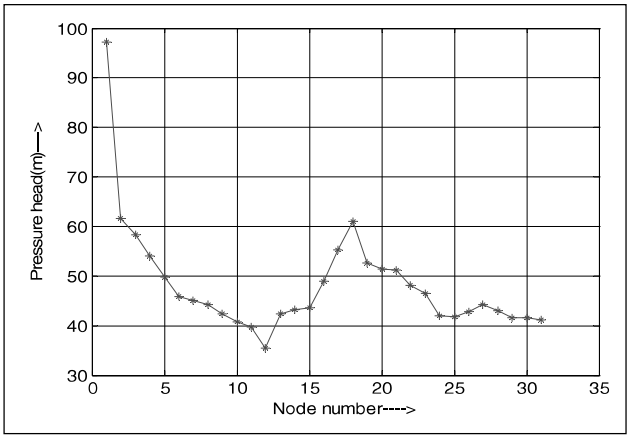

Figure 5 *Pressure head at various nodes of the Hanoi water distribution network (Network cost = 7.44 million units and NRI = 0.8075)*

where m, SI_j and D_j denote total number of demand nodes, satisfaction index and demand at node j, respectively. The membership function derived for the Hanoi network thus represents the satisfaction level of consumers at demand nodes, i.e., $SI_j = \mu_A(y)$.

5. Problem Statement

Hanoi water distribution network is required to be designed for the maximum reliability. The mathematical formulation for this multi-objective reliability based optimization problem is:

Minimize NC = $\sum_{i=1}^{i=n} L_i.C(d_i)$ for $i = 1,..n = 34$ (5)

Maximize NRI (6)

subject to:

$$p_i \geq p_{\min} \quad (7)$$

$$d_i \in B \; \forall \; i \quad (8)$$

$$B = \{40, 30, 24, 20, 16, 12\} \quad (9)$$

where, NC represents network cost, and L_i, d_i and $C(d_i)$ denote length, diameter, and cost of i^{th} link, respectively. However, B is a discrete set of pipe diameters shown in inches, and the respective element wise cost array for the same set of pipe diameters is {278.3, 180.8, 129.33, 98.38, 70.40, 45.73}.

6. Particle Swarm Optimization

Particle Swarm Optimization is a swarm intelligence-based technique developed by Kennedy and Eberhart [27] to solve optimization problems. It is inspired by the social behavior of fish schools where individual members move in synchronization. The maneuver of fish school is governed by the exchange of knowledge earned by the individual member and experience of other members. The population of solution is referred to as swarm, and rows of the population matrix are called as particles. Every particle moves in search space with a velocity influenced by its own best position acquired so far (memory) and the best position obtained by its neighbours both. The velocity and position update equations for the search procedure are:

$$V_{k+1} = V_k \oplus c_1 r_1 \otimes (p_k \Theta x_k) \oplus c_2 r_2 \otimes (g_k \Theta x_k) \quad (10)$$

$$x_{k+1} = x_k \oplus V_{k+1} \quad (11)$$

where c_1 is the cognitive parameter; c_2 is the social parameter; r_1 and r_2 are uniformly distributed random numbers in the range (0-1); k refers to an iteration number; and $\oplus, \Theta, \otimes$ are point wise arithmetic operators.

Equations (10) and (11) representing canonical PSO do not have a check mechanism on particle velocity to restrict it below a threshold (V_{max}), therefore, the velocity update equation in a relatively newer version of PSO [29] is:

$$V_{i+1} = \chi \left[w V_i + c_1 r_1 \otimes (p_i \Theta x_i) + c_2 r_2 \otimes (g_i \Theta x_i) \right] \quad (12)$$

The inertia weight (w) and constriction coefficient (χ) control particles' velocities. χ relating c_1 and c_2 [29] to eliminate the need of an extra parameter is:

$$\chi = \frac{2}{\psi - 2 + \sqrt{\psi^2 - 4\psi}} \quad (13)$$

where $\psi = c_1 + c_2 > 4$

7. Novel Provision for Handling Combinatorial Problem

Every particle of swarm represents a possible solution of the optimization problem and it contains an array of 34 random numbers for the Hanoi network problem whose values fall in the range of (0-1). This range is divided into six intervals [0, 1/6], [1/6, 1/3], [1/3, 1/2], [1/2, 2/3], [2/3, 5/6] and [5/6, 1] for accommodating six pipe diameters as 12, 16, 20, 24, 30, and 40 inches, respectively. If magnitude of an element of a solution array, for example, is 0.3, it would be identified as 16 inch diameter pipe as the value of random number falls between [1/6, 1/3] range. Thus, position of a particle represents a set of 34 elements representing diameters of the links of Hanoi

Table 3 Comparison of the results of the present study with that of other researchers

Present Study → / **Network feature ↓**	**Abebi and Solomatine [32]**	**Liong and Atiquzzaman [33]**	**Chandramouli [4]**	**Present Study**
Cost (million units)	7.84	6.22	7.78	7.4430
Reliability	0.5908	0.5754	0.7323	0.8075
iterations	3055	25402	1800	120
Cost/NRI	13.27	10.81	10.62	9.22
Link index	**Link Diameter**			
1	40	40	40	Given in **Table 2**
2	40	40	40	
3	40	40	30	
4	40	40	30	
5	40	40	30	
6	30	40	30	
7	40	40	24	
8	40	30	30	
9	24	30	20	
10	40	30	40	
11	30	30	30	
12	40	24	24	
13	16	16	30	
14	16	12	40	
15	30	12	24	
16	12	24	20	
17	20	30	24	
18	24	30	20	
19	30	30	40	
20	40	40	40	
21	30	20	40	
22	30	12	24	
23	40	30	40	
24	40	30	40	
25	40	24	20	
26	24	12	40	
27	30	20	30	
28	12	24	24	
29	16	16	30	
30	40	16	40	
31	16	12	30	
32	20	16	40	
33	30	20	40	
34	24	24	40	

network. This provision was adopted for the position of the particles but not for velocity. Rest procedure remains the same to that of newer version of PSO, which incorporates inertia weight and constriction coefficient for controlling particles' velocities. The PSO thus obtained is referred to as Combinatorial Particle Swarm Optimization (CPSO).

8. Application of Combinatorial PSO

An augmented cost function was formulated using objective functions, constraints, and penalty terms.

8.1 Augmented cost function

The lowest and highest costs of the network and their mean were determined. The ratio of deviation of the network cost from the mean to the mean cost was adopted as the first term of the augmented cost function. The second term of the cost function involved inverse function of *NRI* to translate reliability maximization problem into minimization form. Two penalty terms added to the augmented cost function correspond to the demand nodes having negative pressure, and positive pressure below the minimum specified head, respectively. Fixed magnitude of penalty was imposed as:

$$\beta_j = \begin{Bmatrix} 1000 & x_j < 0 \\ 16.5 & 30 \geq x_j \geq 0 \end{Bmatrix} \quad for\ any\ node\ j \qquad (14)$$

8.2 Parameter setting

The inertia weight (ω) was varied linearly from 0.7 to zero. The values of ψ and c_1 were 4.1 (Clerc and Kennedy 2002) and 2.27, respectively. The maximum number of iteration was set as 120 and swarm size was 64.

8.3 Flow chart

The optimization code was written in MATLAB environment to execute combinatorial PSO (CPSO) in conjunction with EPANET tool kit. EPANET [30] is a public-domain software for snapshot and extended time hydraulic and water quality simulation in pressurized pipe networks using gradient method [31]. It provides discharges, nodal heads, and solute concentration in pressurized pipeline for given inputs of pipe roughness, link lengths and pipe diameters. A flow chart depicting the solution procedure is given in Fig. 3.

9. Results and Discussions

A typical convergence characteristics graph for one simulation run of the program that yielded best solution out of ten simulations is shown in Fig. 4. The convergence behaviour of population average cost curve, present generation's best cost particle and the best particle obtained so far is displayed. The merging trend of three curves reflects the appropriate setting of CPSO parameters. Occurrences of spikes along the average cost curve reflect the combinatorial nature of the problem. In fact, average cost of the swarm may shoot up or dip down according to the combination of different diameter pipes chosen for the design of network during iterative process. The data relating to the link diameters, flow velocities and discharges for the best solution are given in Table 2. It may be observed that the network cost and corresponding reliability index obtained by the CPSO (7.44 million units and 0.8075) is found superior to those obtained by Chandramouli [4] (7.78 millions and 0.7323), and Abebi and Solomatine [32] (7.84 millions and 0.5908) as well. A comparison of the optimal solutions obtained by different researchers is [4, 32-33] also given in Table 3. It is observed that the cost reliability ratio (cost/ *NRI*) for the best solution obtained by the present methodology came out to be the lowest as compared to the solutions obtained by other researchers [32-33]. Also, the number of iterations required for yielding the best solution in the present study is 120 as compared to 1800 and 3055 needed by Chandramouli [4] and Abebi and Solomatine [32].

The pressure heads across the different nodes of the network is shown in Fig. 5. The pressure heads at various nodes of the Hanoi network are above the minimum specified pressure of 30 m head and they are close to 45 m at several nodes because of relatively higher network reliability index that requires residual pressures to be in the range of 15-25m head.

Conclusions

The proposed provision for enabling PSO to handle combinatorial optimization problem has demonstrated its capability to serve the intended purpose of yielding the least cost Hanoi water distribution network with significantly high network reliability index. The number of iterations for obtaining the best solutions is also low as compared to that required by GA applied by Savic and Walters [17] and Ant colony optimization applied by Abebi and Solomatine [32]. Further, the optimal design yielded by combinatorial particle swarm optimization resulted nodal pressure heads close to the desired range, hence, this provision is suggested to be applied to PSO to solve other types of multi-objective combinatorial problems.

References

1. L. Perelman, A. Ostfeld, E. Salomons, Cross entropy multiobjective optimization for water distribution systems design. Water Resources Research, 44, W09413, 2008.
2. V. P. Singh, and J. A. Oh, Tsallis entropy-based redundancy measure for water distribution networks. Physica A, 421, 360–376, 2015.
3. P. R. Bhave, and R. Gupta, Analysis of water distribution networks, Narosa publishing pvt. ltd., New Delhi, 2006.
4. S. Chandramouli, Reliability based optimal design of a municipal water supply pipe network. Urban Water Journal, 12(5), 353–361, 2015
5. O. Giustolisi, D. Laucelli, and A. F. Colombo, Deterministic versus stochastic design of water distribution networks. Journal of Water Resources Planning and Management, 135 (2), 117–127, 2009.
6. O. Ekinci, and H. Konak, An optimization strategy for water distribution networks. Water Resources Management, 23 (1), 169–185, 2009.
7. H. J. Kwon, and C.E. Lee, Reliability analysis of pipe network regarding transient flow. KSCE J. Civ. Eng., 12 (6), 409–416, 2008.
8. Y. K. Tung, Evaluation of water distribution network reliability. Vol. 1, Hydraulics and Hydrology in the Small Computer Age, Proc. speciality conference, ASCE Hydraulics Division, Lake Buena Vista, Forida, 1985.
9. R. Revelli, and L. Ridolfi, Fuzzy approach for analysis of pipe networks. Journal of Hydraulic Engineering, 128(1), 93-101, 2002.
10. C. Xu, and I. C. Goulter, Reliability based optimal design of water distribution networks. Journal of Water Resources Planning and Management, ASCE, 125 (6), 352–362, 1999.
11. P. R. Bhave, and R. Gupta, Optimal design of water distribution networks for fuzzy demands. Civil Engineering and Environmental Systems, 21(4), 229-245, 2004.
12. O. Avi, and S. Uri, Incorporating reliability in optimal design of water distribution networks-review and new concepts. Journal of Reliability Engineering and System Safety, 42, 5–11, 1993
13. O. Avi, Water distribution systems connectivity analysis. Journal of Water Resources Planning and Management, ASCE, 131 (1), 58–66, 2005
14. E. Reehuis, Multiobjective robust optimization of water distribution networks. thesis (masters). Leiden University, The Netherlands, 2010.
15. M. Cisty, and Z. Bajtek, Hybrid method for optimal design of water distribution system. International Symposium on Water Management and Hydraulic Engineering, 235–246, Ohrid, Macedonia. Ss.Cyril and Methodicy University in Skopje, Ohrid, Macedonia: Faculty of Ci vil Engineering, 2009.
16. R. Roy, S. Dehuriand, and S. B. Cho, A novel particle swarm optimization algorithm for multi-objective combinatorial optimization problem. International Journal of Applied Metaheuristic Computing, 2(4), 41-57, October-December, 2011.
17. D. A. Savic, and G. A. Walters, Genetic Algorithms for least cost design of water distribution networks. Journal of Water Resources Planning and Management, ASCE, 123 (2), 67–77, 1997.
18. Z. Y. Wu, and T. Walski, Self-adaptive penalty approach compared with other constraint-handling techniques for pipeline optimization. Journal of Water Resources Planning and Management, ASCE, 131 (3),181–192, 2005.
19. M.Van Dijk, S. J. Van Vuuren, and J. E. Van Zyl, Optimizing water distribution systems using a weighted penalty in a genetic algorithm. Water SA, 34 (5), 537–548, 2008
20. L. A. Zadeh, Fuzzy Sets. Infection Control, 8, 338–353, 1965.
21. L. A. Zadeh, Fuzzy sets, usuality and commonsense reasoning. EECS Technical Report, University of California, Berkeley, 1985.
22. T. J. Ross, Fuzzy logic with engineering applications. McGraw-Hill, New York, 1995.
23. A. Kaufmann, and M. M. Gupta, Introduction to fuzzy arithmetic: Theory and applications. Van Nostrand Reinhold, New York, 1991.
24. R. Gupta, and P. R. Bhave, Fuzzy parameters in pipe network analysis. Civil Engineering and Environmental Systems, 24(1), 33-54, 2007.
25. C. C. Lee, Fuzzy logic in control systems: fuzzy logic controller – I. IEEE Transactions on Systems, Man and Cybernetics, 20(2), 404-435, 1990.
26. D. McNeill, and P. Freiberger, Fuzzy logic. Simon & Schuster, New York, 1993.
27. J. F. Kennedy, and R. C. Eberhart, Particle swarm optimization. Proc. of the IEEE Int. Conf. on Neural Networks, IEEE Service Canter, Piscataway, NJ, 1942–1948, 1995.
28. R. C. Eberhart, and Y. Shi, Comparing inertia weights and constriction factors in Particle Swarm Optimization. Proceedings of the Congress on Evolutionary Commutating, 84–88, 1998.
29. M. Clerc, and J. F. Kennedy, The particle swarm explosion, stability and convergence in a multidimensional complex space. IEEE Transactions on Evolutionary Computation, 6 (1), 58-73, 2002.
30. L. A. Rossman, EPANET 2, users manual. National Risk Management Research Laboratory, U.S. Environmental Protection Agency, Cincinnati, Ohio, 2000
31. E. Todini, and S. Pilati, A gradient method for the analysis of pipe networks. International Conference on Computer Application for Water Supply and Distribution. Leicester Polytechnic, U.K.,1987
32. A. J. Abebi and D. P. Solomatine, Application of global optimization to the design of pipe networks In: Proc. 3rd International Conference on Hydroinformatics. Copenhagen: Balkema, 1–8, 1998.
33. S. Y. Liong, and M. Atiquzzaman, Optimal design of water distribution network using shuffled complex evolution. Journal of the Institute of Engineers (Singapore), 44, 93–107, 2004

Life Cycle Reliability and Safety Engineering
Vol.5 Issue 3 (2016) 16-20

Address of Geo-hydrological Problem using Lattice Boltzmann and Differential Quadrature Methods

D. Datta[1], T.K.Pal[2]
[1]*Radiological Physics & Advisory Division, BARC, Mumbai, India*
[2]*Technology Development Division, BARC, Mumbai, India*
Email: ddatta@barc.gov.in

Abstract:

This paper addresses the geo-hydrological problems through a generalized advection- dispersion equation (GADE). Paper presents the solution of GADE with time dependent boundary conditions using Lattice Boltzmann Method (LBM) and Differential Quadrature Method (DQM). In the LBM based scheme, ADE is solved using a D2Q5 lattice model together with single relaxation time (SRT) and Bhatnagar-Gross-Krook (BGK) collision operator. In the DQM based scheme, time derivative is approximated using forward difference and the spatial derivatives using polynomial based DQM. Numerical results are compared with analytical solutions and good agreement between the two results is established.

Keywords: Advection-dispersion equation, lattice Boltzmann method, Differential Quadrature

1. Introduction:

Generalized Advection-Dispersion Equation (GADE) appears in many fields of science and technology including geo-hydrology, for example physical processes that are involved with transport of non-reactive solute through geological porous media in the presence of ground water flow are advection of solute with the velocity of ground water, molecular diffusion of solute due to concentration gradient, and dispersion of solute due to porous structure of the geological materials (rock, soil etc) and spatial heterogeneity of the geological formation. Therefore, transport process of non-reactive solute through geological media is modeled as an ADE.

Numerical solution of a partial differential equation (here it is ADE) is generally carried out using traditional numerical techniques, such as Finite Difference Method (FDM), Finite Element Method (FEM), and Finite Volume Method (FVM) etc. Lattice Boltzmann method (LBM) and Differential Quadrature Method (DQM), which are relatively new in this field, have been extensively used as an alternate numerical technique for simulation of various flow and transport related problems [1, 2, 3].

The rest of the paper is organized as follows. Mathematical formulation of generalized ADE is given in Section 2. Numerical schemes of ADE using LBM and DQM are developed in Section 3 and 4, respectively. Results and discussions are elaborated in Section 5. Finally conclusions are drawn in Section 6.

2. Mathematical Formulation of Generalized Advection-Dispersion Equation

The generalized time dependent 2D ADE with constant coefficients for a general scalar variable $u(x,y,t)$ can be written as

$$\frac{\partial u(x,y,t)}{\partial t} = \alpha_x \frac{\partial^2 u(x,y,t)}{\partial x^2} + \alpha_y \frac{\partial^2 u(x,y,t)}{\partial y^2} - \beta_x \frac{\partial u(x,y,t)}{\partial x} - \beta_y \frac{\partial u(x,y,t)}{\partial y} \quad (1)$$

The time dependent boundary conditions are

$$u(0,y,t) = a\, e^{bt}(1 + e^{-yc_y})$$
$$u(1,y,t) = a\, e^{bt}(e^{-c_x} + e^{-yc_y})$$
$$u(x,0,t) = a\, e^{bt}(e^{-xc_x} + 1)$$
$$u(x,0,t) = a\, e^{bt}(1 + e^{-yc_y})$$
$$u(x,1,t) = a\, e^{bt}(e^{-xc_x} + e^{-c_y}) \quad t > 0$$

here

$$c_x = \frac{-\beta_x - \sqrt{\beta_x{}^2 + 4b\alpha_x}}{2\alpha_x}$$

$$c_y = \frac{-\beta_y - \sqrt{\beta_y{}^2 + 4b\alpha_y}}{2\alpha_y}$$

Space dependent initial condition is

$$u(x, y, 0) = a\,(e^{-xc_x} + e^{-yc_y}) \quad 0 \le x, y \le 1$$

Analytical solution of the above formulation can be written as

$$u(x, y, t) = a\, e^{bt}(e^{-xc_x} + e^{-yc_y}) \tag{2}$$

3. Numerical Formulation: Lattice Boltzmann Method

LBM is a particle based simulation technique, which investigates the dynamical behavior of a fluid system using statistical mechanics. The LBM method is based on the numerical simulation of a time-, space- and velocity-discrete Boltzmann type equation. The propagation and interaction of the particles of an 'artificial computer fluid' is simulated in terms of time evolution of a density distribution function, representing an ensemble average of the particle distribution. Working equation of a SRT LBM with Bhatnagar-Gross-Krook (BGK) collision operator can be written in the following form:

$$f_i(\vec{r} + \vec{e_i}\Delta t^*, t + \Delta t^*) = f_i(\vec{r}, t) + \Omega_i^{BGK}(\vec{r}, t)$$

$$\Omega_i^{BGK}(\vec{r}, t) = \frac{\Delta t^*}{\tau}\left[f_i^{eq}(\vec{r}, t) - f_i(\vec{r}, t)\right] \tag{3}$$

where $\vec{r}$ is position vector, e_i is velocity vector along *i*-th direction, f_i represents particle's density distribution function, and time t, τ is relaxation time, Δt^* is lattice time step in lattice, Ω_i^{BGK} is BGK collision operator. f_i^{eq} is equilibrium particle's density distribution function and can be written as:

$$\mathrm{f_i^{eq}}(\vec{\mathrm{r}}, \mathrm{t}) = \mathrm{w_i u}(\vec{\mathrm{r}}, \mathrm{t})\left(1 + \frac{\vec{\mathrm{e_i}}.\vec{\beta_\mathrm{j}}}{\mathrm{e_s^2}}\right) \tag{4}$$

where are the weights for particle's density distribution along *i*-th direction in the velocity space and its value depends upon lattice structure, is "pseudo-sound-speed" [LT-1]. Various lattice structures used in LBM are D1Q2, D1Q3, D1Q5 etc for 1D lattice, D2Q4, D2Q5, D2Q9 for 2D lattice, and D3Q15, D3Q19 for 3D lattice. In a DnQm lattice structure, n represents the dimension of the problem and m represents number of discrete velocity vectors in the velocity space. Shapes of various lattices are shown in Fig. 1. for various lattices are given in Table 1.

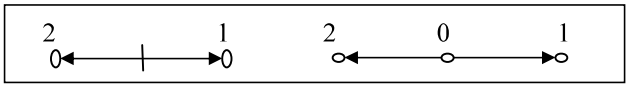

Fig. 1a: D1Q2 *Fig. 1b: D1Q3*

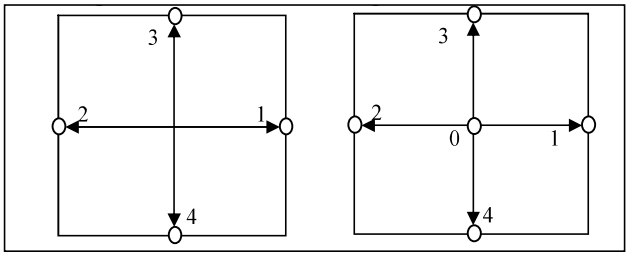

Fig. 1c: D2Q4 *Fig. 1d: D2Q5*

Table 1: for various 1d and 2D lattices,

Lattice	Weights (wi)	"pseudo-sound-speed" (e_s)
D1Q2	1/2 for α = 1 and 2	$e/\sqrt{2}$
D1Q3	4/6 for α = 0 1/6 for α = 1 and 2	$e/\sqrt{3}$
D2Q4	1/4 for α = 1, 2, 3, 4	$e/\sqrt{2}$
D2Q5	2/6 for α = 0 1/6 for α = 1, 2, 3, 4	$e/\sqrt{2}$

Concentration of solute are expresses as the first order moment of the distribution function

$$\mathrm{C}(\vec{\mathrm{r}}, \mathrm{t}) = \sum_{\alpha} f_\alpha(\vec{r}, t) \tag{5}$$

For the 2D ADE given in Eq. (1), equilibrium distribution functions as given in Eq. (4) for a D2Q5 lattice can be written as:

$$\begin{aligned}
\mathrm{f_0^{eq}}(\vec{\mathrm{r}}, \mathrm{t}) &= \frac{2}{6}u(x, y, t)\\
\mathrm{f_1^{eq}}(\vec{\mathrm{r}}, \mathrm{t}) &= \frac{1}{6}u(x, y, t)(1 + 3\beta_x)\\
\mathrm{f_2^{eq}}(\vec{\mathrm{r}}, \mathrm{t}) &= \frac{1}{6}u(x, y, t)(1 + 3\beta_y)\\
\mathrm{f_3^{eq}}(\vec{\mathrm{r}}, \mathrm{t}) &= \frac{1}{6}u(x, y, t)(1 - 3\beta_x)\\
\mathrm{f_4^{eq}}(\vec{\mathrm{r}}, \mathrm{t}) &= \frac{1}{6}u(x, y, t)(1 - 3\beta_y)
\end{aligned} \tag{6}$$

4. Numerical Formulation: Differential Quadrature Method

DQM is numerical technique for solution of differential equations. Historically it was developed

as an analogous to numerical integration technique called numerical quadrature. In numerical quadrature, definite integral is approximated as weighted some of integrand values at a group of points in the domain of integration, similarly in DQM, differentiation of a piecewise continuous function is approximated as weighted some of functional values at certain discrete points in the domain of continuity called nodes. Bellman was the pioneer of DQM and he used the technique to solve differential equations [6]. Since then, the technique has gone through various development works [3, 4]. Mathematically DQM can be written as

$$f_x^{(k)}(x_i) = \left.\frac{\partial^k f(x)}{\partial x^k}\right|_{x=x_i} = \sum_{j=1}^{N} A_{ij}^{(k)} f(x_j) \qquad (7)$$

where x_j are the discrete nodes in the domain at which function values are known, $f(x_j)$ are the function values at these nodes, N is the total number of such nodes, and $A_{ij}^{(k)}$ are the weighting coefficients for the order k^{th} derivative of the function, therefore for a N point DQM, $A_{ij}^{(k)}$ are the elements of a N×N matrix.

Weighting coefficients of DQM are not related to any special problem and only depends on the grid spacing. Hence, most demanding task in DQM is to calculate weighting coefficient matrix for a given discrete nodes. Determination of weighting coefficients is carried out using approximation theory where the function under differentiation is first approximated. Based on the procedure of approximating the function, we have various kind of DQM such as, Polynomial DQM (PDQM) where the function is approximated as a polynomial, Fourier Expansion Base DQM (FDQM) where the function is approximated by a Fourier series expansion etc. Shu et al carried out a detailed study on determination of weighting coefficients. [7]. DQM has been used by researcher to solve Advection-Diffusion Equation [8, 9].

2D ADE as given mathematically in Eq. (1), after approximating time derivative using forward difference and the spatial derivatives using PDQM, can be written as Eq. (8)

$$\frac{u(x_i, y_j, t+\Delta t) - u(x_i, y_j, t)}{\Delta t} = \alpha_x \sum_{\substack{k=1 \\ N_x}}^{N_x} A_{k,j}^{(2)} u(x_k, y_j, t) + \alpha_y \sum_{\substack{k=1 \\ N_y}}^{N_y} B_{i,k}^{(2)} u(x_i, y_k, t) - \beta_x \sum_{k=1} A_{k,j}^{(1)} u(x_k, y_j, t) - \beta_y \sum_{k=1} A_{i,k}^{(1)} u(x_i, y_k, t) \quad (8)$$

where Δt is discrete time step, N_x, N_y are the number of grid points along x and y directions, respectively, A^1, A^2, B^1, B^2 are the weighting coefficient matrices. Simplified form of Eq. (8) can be written as:

$$u(x_i, y_j, t+\Delta t) = u(x_i, y_j, t) + \Delta t \times M_{dqm}$$

where

$$M_{dqm} = \alpha_x \sum_{k=1}^{N_x} A_{k,j}^{(2)} u(x_k, y_j, t) + \alpha_y \sum_{k=1}^{N_y} B_{i,k}^{(2)} u(x_i, y_k, t) - \beta_x \sum_{k=1}^{N_x} A_{k,j}^{(1)} u(x_k, y_j, t) - \beta_y \sum_{k=1}^{N_y} A_{i,k}^{(1)} u(x_i, y_k, t)$$

Elements of the weighting matrixes are calculated using polynomial approach known as PDQM. This approach is also known as Quan and Chang's approach (Quan and Chang 1998a, 1998b, Shu 2000). In this approach, weighting coefficients are written as

$$A_{ij}^{(1)} = \frac{L(x_i)}{(x_i - x_j)L(x_j)}, \quad A_{ii}^{(1)} = -\sum_{j=1}^{N} A_{ij}^{(1)} \quad i \neq j$$

$$A_{ij}^{(2)} = 2A_{ij}^{(1)}\left(A_{ii}^{(1)} - \frac{1}{(x_i - x_j)}\right)$$

$$A_{ii}^{(2)} = -\sum_{j=1}^{N} A_{ij}^{(2)} \quad i \neq j$$

where $L(x_i) = \prod_{j=1}^{N}(x_i - x_j)$, $i \neq j$ is the first derivative of polynomial function of degree N. The locations of grid points can be taken at uniform intervals or non uniform interval. Previous studies reveal that non-uniform mesh from the roots of orthogonal polynomials of functions can greatly enhance the accuracy of the quadrature solution in comparison to uniform mesh. Non-uniform grid points using Chebyshev-Gauss-Lobatto (CGL) grid points can be written as

$$r_i = \frac{1}{2}\left(1 - \cos\frac{i-1}{N-1}\pi\right) \quad i = 1, 2, \ldots, N$$

Uniform grid points can be written as

$$r_i = i * \frac{R}{N-1} \quad i = 0, 1, 2, \qquad \ldots N-1$$

5. Results and Discussions

A study on dependency of numerical stability of the lattice Boltzmann (LB) and differential quadrature (DQ) solutions on Peclet number (*Pe*) is carried out. Peclet number is defined as

$$Pe_x = \frac{\Delta x \times \beta_x}{\alpha_x}, \; Pe_y = \frac{\Delta y \times \beta_y}{\alpha_y}$$

where Pe_x and Pe_y are Peclet numbers along x and y direction, respectively. The simulations are carried out on a domain which ranges from 0 to 1 in both x and y directions using equal lattice length along x and y directions. The various parameters used in the simulations are given in the Table 2.

Table 2: parameters used in the simulation

Sr. No.	Δx=Δy	$\alpha_x = \alpha_y$	$\beta_x = \beta_x$	$Pe_x = Pe_x = Pe$
1	0.1	0.1	0.1	0.1
2	0.2	0.1	0.1	0.2
3	0.05	0.1	1.0	0.5
4	0.1	0.1	1.0	1
5	0.1	0.01	0.1	1
6	0.2	0.01	0.1	2
7	0.2	0.1	1.0	2
8	0.05	0.01	1.0	5
9	0.1	0.01	1.0	10
10	0.2	0.01	1.0	20

Results of the simulations are shown in tabular form in Table 3.

Table 3: stability at various inputs

Sr. No.	Grid Points	$Pe_x = Pe_x = Pe$	Solution	
			LBM	DQM
1	11	0.1	Stable	Stable
2	6	0.2	Stable	Stable
3	21	0.5	Stable	Unstable
4	11	1	Stable	Stable
5	11	1	Stable	Stable
6	6	2	Stable	Stable
7	6	2	Stable	Stable
8	21	5	Stable	Unstable
9	11	10	Stable	Unstable
10	6	20	Stable	Unstable

Graphical contour plots of u(x,y,t) at time t = 1.0 unit for Case 1 are shown in Fig 2.

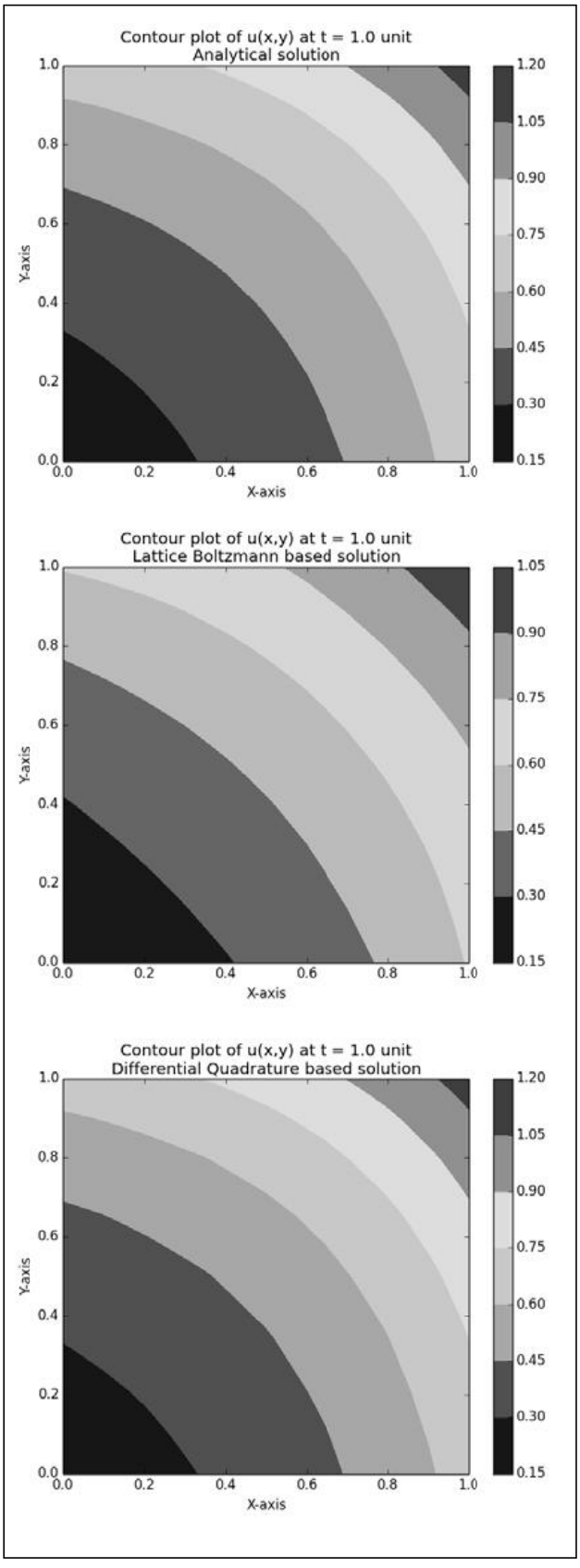

Fig 2: Contour plots of u(x, y, 1) at time 1.0 unit for Case 1.

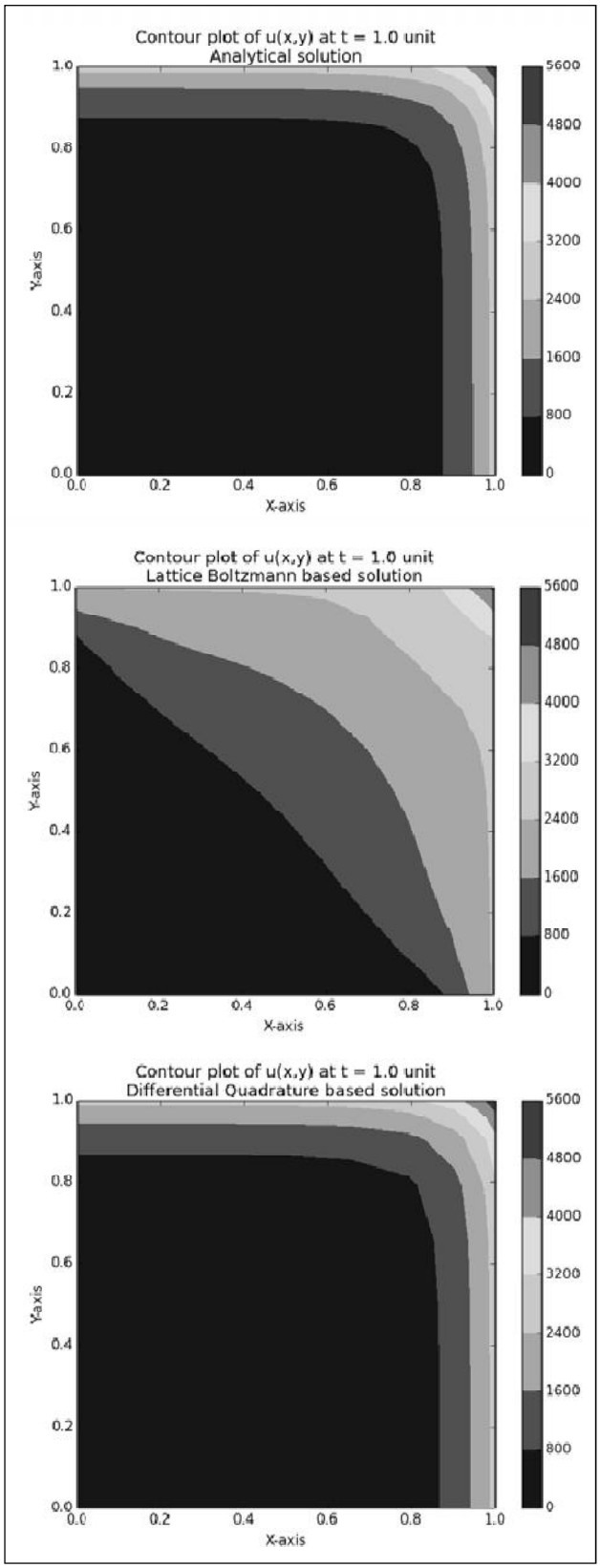

Fig 3: Ccontour plots of u(x,y,t) at time t = 1.0 unit for Case 4

6. Conclusions

The Table 3 shows that stability of LB solutions are better compared to DQ solutions at high Peclet number. From the contour plots, as shown in Fig 2 and Fig 3, we can say that accuracy of DQ solutions is better than LB solution at a particular value of Peclet number.

References

1. Chen S, Doolen GD. Lattice Boltzmann method for fluid flows. Annu Rev Fluid Mech; 1998; 30:329–64.
2. S. Succi. The Lattice Boltzmann Equation for Fluid Dynamics and Beyond. Oxford University Press, New York, 2001.
3. Wolf-Gladrow DA. Lattice-Gas Cellular Automata and Lattice Boltzmann Models: An Introduction. Springer: New York, 2000.
4. J.G. Zhou. A lattice Boltzmann method for solute transport. Int J Numer Meth Fluids, 61 (8) (2008), pp. 848–863.
5. Ginzburg, I.: Equilibrium-type and link-type lattice Boltzmann models for generic advection and anisotropic-dispersion equation. Adv. Water Resour. 28, 1171–1195 (2005)
6. Ginzburg, I.: Truncation errors, exact and heuristic stability analysis of two-relaxation-times lattice Boltzmann schemes for anisotropic advection–diffusion equation. Commun. Comput. Phys. 11, 1439–1502
7. Servan-Camas, B., Tsai, F.T.-C.: Lattice Boltzmann method with two relaxation times for advection–diffusion equation: third order analysis and stability analysis. Adv. Water Resour. 31, 1113–1126 (2008)
8. H. Yoshida, M. Nagaoka, Multiple-relaxation-time lattice Boltzmann model for the convection and anisotropic diffusion equation. J. Comput. Phys., 229 (2010), pp. 7774–7795.
9. R.Z. Huang, H.Y. Wu, A modified multiple-relaxation-time lattice Boltzmann model for convection–diffusion equation. J. Comput. Phys., 274 (2014), pp. 50–63.
10. Perko, J., Patel, R. A.: Single-relaxation-time lattice Boltzmann scheme for advection–diffusion problems with large diffusion-coefficient heterogentities and high-advection transport. Phys. Rev. E 89, 053309 (2014)
11. Janez Perko and Ravi A. Patel, Diffusion velocity lattice Boltzmann formulation applied to transport in macroscopic porous media. Int. J. Mod. Phys. C 25, 1441006 (2014)
12. Zhang, X., Bengough, A.G., Crawford, J.W., Young, I.M.: A lattice BGK model for advection and anisotropic dispersion equation. Adv. Water Resour. 25, 1–8 (2002)
13. Suga, S.: Stability and accuracy of lattice Boltzmann schemes for anisotropic advection–diffusion equations. Int. J. Mod. Phys. C 20, 633–650 (2009)

Life Cycle Reliability and Safety Engineering
Vol.5 Issue 3 (2016) 21-29

Radon in Ground Water and Soil as a Potential Tracer for Uranium Exploration and Earthquake Precursory Studies

B. K. Sahoo* and J. J. Gaware
Radiological Physics & Advisory Division
Bhabha Atomic Research Centre, Mumbai, 400 085
**Email:bijay@barc.gov.in*

Abstract

Radon, produced by radioactive decay of the trace amounts of uranium present in most rock is considered as a natural tracer for uranium exploration and studying earthquake precursory phenomena such as changes of radon concentration due to stress release from earth crust. Radon emitted from rocks containing uranium can partly dissolve and remain in ground water, subject to radioactive decay, until dispensed and aerated. Hence, a measurement of dissolved radon in ground water is a key path finder for uranium deposit. The paper discusses formulation and modeling of radon transport in soil media and its usefulness for interpretation of measured radon data with uranium deposit and stress release from earth crust. Analytical models were derived from basis radon transport theory of porous media considering diffusion as well as advection transport in addition to radon emanation and radioactive decay in the soil pore. Analysis of the model solutions indicates that radon monitoring in sub-soil is more reliable for stress release and earthquake precursory studies than deep soil sampling. On the other hand, radon monitoring in deep soil, preferably in ground water, can be applied for detecting the uranium deposit in certain areas. But it is necessary to measure ^{226}Ra along with radon to compensate the contribution of radon from dissolved ^{226}Ra in the water. The compensated radon activity is the actual indicator of ^{226}Ra and uranium content in rocks at the vicinity of ground water source. Results of two experimental case studies were also presented to validate the above prediction of model.

1. Introduction

Geophysical methods based on radon (^{222}Rn) monitoring have received considerable attention in last few decades for uranium prospecting and studying the earthquake precursory process [1, 2, 3, 5, 6, 10, 12]. ^{222}Rn, the sixth member in the decay series of ^{238}U, is a chemically inert gas and is produced by process of radon emanation from soil grain containing trace amounts of uranium. Radon is considered as a natural tracer for uranium exploration and studying earthquake precursory phenomena such as changes of radon concentration due to pre-seismic stress release from earth crust. Radon emanated from soil grain is transported to atmosphere through porous media of soil. Radon transport in soil pore is mainly governed by two physical processes namely, diffusion and advection (Nazaroff, 1992). [9] Different transport models have been developed to study the anomalous behavior of soil radon in geothermal fields, thermal spas, active faults, volcanic processes and seismo-tectonic environments. [18], [17], [13], [7], [16]

Radon measurement in soil pore has been extensively used in uranium prospecting and exploration, particularly in finding out the extension of the concealed bodies [1] Fleischer and Antonio, 1978; [6][2]. Same time, radon data in soil pore has been used for finding anomalous behavior of radon in relation to earthquake events [3, 5, 12, 10]. The porosity, grain size, and flow velocity of the driving gas affect the monitored concentration of radon in soil gas. In view of this, the correct interpretation of real-time monitored data of radon and its correlation with seismic events requires better understanding of the radon transport process in soil pore and its perturbation during earthquake events.

Radon emitted from rocks containing uranium can partly dissolve and remain in ground water, subject to radioactive decay, until dispensed and aerated. Hence, a measurement of dissolved radon in ground water is a key path finder for uranium deposit. Occasionally presence of dissolved radium in ground water makes problem more complicated for accurate interpretation of radon data in the context of locating

uranium deposit.Generally, it has been demonstrated that methods based on the detection of radon in water are reconnaissance methods and should be used only in the reconnaissance phase of uranium exploration. Methods based on the detection of radon in soil gas have been used in both the reconnaissance and detailed phases of uranium exploration, where they should be integrated into the exploration programme along with other geochemical and geophysical methods. A number of problems attend the collection and interpretation of data from radon surveys. Since these are, to a large extent, geochemical problems, sound knowledge of the geochemical dispension of radon and its precursors must be applied to the problem. The paper discusses formulation and modeling of radon transport in soil media and its usefulness for interpretation of measured radon data with uranium deposit and stress release from earth crust. Results of two experimental case studies were also presented to validate the model hypothesis.

2. Modeling radon transport in soil media

Radon migrates from rocks, ore bodies, soil grains to environment by two fundamental processes (Fig.1). The first stage is emanation from the material and the second is exhalation from the matrix through different transport processes. ([9], [4]) *Emanation* is the process by which radon atom escape from the solid mineral grains to the air-filled pores. *Exhalation* is the process of transport of radongas from air-filled pores to the atmosphere.

Although the detailed processes responsible for radon emanation from grains is not fully understood, it is believed that the main contribution to the emanation comes from the recoil processes. [15] Influence of temperature on radon emanation is relatively small but moisture content has a large impact on it [11]. This is because a radon atom entering a pore that is filled or partially filled with water has a higher probability of being stopped in the pore volume without crossing the pore space and being exhaled out in the atmosphere.

Transport of radon from pore space to the environment takes place mainly by diffusion, and in some cases, because of darcian flow (Advection). There are many external factors that can influence the diffusivity and thereby the exhalation rate. [14] Rainfall, snowfall, freezing and increase in atmospheric pressure results in decrease of exhalation rate, whereas increase in wind speed and temperature can increase it. We have discussed below the formulation of radon transport and its solution to a one dimensional soil media.

2.1. Diffusion Transport

Consider a porous matrix such as soil (Fig 1), in which radon is continuously released to the pore volume of the matrix due to the emanation from the grains containing ^{226}Ra. Let S be the radon activity released into unit volume of the pore space per unit time by the above process. Assuming that radon is transported in the pore volume by the process of diffusion through the pores, one may define a local flux density F_p representing the activity of radon crossing per unit pore area per unit time. Let C_p be the pore space radon concentration (i.e. radon activity / volume of pore space) at any point at a given time. The general diffusion equation is obtained by a limiting process of the time rate of change of radon activity in an infinitesimal pore volume arising due to the difference between the generation rate and losses due to leakage rate and radioactive decay (with decay constant of λ), this is given by:

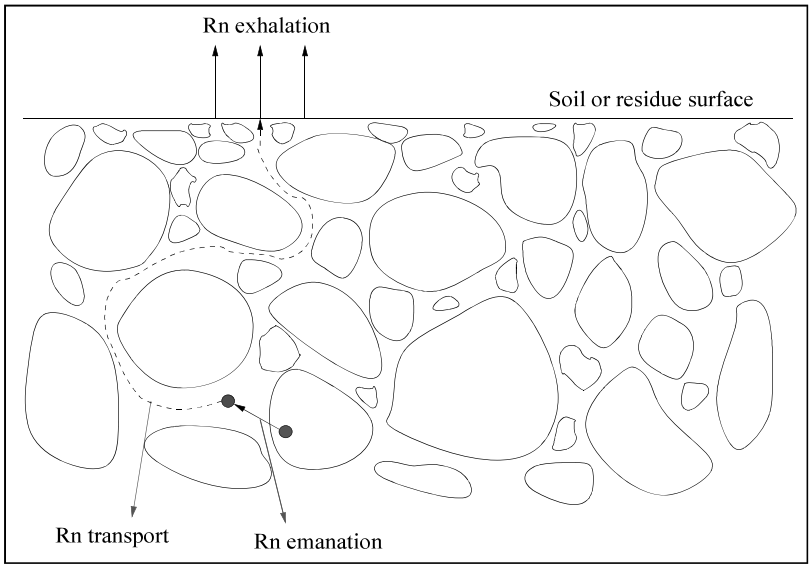

Fig 1: Process of radon generation and transport in porous soil media

$$\frac{\partial C_p}{\partial t} = S - \nabla . F_p - \lambda C_p \qquad (1)$$

In general, F_p is composed of two components (i) pressure driven flux

and (ii) gradient driven diffusive flux. Generally in most situations, the pressure difference sustained between the pore space and the atmosphere is sufficiently small to cause significant pressure induced flux as compared to diffusion driven flux and hence the former is neglected. For a one-dimensional system, the diffusion flux is expressed in terms of the concentration gradient by applying Fick's law of diffusion as follows:

$$F_p = -D\frac{\partial C_p}{\partial z} \tag{2}$$

Where, D is the radon diffusion coefficient in the pore space in the soil matrix. In a strictly dry matrix, it is the product of molecular diffusion coefficient in air (D_M) in the pore space and tortuosity (τ) that accounts for the tortuous path traversed by the radon atoms along the pores. However, in general, soil pore contain moisture and radon atoms will diffuse both in the air and water phases resulting in lowering of the diffusion coefficient (D) in the pore space.

Substitution of Eq.(2) in Eq.(1) yields the following diffusion equation:

$$\frac{\partial C_p}{\partial t} = S + D\frac{\partial^2 C_p}{\partial z^2} - \lambda C_p \tag{3}$$

If R is the radium content of the matrix (i.e. Radium activity in the soil grain / mass of the matrix), ρ is the bulk density of the matrix (i.e. mass of the matrix / bulk volume of the matrix), E is the radon emanation factor from soil grain to pore volume and n_T is the total porosity of the matrix (i.e. total pore volume/ bulk volume), then S can be expressed as:

$$S = \frac{\lambda R \rho E}{n_T} \tag{4}$$

With this, Eq. (3) can be simplified to

$$\frac{\partial C_p}{\partial t} = D\frac{\partial^2 C_p}{\partial z^2} - \lambda C_p + \frac{\lambda R \rho E}{n_T} \tag{5}$$

While the flux F_p above refers to unit pore area, the exhalation flux at the soil surface refers to the bulk area that includes both pore area and the area covered by the solid materials. Upon assuming the fractional pore area at the surface to be the same as the fractional pore volume of the bulk of the soil matrix, the exhalation flux density may be related to the pore space concentration as follows:

$$F = n_T F_p = -n_T D\frac{\partial C_p}{\partial z} \tag{6}$$

In dry soil matrix, the pores will be filled only with air, and hence C_p will be the same as the concentration C_a in pore air. In the case of soil pore containing moisture, the radon atoms in the pore volume will be distributed partly in air and partly in water in proportion to the water/air partition coefficient of radon. It is more convenient to recast the diffusion equation in terms of C_a so as to develop consistent formulations and interface boundary conditions to address multi-layer problem involving covers having different moisture contents and material properties. If C_w ,C_a, denote radon concentration in water and in air and if n_w , n_a are air-filled and water filled porosities respectively, then material conservation requires that:

$$n_T C_p = n_a C_a + n_w C_w \tag{7}$$

The law of equilibrium partitioning relates C_w to C_a as follows:

$$C_w = K.C_a \tag{8}$$

where, K is the water/air partition coefficient. Upon combining Eq.(8) with Eq.(7), one arrive at

$$n_T C_p = C_a(n_a + Kn_w) = n_e.C_a \tag{9}$$

where,

$$n_e = (n_a + Kn_w). \tag{10}$$

The quantity n_e denotes the partition corrected porosity. It may be expressed more conveniently in terms of the volumetric moisture saturation (m), defined as $m=n_w/n_T$, as follows:

$$n_e = n_T\,[1-(1-K)m]. \tag{11}$$

With this, Eq. (5) may be recast in terms of C_a as follows:

$$\frac{\partial C_a}{\partial t} = D\frac{\partial^2 C_a}{\partial z^2} - \lambda C_a + \frac{\lambda R \rho E}{n_e} \tag{12}$$

Under steady state condition, Eq. (12) becomes

$$D\frac{\partial^2 C_a}{\partial z^2} - \lambda C_a + \frac{\lambda R \rho_B E}{n_e} = 0 \tag{13}$$

The corresponding expression for flux is:

$$F = -n_e D \frac{\partial C_a}{\partial z} \tag{14}$$

The formulation of the diffusion equation in terms of radon concentration in the air phase (C_a) and partition corrected porosity (n_e) enables a direct applications to multi-layer problem since both C_a and F will satisfy continuity requirement at the interface of the two layers even if their moisture content and porosities are different from each other. Hence forth, air phase radon concentration (C_a) is simply referred as the radon concentration in soil pore (C)and partition corrected porosity (n_e) is referred as porosity of soil (n). With this, Eq. (14) can be re-expressed as

$$D\frac{\partial^2 C}{\partial z^2} - \lambda C + \lambda \frac{R\rho E}{n} = 0 \tag{15}$$

The boundary conditions applicable to a soil matrix as shown in Fig. 2 may be written as:

$$C(z = -\infty) = R\rho E / n = C_\infty \tag{16}$$

$$C(z = 0) = 0 \tag{17}$$

Eq. (17) implies that once the radon atom reaches the atmosphere, it is immediately transported by the wind fields. Defining the radon diffusion length in soil as

$l = \sqrt{D/\lambda}$,

the solution of this equation may be derived as:

$$C(z) = C_\infty \{1 - \exp(z/l)\} \tag{18}$$

Eq. (18) represents the vertical profile of radon concentration in the soil matrix. The concentration increases exponentially as soil depth increases and after a certain depth (~ 3l) the concentration saturates (Fig. 2).

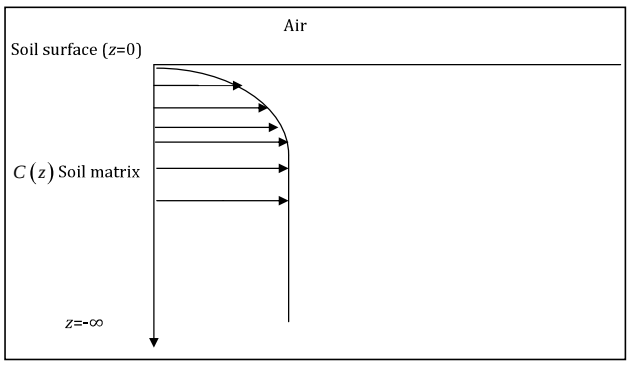

Fig. 2: A schematic of coordinate in a soil matrix and pictorial demonstration of depth profile of radon in soil pore

Similarly the radon flux at the soil surface (F_s) can be estimated as:

$$F_s = -nD\left.\frac{dC(z)}{dz}\right|_{z=0} = \frac{nD}{l}C_\infty = \lambda l R\rho E \tag{19}$$

Eq. (19) indicates that it is necessary to measure the soil parameters such as radium content, radon diffusion length in soil, radon emanation factor and bulk density to estimate the radon exhalation flux from the soil surface.

Another simple way to estimate radon flux density is by using radon mass exhalation rate. The radon mass exhalation rate, J_m(Bq kg^{-1} h^{-1}), is defined as the radon activity released per unit time from unit mass of the matrix. It is generally measured using the closed chamber technique. If the thickness of the sample is far less (~ 10 times) than the radon diffusion length in the matrix, then the radon mass exhalation rate may be considered as the radon production rate in the pore volume of the matrix due to emanation from the grain. Typically, radon diffusion length in soil is about 1 m and samples used for measurement are limited to about 0.1 m. Hence in all practical cases, the measured radon mass exhalation rate from a soil sample may be considered as the radon production rate in the pore volume. Mathematically, it is expressed as:

$$J_m = RE\lambda \tag{20}$$

With this, the formula for radon flux density given in Eq. (19) may be simplified to

$$F_s = J_m \rho l \tag{21}$$

From Eq. (21), it is observed that the major parameter required for computing the radon flux density is the radon mass exhalation rate (J_m) and radon diffusion length in soil (l) and it suggest that radon exhalation from ground is linearly proportional to radon mass exhalation rate of soil sample collected from same location and a X-Y plot between these parameters should yield an y-intercept value of nearly 0. However, in situation where both diffusion and advection transport take place, the X-Y plot may result a non-zero y-intercept. Hence, a significant positive value of y-intercept can be considered as a measure of advection contribution and stress release from earth crust.

2.2. Diffusion-Advection Transport

In addition to diffusion, advection may transfer radon over a wide range of distances, depending on the porosity and velocity of the carrier fluid. Due to this reason, soil gas radon has been established as a powerful tracer used for a variety of purposes, such as exploring uranium ores, locating geothermal resources and hydrocarbon deposits. Eq. (1) may be modified to include the advection process as follows:

$$D\frac{\partial^2 C(z)}{\partial z^2} - u\frac{\partial C(z)}{\partial z} - \lambda C(z) + \lambda C_\infty = 0 \qquad (22)$$

Where u= velocity of carrier gas *(m/s)*

The additional second term represents the loss of radon in the pore space of the soil by the process of advection. The boundary conditions remain unaltered as given by Eqs. (16) and (17).

An analytical steady state solution of Eq (22) is given as

$$C(z) = C_\infty + C_1 e^{\left(\frac{u}{2D}+\sqrt{\frac{u^2}{(2D)^2}+\frac{\lambda}{D}}\right)z} + C_2 e^{-\left(\frac{u}{2D}+\sqrt{\frac{u^2}{(2D)^2}+\frac{\lambda}{D}}\right)z} \qquad (23)$$

Using the boundary conditions, the exact solution of the advection inclusive Eq (23) may be written as

$$C(z) = C_\infty + (C_0 - C_\infty)e^{\left(\frac{u}{2D}+\sqrt{\frac{u^2}{(2D)^2}+\frac{\lambda}{D}}\right)z} \qquad (24)$$

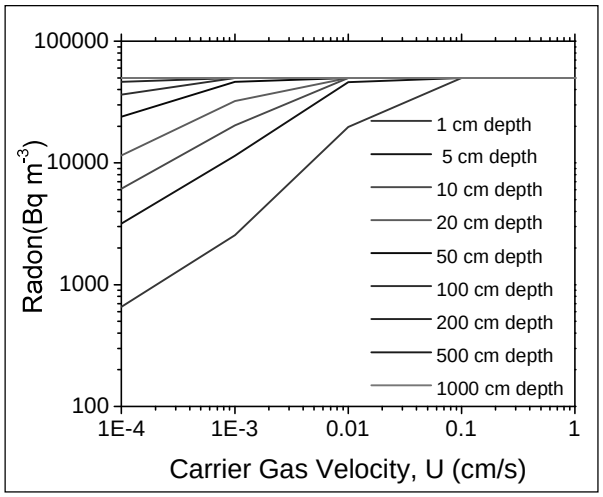

Fig. 3: Perturbation effect of carrier fluid flow on radon concentration in soil pore at different soil depths.

With this model, Let us analyze the effect of velocity of carrier fluid, which may arise from stress release from earth crust, on radon concentration profile in sub soil. Table 1 presents the predicted values of radon concentration in soil pore space at a depth of 0.05 m and 0.1 m without any carrier fluid movement (diffusion transport) and with carrier fluid movement of velocity ranging from 10^{-7} m/s to 10^{-1} m/s. As it can be seen from the table 1, there is a significant perturbation of radon concentration due to movement of carrier fluid as compared to diffusion driven radon profile. Radon concentration increases at a very low velocity of about 10^{-7} m/s for both depths of 0.05 m and 0.1 m but saturates at a velocity of about 10^{-2} m/s for radon concentration at a depth of 0.05 m while it saturates at a less velocity of about 10^{-3} m/s for radon concentration at a depth of 0.1 m.

Fig. 3 gives the plot of perturbed radon concentration against velocity of carrier fluid at soil depth varying from 0.01 m to 10 m. As one can notice, more is the depth of soil, radon concentration saturates at less value of carrier fluid velocity. Beyond a soil depth of 1 m, radon concentration has almost no impact by the carrier gas velocity as it has been pre-saturated by diffusion driven process. These results suggest that for studying the stress release from earth crust via radon perturbation, it is necessary to sample the radon from sub soil rather than deep soil. However, this argument is applicable to a homogeneous soil media where radioactivity distribution is nearly uniform throughout the soil.

Table 1: Radon concentration at a depth of 0.05 m and 0.1 m for various carrier fluid velocities

Velocity of Carrier fluid, u (m/s)	Radon (Bq/m^3) at depth of 0.05 m	Increase of radon from base value (%)	Radon (Bq/ m^3) at a depth of 0.1 m	Increase of radon from base value (%)
0	2448	**0**	4767	**0**
10^{-7}	2505	2	4876	2
10^{-6}	3076	23	5954	22
10^{-5}	10996	257	19568	228
10^{-4}	45383	340	49574	153
10^{-3}	50000	10	50000	1
10^{-2}	50000	0	50000	0
10^{-1}	50000	0	50000	0

Let us consider a case of in- homogeneous soil media having a uranium ore body deposit at certain

depth of soil (say it is more than 2 to 3 times of radon diffusion length in soil). Figure 4 represents a pictorial demonstration of radon concentration profile in a homogeneous soil medium and an in-homogeneous soil medium with uranium deposit and its effect by carrier fluid flow during stress release from earth crust. Comparison between original and perturbed profile of radon in the above two media indicate that there is a definite perturbation of carrier fluid velocity on sub-soil radon concentration in both homogenous and in-homogeneous soil media. This suggests that sub-soil sampling based method is a reliable method for stress release detection and then correlating to earthquake phenomena. On the other hand, there is no definite perturbation of carrier fluid velocity on the deep soil radon concentration. In the case of homogenous soil media, there is no effect of carrier fluid on the original profile of radon concentration while the effect can be positive, negative or neutral depending upon the magnitude of carrier fluid velocity and exact location of sampling point with respect to position of Uranium ore body deposit in the case of in-homogeneous soil media. Hence, deep soil sampling including radon measurement in ground water may not be a reliable method for earthquake precursory study.

Deep soil sampling methods, rather, will be useful for uranium exploration programme. Swallow deposit of uranium ore (within 2-5 m from surface) can be easily established by soil probe radon profiling method in a selected zone which may yield a similar profile of radon as shown in fig 4 in the case of in-homogenous soil media. For finding uranium deposit at deeper level, measurement of radon in ground

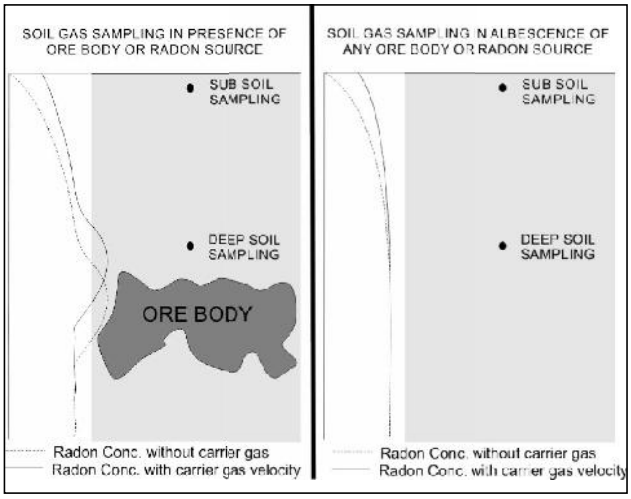

Fig. 4: Pictorial representation of radon concentration profile for soil medium with and without uranium deposit and its effect by carrier gas flow during stress release from earth crust.

water will be a preferable method. It is well known that radon emitted from rocks containing uranium can partly dissolve and remain in ground water, subject to radioactive decay, until dispensed and aerated. Occasionally presence of dissolved radium in ground water makes problem more complicated for accurate correlation of radon with uranium deposit in local rocks. Radium is being very long lived (half life ~1600 yrs) as compared to radon (half life ~3.82 days), ground water containing radium can be transported to a longer distance before its decay. Hence, radon contributed from dissolved radium in water may not be an indicator of uranium deposit in the local rock. In view of this, measurement of total dissolved radon and radium concentration together in ground water (such as water sample from hand pump and bore-well) will be necessary to have a proper correlation analysis of radon with uranium content of rocks in the vicinity of ground water. Continuous monitoring of radon in deep soil pore space or in ground water and analyzing the perturbation of carrier gas flow on radon concentration during stress release from earth crust is a another way of getting information of uranium deposit at much deeper level of soil.

3. Experimental Case Study

Measurements of radon in soil pore, ground water, in-situ radon exhalation from ground and their correlation with radioactivity and exhalation rate of soil samples are some of the techniques, which can be adopted for Uranium exploration and earthquake precursory research programme. Though, some of these methods are already in use but need to be updated or re-designed considering the advances in the radon instrumentations and models. Two case studies were conducted to check the feasibility of proposed radon tracer methods toward application of Uranium exploration and detection of stress release from earth crust and its correlation with earthquake event. Case-1 study was aimed at measurement of radon in ground water at normal and Uranium mineralized zones and studying the relative difference of radon concentration between two locations. Case-2 study was aimed at effect of stress release on the radon concentration in sub-soil of a seismic prone site. Method of measurements and the results obtained is discussed below

3.1. Radon in ground water

Ground water samples were collected from various hand pumps located in a Uranium mineralized

zone and a normal region to measure the dissolved radon content in the water samples. Water samples were collected in a leak tight sampling glass bottle (capacity 60 ml). While sampling into the bottle, caution was taken to avoid formation of bubble/ agitation in the water sample. This was carried out by gently transferring the sample by putting one end of a sampling tube inside the hand pump and other end put at the bottom of the sampling bottle held in a water bucket. The bottles was filled completely and the volume in bottle replaced 4 to 5 times with the water sample without leaving any air volume, and close tightly inside the water medium of the bucket to avoid any leakage. Radon bubbling method using a continuous radon monitor (Smart RnDuo, BARC, Mumbai) [4] was used for measurement of radon in the water sample. The monitor is based on detection of alphas emitted from sampled radon and its decay products in a scintillation cell (ZnS:Ag) . Air is sampled into the scintillation cell (153 cc) through a "progeny filter" and "Pinhole plate" eliminating progenies and thoron (^{220}Rn). The "diffusion-time delay" given by pinhole plate does not allow the short lived thoron (^{220}Rn, half- life 55.6 sec) to pass through them acting as "thoron barrier". The alpha scintillations from radon and its decay products formed inside the cell are continuously counted for a user-programmable counting interval by the Photo Multiplier Tube and the associated counting electronics. The alpha counts obtained are processed by a microprocessor unit built with a smart algorithm to display the concentration of radon and other related parameters.

A schematic diagram of the experimental set up is shown in Fig.5. Measurements were carried out at the site immediate after sampling (within 30 minutes) to avoid any decay of radon in the sample. Sampling bottle containing the water sample was gently fitted to the water bubble as shown in fig. 5 after ensuring the correct connection of the monitoring system with water bubbler. Pump of the measurement system was kept on for initial 2-3 minutes before measurement so that by the process of bubbling, dissolved radon in the water bottle is transferred to the scintillation chamber of the measurement system. Measurements were made in 15 minute cycle interval for about one hour to get a representative value of radon in the water sample. The radon concentration in water ($C_{w,}$ Bq/L) was estimated from the measured radon concentration (C_{air}, Bq/m^3) as follow [19]

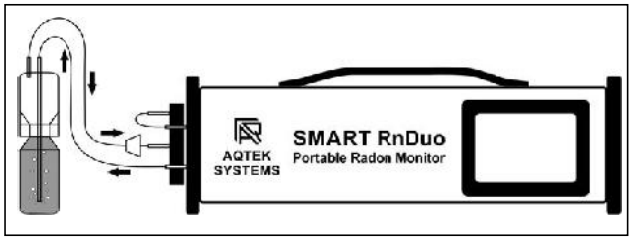

Fig. 5: Set-up for measurement of radon in water sample

$$C_w = \frac{C_{air}}{1000}\left(K + \frac{V_{air}}{V_{w,}} \right) \quad (25)$$

Where K is partition coefficient of radon in liquid with respect to air (=0.25 for water), V_{air} is volume of air enclosed in the closed loop setup (m^3) (Bubbler volume + tubings volume + detector volume) and V_w is volume of water in sampling bottle (m^3).

The estimated C_w may have two components i.e one is the contribution from dissolved ^{226}Ra in the water sample and other is the actual dissolved fraction of radon emitted from rocks in the vicinity of ground water source. The former, sometime, is referred as the supported radon fraction (C_{ws}) while the later is referred as the unsupported radon fraction (C_{wu}). The unsupported radon activity, which is the indicator of uranium content in the rock, was estimated by subtracting the measured ^{226}Ra concentration in the water, assumed to be equilibrium with supported radon activity (C_{ws}). The ^{226}Ra concentration of the water sample was analyzed by the standard radon emanometry method which is discussed elsewhere [8]

Table 2 provides the results of total dissolved radon, ^{226}Ra and unsupported radon activity concentration of the ground water samples collected from Uranium mineralized zone and normal zone of the survey region. Table 2 clearly indicates that there is an elevated level of radon concentration in ground water samples collected from Uranium mineralized zone as compared to normal regions. This proves the hypothesis that higher level of radon in ground water is an indicator of Uranium deposit in the region. Hence, the method can be applied to unknown regions to get the information of Uranium deposit from the measured level of radon concentration in ground water samples.

3.2 Radon monitoring in sub-soil of a seismic fault region

As predicted by model, Radon monitoring in sub-soil will be more reliable to detect the stress release from earth crust as compared to deep soil sampling. A very low carrier gas velocity (~ µm/s) due to pre-

Table 2: Results of total dissolved radon, 226Ra and unsupported radon activity concentration of the ground water samples collected from Uranium mineralized zone and normal zone of the survey region.

Sample no	Uranium Mineralised Zone			Normal Zone		
	C_w (Bq/L)	C_{Ra}(mBq/L)	C_{wu}(Bq/L)	C_w(Bq/L)	C_{Ra}(mBq/L)	C_{wu}(Bq/L)
1	483±4	240	483	10.5±0.7	13±6	10.5
2	526±5	322	526	8.2±0.5	12±5	8.2
3	763±6	385	763	9.6±0.6	11±5	9.6
4	645±6	367	645	8.6±0.5	15±6	8.6
5	586±5	295	586	11.2±0.7	16±7	11.2
Average±SD	601±109	322±58	600±109	9.6±1.3	13±2	9.6±1.3

seismic stress release can result in very significant changes in radon concentration at sub soil level. To validate this hypothesis, a soil gas radon monitoring station was established near a seismic fault region. The experimental set up for in-situ measurement of radon in soil gas is shown in fig.6. Soil probe was inserted to a depth of 10 cm of the soil matrix. Sampling tube were connected in a recirculation loop manner as shown in the fig 6 between soil probe and a continuous radon monitor (Smart RnDuo, BARC, Mumbai) for sampling and measurements. Monitor was operated in a 15 minute cycle interval. In this 15 minute cycle, sampling was carried out automatically by pump of the monitor for only initial 5 minutes and hence counts obtained during initial 5 minutes will be a measure of both radon and thoron. Subsequently, there was an intentional delay of 5 minutes to ensure decay of thoron atom (half life 55.6 s) in the scintillation

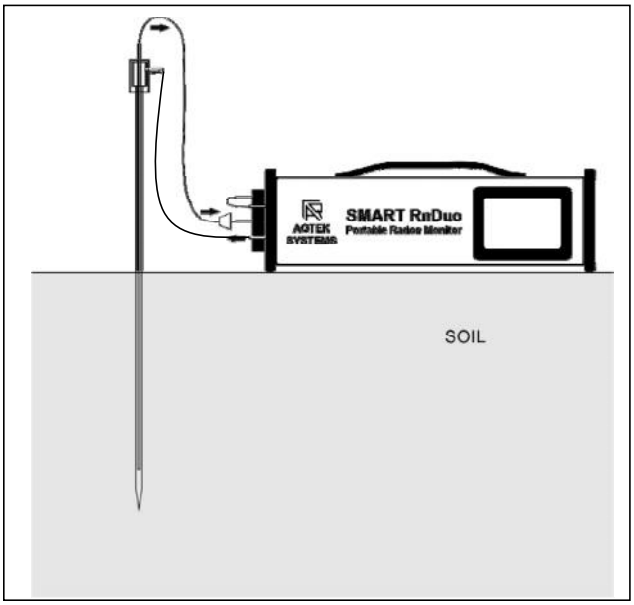

Fig.6: Set-up for continuous monitoring of radon in sub-soil pore space

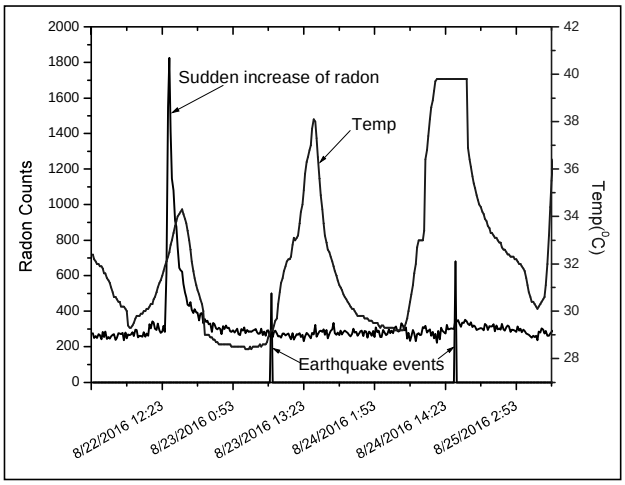

Fig.7: Effect of pre-seismic stress release on the radon concentration in sub-soil

chamber and further counting for another 5 minutes will give the counts due to radon. At end of each 15 minutes cycle, both radon and thoron counts were recorded by the monitor.

Fig. 7 shows the plot of measured radon counts and environmental temperature with Indian Standard Time (IST). Two earthquake events of magnitude 5.0 and 6.8 were taken place on 23/08/2016 7:41 and 24/08/2016 16:04 within the Indian tectonic plate boundary at Myanmar during the investigation period is also indicated in the fig 7. As one can notice, there was a sudden increase of radon concentration prior to these earthquake events. Correlation with environmental temperature suggests that this sudden increase of radon cannot be attributed to diurnal variation of temperature. However, this can be a result of pre-seismic stress release prior to these earthquakes. But more data from multiple locations need to be gathered to prove such hypothesis. The preliminary investigations suggest that radon monitoring in sub -soil in certain well planned locations in form of a network could be more reliable to study the pre-

seismic stress behavior in the earth crust and possibly the prediction of earthquake.

4. Conclusion

Analytical models were derived from basis radon transport theory of porous media considering diffusion as well as advection transport in addition to radon emanation and radioactive decay in the soil pore. Analysis of the model solutions indicates that radon monitoring in sub-soil is more reliable for stress release and earthquake precursory studies than deep soil sampling. Pre-seismic stress release could be easily captured in sub soil monitoring as demonstrated in the experimental case study. Sub-soil radon monitoring at several places in form of a network could be more reliable to study the pre-seismic stress behavior in the earth crust which may be useful to track the locations of stress build up and the direction of pressure wave propagation before the earthquake event.

On the other hand, radon monitoring in deep soil preferably in ground water can be used for detecting the uranium deposit in certain areas. Experimental case study carried out in this work suggest that radon level in ground water samples collected from a uranium mineralized zone was substantially high as compared to samples collected from normal region. But it is necessary to measure ^{226}Ra along with radon to compensate the contribution of radon from dissolved ^{226}Ra in the water. The compensated radon activity is the actual indicator of ^{226}Ra and uranium content in rocks presents in the vicinity of ground water source and hence, this quantity must be estimated for the purpose of uranium exploration.

Acknowledgement:

Authors would like to thank Dr. B.K. Sapra, Head, Environmental and Bio-Dosimetry Section, Dr. D. Datta, Head, Radiological Physics and Advisory Division and Dr. K.S. Pardeepkumar, Associate Director, Health, Safety and Environment Group of Bhabha Atomic Research Centre, Mumbai for their encouragements and supports.

References

1. Alekseev V.V., Grammckou A.G., Tafeev G.P. (1959). Radiometric methods in the Prospecting and Exploration of Uranium Ores. Translation Series USAEC-3730, Book 2.
2. Durrance Eric Michael (1986). Radioactivity in Geology. Principle and Application. Pub Ellis Hoorwool Ltd Eng., 403
3. Fleischer RL (1981) Dislocation model for radon response to distant earthquakes. Geophys Res Lett 8: 477-480.
4. Gaware J.J., Sahoo B.K., Sapra B.K., Mayya Y.S., 2011. Development of online radon and thoron monitoring systems for occupation and general environments.BARC News Letter. Issue No: 318, 45 -51.
5. Ghosh D, Deb A, Dutta S, Sengupta R, Samanta S (2012) Multifractality of radon concentration fluctuation in earthquake related signal. Fractals 20: 33-39.
6. Hambleton-Jones B.B., and Smit M.C.B., 1980 ROAC- A new dimension in radon prospecting.
7. Holford, D. J., Schery, S. D., Wilson, J. L., and Phillips, F. M. (1993). Modeling radon transport in dry, cracked soil. Journal of Geophysical Research Solid Earth, 98(B1),567-580.
8. Maharana M., Eappen K.P., Sengupta D., (2010).Radon emanometric technique for ^{226}Ra estimation. Journal of Radioanalytical and Nuclear Chemistry 285(3): 469-474
9. Nazaroff, W.W., 1992. Radon transport from soil to air.,Rev. GEophys., 30, 137 – 160.
10. Oh, Y. and Kim, G. A radon-thoron isotope pair as a reliable earthquake precursor. *Sci. Rep.* **5**, 13084; doi: 10.1038/ srep13084 (2015).
11. Peter Bossew., 2003. The radon emanation power of building materials, soils and rocks., Applied Radiation and Isotopes., 59, 389 – 392.
12. Petraki E, Nikolopoulos D, Panagiotaras D, Cantzos D, Yannakopoulos P, et al. (2015) Radon-222: A Potential Short-Term Earthquake Precursor. J Earth Sci Clim Change 6: 282. doi:10.4172/2157-7617.1000282
13. Rogers V. C. and Nielson K. K., (1991). Multiphase radon generation and transport in porous material, Health Phys. 60(6), 807–815.
14. Sahoo B.K., Mayya Y.S., (2010). Two dimensional diffusion theory of trace gas buildup in soil chambers for flux measurements. Agric. and Forest Meteorol, 150, 1211-1224.
15. Sahoo B.K., Nathwani D., Eappen K.P., RamachandranT.V., Gaware J.J., MayyaY.S.,(2007).Estimation of radon emanation factor in Indian building materials., Rad. Meas. 42,1422-1425.
16. Sahoo B.K., Mayya Y.S, Sapra B.K., Gaware J.J. Banerjee K.S. and Kushwaha, H.S., 2010 Radon exhalation studies in an Indian Uranium tailings pile, Radiation Measurements, 45, pp. 237-241.
17. Schery, S. D., Holford, D. J., Wilson, J. L., and Phillips, F. M. (1988). The flow an diffusion of radon isotopes in fractured porous media Part 2, Semi-infinite media. Radiation Protection Dosimetry, 24(1-4), 191-197.
18. Tanner A.B., (1966). Radon migration in the ground, a review, Natural Radiation Environment, Ed Adams and Lowder.
19. TirumaleshKeesari, Hemant V., Mohokar , BK Sahoo, G. Mallesh. 2014. Assessment of environmental radioactive elements in groundwater in parts of Nalgonda district, Andhra Pradesh, South India using scintillation detection methods. J RadioanalNuclChem 302:1391–1398

Life Cycle Reliability and Safety Engineering
Vol.5 Issue 3 (2016) 30-40

Impact of Linguistic Proposition of Weather Stability in Gaussian Plume Model

Subrata Bera, A. J. Gaikwad

Nuclear Safety Analysis Division, Atomic Energy Regulatory Board, Mumbai-400094, India
Email: sbera@aerb.gov.in

Abstract

Conventional method to estimate the concentration of air pollution uses crisp/precise input meteorological parameters in Gaussian plume model. In general, identification of weather class (Class A to Class F) as per Pasquill Gifford definition is based on linguistic preposition for combined variation of wind speed and solar radiation. Decimal weather class in the scale of 6, instead of Pasquill-Gifford class, has been developed using soft computing for detailed representation of weather stability class and enhancement of empirical formulae of coefficient of dispersion. In the decimal weather stability class, weight fraction of composite weather class has also been estimated. The empirical formulae for composite weather class have also been developed and used for atmospheric dispersion calculation using Gaussian plume model. Interval arithmetic with fuzzy alpha-cut technique has been developed to carry out classical arithmetic operations for imprecise variables. The tracking of all interim parameters arisen during evaluation of Gaussian plume function has been carried out to get the information on transformation of membership function due to various Fuzzy arithmetic operations. The effect of composite weather stability class on pollutant concentration reduction factor has been analyzed. The variation of concentration reduction factor with downwind distances has been estimated for various composite weather stability classes. The uncertainty in concentration reduction factor arisen due to the imprecise parameters has also been estimated.

Keywords: Soft computing, Fuzzy set theory, Atmospheric dispersion, decimal weather stability class, Interval arithmetic, Uncertainty

1 Introduction

Quantification of pollution content in the atmosphere, in general, is being carried out using precise inputs related to meteorological, demographical and topographical data to the various atmospheric dispersion models such as Gaussian plume model, Gaussian puff model, Lagrangian particle model, etc [1]. All the models need details correlation formulae for the coefficient of dispersion along the transverse and vertical direction to transport pollutant from the source. Safety Guide of Atomic Energy Regulatory Board (AERB) [2] has suggested weather stability class based correlation formulae, which are to be used for atmospheric dispersion calculation. However, the definition of the weather stability class is imprecise in the sense that boundary region may have combined effect of more than one class[2]. Apart from the weather class, the meteorological data containing wind speed, solar radiation may have uncertainty due to the measurement error that lead to impreciseness on input data. Hard computing, which is based on the concept of precise modeling and analyzing to yield accurate result, do not tolerant to imprecision, uncertainty, partial truth and assumption. However, soft computing is an approach to deal with imprecise data or modeling. It is a computationally intelligent technique, which posses' human like expertise. It can adapt to the changing environment and can learn to do better. Fuzzy Logic is one of the soft computing platforms. The Fuzzy Set Theory (FST) was first introduced by Zadeh (1965). FST deals with imprecise variable with suitable Membership Functions (MFs), which are the key element in FST. Imprecise variables may have various types of MFs such as Triangular, Trapezoidal, single sided Trapezoidal, Gaussian, sigmoid etc. Various aspect of FST has been discussed by Timothy J. Ross [3]. Various attempts were made to employ FST in atmospheric dispersion modeling to quantify weather stability class with combined variation of wind speed and cloud cover [4, 5], and non-probabilistic sensitivity and uncertainty in

atmospheric dispersion calculation [6]. In this paper, it is attempted to develop decimal weather stability class (WSC) in the scale of 6 with combined variation of wind speed and solar radiation. The important element for Gaussian plume model is the coefficient of dispersion in transverse and vertical direction. Coefficient of dispersion is strongly dependent on WSC. In the new decimal WSC, weather class is composed of any number of basic Pasquill Gifford (PG) weather classes (i.e. Class-A, class-B, Class-C, Class-D, Class-E and Class-F) with weighting factor. The empirical formulation for coefficient of dispersion has been estimated using weighting factor of composite weather class. The composite weather stability class has been used for atmospheric dispersion analyses. The estimation of air pollution concentration through Gaussian plume model requires many classical mathematical operations. In the FST, classical mathematical operation is not valid. Equivalent mathematical operation in FST has been developed using fuzzy interval techniques with α-cut [7,8,9,10]. These fuzzy arithmetic operations have been used during evaluation of Gaussian Plume Function (GPF). Tracking of all interim parameter generated during various fuzzy arithmetic operations has been made in this analysis. Input parameters in the Gaussian plume model are imprecise in the sense that their spread is around the most likely value and this enforces the fuzzy analyst to consider them as a triangular fuzzy membership function. Triangular membership functions for imprecise parameters have been considered in this analysis. The variation of concentration reduction with downwind distance has been estimated for various decimal classes. Equivalent classical value of concentration reduction factor along with various uncertainty ranges can be found out using estimation of prototype value and various quartile sets. The value of prototype is being estimated using triangular membership function with α-cut equal to 1.0. Deviation from prototype value also estimated by upper quartile set, middle quartile set, lower quartile set and support set by alpha cut technique on membership function. Sensitivity of input parameters also evaluated using Hartley-like measure. Lowest Hartley-like measure corresponds to the most sensitive parameter.

2 Atmospheric Dispersion Modeling with Gaussian Plume Model

Many formulae for atmospheric dispersion estimation to take into account various conditions such as ground level release, ground level concentration and elevated release, centre line ground level concentration, etc have been prescribed in AERB safety document [2]. For simplicity, the formula corresponding to the centre line ground level concentration has been used to demonstrate the effect of composite weather stability class on concentration reduction factor of pollutant and given in the Equation 1.

$$c(x,0,0) = \frac{Q}{\pi u s_y s_z} exp\left(-\frac{H^2}{2s_z^2}\right) \quad (1)$$

where C is steady state concentration of the effluent (x,0,0) (Bq/m3); Q is source strength (Bq/sec); u: mean wind speed (m/sec); S_y=cross wind dispersion parameter (m); S_z=vertical dispersion parameter (m); H=effective stack height (stack height + plume rise)

Under neutral condition plume rise = $3D_i\left(\frac{w}{u}\right)$

where, D_i is Stack Internal diameter (m); w is plume exit velocity (m/s)

Dispersion coefficients S_y, S_z depend on the atmospheric stability class and increase with downwind distance. AERB safety document [2] has suggested formulae for dispersion coefficients, which are given below

$$S_y = A_y x^{0.9031} \quad \& \quad S_z = A_z x^q + R \quad (2)$$

where, the value of downwind distance (x) is units of meter. The parameters are used in the Equation 2 are strongly depended on WSC. For the various WSC, the values of these parameters are given in the Table 1.

Table 1 P-G Model parameters

Pasquill type	Ay	X<0.1 km			0.1 km <x<1.0 km			x>1.0 km		
		Az	q	R	Az	q	R	Az	q	R
A	0.3658	0.192	0.936	0	0.00066	1.941	9.27	0.00024	2.094	-9.6
B	0.2751	0.156	0.922	0	0.038	1.149	3.3	0.055	1.098	2.0
C	0.2089	0.116	0.905	0	0.113	0.911	0	0.113	9.11	0.0
D	0.1471	0.079	0.881	0	0.222	0.725	-1.7	1.26	0.516	-13.0
E	0.1046	0.063	0.871	0	0.211	0.678	-1.3	6.73	0.305	-34.0
F	0.0722	0.053	0.814	0	0.086	0.74	-0.35	18.05	0.18	-48.6

Definition of weather stability class is needed for selection of WSC during the calculation of coefficient of dispersion. Weather stability class is decided by the combination of wind speed and solar radiation. With the variation of wind speed and solar radiation, a look-up table for weather stability class has been given in the Table 2.

Table 2 Modified stability classification table

Wind speed u (m/s)	Stability Class			
	Solar Insolation RD(langley/h) during day			
	Rd>= 50	25<= Rd<50	12.5<= Rd<25	Rd<12.5
U<2.0	A	A-B	B	D
2<=u<3	A-B	B	C	D
3<=u<4	B	B-C	C	D
4<=u<6	C	C-D	D	D
u>=6	C	D	D	D

From the Table 2, it is found that weather stability class is not precisely defined in some combination of wind speed and solar radiation. In those combinations of wind speed and solar radiation, weather stability class has to be selected one class out of two classes. Apart from this imprecision, it is also found that there may be combination of adjacent classes at the boundary, which is to be considered for atmospheric dispersion calculation. To deal with that impreciseness of definition of weather stability class, it is required to employ soft computing for development of decimal weather stability class instead of single weather stability class. In this work, fuzzy logic based soft computing has been used to deal with imprecise data and model.

3. Fuzzy Set Theory

In this section, fuzzy mathematics including fuzzy membership function, interval arithmetic with α-cut techniques, and arithmetic operation on fuzzy variables will be discussed. In the classical set theory, mathematical operation performs on crisp data. However, fuzzy set theory deals with imprecise data or uncertain data. The degree of impreciseness is defined by membership function with the scale of 0 to 1. Various types of membership functions such as triangular, trapezoidal, Gaussian, sigmoid, etc are used in the fuzzy set theory. In the atmospheric dispersion calculation, arithmetic operations such as addition, subtraction, multiplication and division are needed to evaluate the Gaussian plume function as given in equation 1. In the development of fuzzy arithmetic, triangular membership function with interval arithmetic has been used. A graphical representation of a fuzzy variable (X) with triangular membership function has been shown in the Figure 1. Base of the triangle (l-m-r) is known as support of the fuzzy variable X. In the interval notation fuzzy variable can be represented as [l, m, r]. It means that the value of the membership function at middle point(i.e m) is unity, however, zero at both left boundary (i.e. l) and right boundary(i.e. r). The value of membership function decides the degree of impreciseness. The value of membership function equal to unity represents the crisp (or precise) value of the fuzzy variable X. The degree of impreciseness increases when the value of membership function decreases from unity. It becomes maximum at the support of the fuzzy variable X. The methodology used for definition of imprecise variable with fuzzy membership function is known as fuzzification.

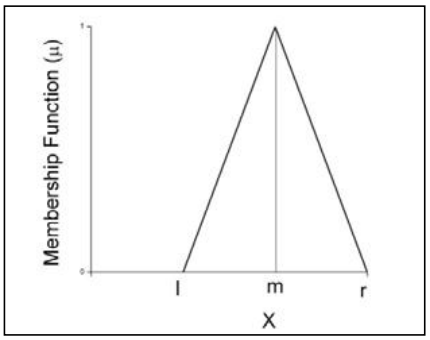

Figure 1 Fuzzy variable with triangular membership function

Mathematical formulation of a fuzzy variable with triangular membership function bounded in the interval [l, m, r] is given in the equation (3)

$$\mu_X(x) = \begin{cases} \frac{x-l}{m-l} & , l \le x \le m \\ \frac{r-x}{r-m} & , \ m \le x \le r \end{cases}$$

Any mathematical expression involving fuzzy variables requires equivalent arithmetic operations with fuzzy variable to obtain its functional value. Arithmetic operations may be addition, subtraction, multiplication, division, polynomial form, logarithmic, exponential, etc. In this paper, equivalent fuzzy arithmetic operation has been demonstrated with combination of fuzzy alpha-cut techniques and principle of interval arithmetic.

Fuzzy alpha-cut techniques:

Given a fuzzy set A in X and any real number alpha $\alpha \in [0,1]$, then α-cut or α-level or cut worthy of A denoted by ${}^{\alpha}A = \{x \in X : \mu_A(x) \ge \alpha\}$

For a fuzzy variable X with triangular membership function in the interval [a, b, c], α-cut interval can be represented and defined as

$$^{\alpha}X = [a + (b-1)\alpha, c - (c-b)\alpha] \quad (4)$$

Interval arithmetic:

For close intervals, let define two intervals A and B in the following manner.

A=[a1, a2]

B=[b1, b2]

Then rule of interval arithmetic is given for following arithmetic operations:

1. Addition: A+B=[a1+b1, a2+b2]
2. Subtraction: A-B=[a1-b2,a2-b1]
3. Multiplication: A.B=[Min(a1b1,a1b2,a2b1,a2b2),Max(a1b1,a1b2,a2b1,a2b2)]
4. Division: A/B=[Min(a1/b1,a1/b2,a2/b1,a2/b2),Max(a1/b1,a1/b2,a2/b1,a2/b2)] If B/=0

Equivalent fuzzy arithmetic operation:

Let X and Y are fuzzy variable with triangular membership function in the interval [a, b, c] and [p, q, r] respectively. Hence

$$\mu_X(x) = \begin{cases} \frac{x-a}{b-a} & , a \le x \le b \\ \frac{c-x}{c-b} & , \ b \le x \le c \end{cases} \quad (5)$$

$$\mu_Y(x) = \begin{cases} \frac{x-p}{q-p} & , p \le x \le q \\ \frac{r-x}{r-q} & , \ q \le x \le r \end{cases} \quad (6)$$

Then α-cut value of X and Y are defined as

$$^{\alpha}X = [a + (b-a)\alpha, c - (c-b)\alpha] \quad (7)$$

$$^{\alpha}Y = [p + (q-p)\alpha, r - (r-q)\alpha] \quad (8)$$

Addition of X and Y:

In the addition operation, the interval arithmetic with α-cut value has been used to get resultant membership function and modified interval. The final membership function is given below.

$$\mu_{X+Y}(x) = \begin{cases} \frac{x-(a+p)}{(b+q)-(a+p)} & , (a+p) \le x \le (b+q) \\ \frac{(c+r)-x}{(c+r)-(b+q)} & , \ (b+q) \le x \le (c+r) \end{cases}$$

Similarly, final membership functions for other mathematical operations are given below.

Subtraction:

$$\mu_{X-Y}(x) = \begin{cases} \frac{x-(a-r)}{(b-q)-(a-r)} & , (a-r) \le x \le (b-q) \\ \frac{(c-p)-x}{(c-p)-(b-q)} & , (b-q) \le x \le (c-p) \end{cases}$$

Multiplication:

Let A=(b-a)(q-p)

B=p(b-a)+a(q-p)

C=ap-x

P=(c-b)(r-q)

Q=r(c-b)+c(r-q)

R=cr-x

Then

$$\mu_{X\times Y}(x) = \begin{cases} \frac{-B+\sqrt{B^2-4AC}}{2A} & , (ap) \le x \le (bq) \\ \frac{-Q-\sqrt{Q^2-4PR}}{2P} & , (bq) \le x \le (cr) \end{cases} \quad (11)$$

Division:

$$\mu_{\frac{X}{Y}}(x) = \begin{cases} \frac{xr-a}{(b-a)+(q-p)x} & , \left(\frac{a}{r}\right) \le x \le \left(\frac{b}{q}\right) \\ \frac{c-px}{(c-b)-(q-p)x} & , \left(\frac{b}{q}\right) \le x \le \left(\frac{c}{p}\right) \end{cases} \quad (12)$$

Exponential:

$$\mu_{EXP(X)}(x) = \begin{cases} \frac{\ln(x)-a}{(b-a)} & , EXP(a) \le x \le EXP(b) \\ \frac{c-\ln(x)}{(c-b)} & , EXP(b) \le x \le EXP(c) \end{cases} \quad (13)$$

Logical operation of Fuzzy variables

$$Union: \ \mu_{X\cup Y}(x) = Max(\mu_X, \mu_Y) \quad (14)$$

$$Intersection: \ \mu_{X\cap Y}(x) = Min(\mu_X, \mu_Y) \quad (15)$$

$$Compement: \mu_{\bar{X}}(x) = 1 - \mu_X \quad (16)$$

4 Fuzzy Inference Engine

Let A and B are two universe of discourse of fuzzy sets having m and n number of elements respectively, then A and B can be represented as

$$A = \{\emptyset, \{A_1\}, \{A_2\}, \dots, \{A_m\}\} \quad (17)$$

$$B = \{\emptyset, \{B_1\}, \{B_2\}, \dots, \{B_n\}\} \quad (18)$$

If C is the another universe of discourse having r number of elements and represented as

$$C = \{\emptyset, \{C_1\}, \{C_2\}, \dots, \{C_r\}\} \tag{19}$$

As fuzzy inference system is the way of mapping input space to an output space using fuzzy logic, the output variable C can be formulated using various combination of A and B. In a mathematical formulation, Fuzzy inference rule base can be represented as

$$\text{IF}\{(A=\{A_i\}).\text{AND}.(B=\{B_j\})\text{THEN}\{C=\{C_k\}\} \tag{20}$$

where i, j and k can varied from 1 to m, n and r respectively. The total number of rules can be formed is m times n. Selection of C_k is based on the judgment.

Fuzzy relation between two set (Binary Relationship) can be represented by Relation matrix or Sagittal diagram. In general Cartesian product techniques are used to obtain fuzzy relationship. If the product of two fuzzy variables X, Y produces another fuzzy variable R then R(x,y)=X(x) x Y(y). membership function of R is represented by

$$\mu_R(x,y) = \mu_{X\times Y}(x,y) = Min\big(\mu_X(x), \mu_Y(y)\big) \tag{21}$$

Let us take example for demonstration of relation matrix and Sagittal diagram. If universe of discourse of fuzzy set X and Y represented by X={1,2,3} and Y={a,b,c} then the maximum possible binary relationship formation has been shown in Figure 2 in the form of Sagittal diagram. In the sagittal diagram line represents the existing binary relationship.

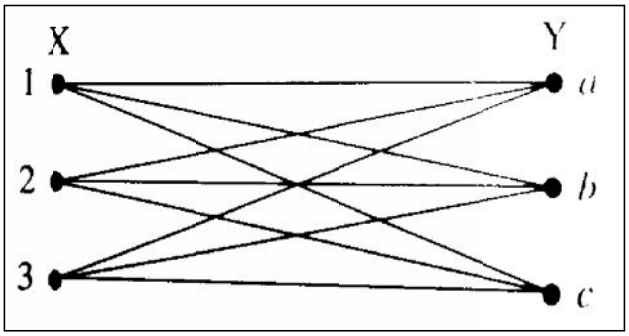

Figure 2 Sagittal diagram to represent binary relationship

The relation matrix representation of the Sagittal diagram has been given below.

$$R = \begin{matrix} \\ 1 \\ 2 \\ 3 \end{matrix} \begin{matrix} a & b & c \end{matrix} \begin{bmatrix} 1 & 1 & 1 \\ 1 & 1 & 1 \\ 1 & 1 & 1 \end{bmatrix} \tag{22}$$

In the relation matrix, unity represents the existing binary relationship.

If A belongs to its more than one element than aggregation operator has to be used to obtain the crisp value of C, this method is also known as defuzzification.

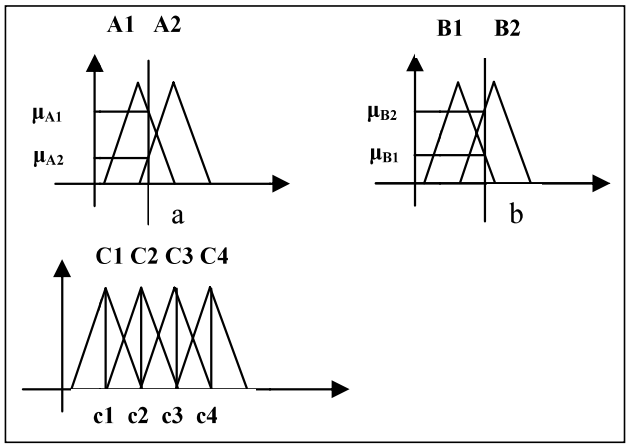

Figure 3 Universe of discourse of A, B and C

Let us take an example to demonstrate the defuzzification methodologies with two fuzzy variables having two elements with triangular membership function. These are A = {A1, A2} and B={B1, B2}. One output variable is considered whose universe of discourse having 4 elements (such as C1, C2, C3, C4)

Fuzzy Interface rule base:

IF(A=A1.AND.B=B1) THEN C=C1

IF(A=A1.AND.B=B2) THEN C=C2

IF(A=A2.AND.B=B1) THEN C=C3

IF(A=A2.AND.B=B2) THEN C=C4

For the defuzzification,

For a particular value of A (say a), there will be two membership function values due to the fact that line A=a is passing through two elements.

Let weighting factors defined as

$$W_1 = \frac{\min\left(\mu_{A1}, \mu_{B1}\right)}{\min\left(\mu_{A1}, \mu_{B1}\right) + \min\left(\mu_{A1}, \mu_{B2}\right) + \min\left(\mu_{A2}, \mu_{B1}\right) + \min\left(\mu_{A2}, \mu_{B2}\right)}$$

$$W_2 = \frac{\min\left(\mu_{A1}, \mu_{B2}\right)}{\min\left(\mu_{A1}, \mu_{B1}\right) + \min\left(\mu_{A1}, \mu_{B2}\right) + \min\left(\mu_{A2}, \mu_{B1}\right) + \min\left(\mu_{A2}, \mu_{B2}\right)}$$

$$W_3 = \frac{\min\left(\mu_{A2}, \mu_{B1}\right)}{\min\left(\mu_{A1}, \mu_{B1}\right) + \min\left(\mu_{A1}, \mu_{B2}\right) + \min\left(\mu_{A2}, \mu_{B1}\right) + \min\left(\mu_{A2}, \mu_{B2}\right)}$$

$$W_4 = \frac{\min\left(\mu_{A2}, \mu_{B2}\right)}{\min\left(\mu_{A1}, \mu_{B1}\right) + \min\left(\mu_{A1}, \mu_{B2}\right) + \min\left(\mu_{A2}, \mu_{B1}\right) + \min\left(\mu_{A2}, \mu_{B2}\right)}$$

Then $C = W_1c_1 + W_2c_2 + W_3c_3 + W_4c_4$

5. Results and Discussions

Decimal scale of weather stability class:

However, the definition of weather stability class based on wind speed and solar radiation, as given in the Table 2, is imprecise. It is found that weather stability class has to be chosen one among two classes for some combination of wind speed and solar radiation. In those case, weather stability class can be selected either lower class or upper class. Apart from the double class definition there may exist an overlapping of weather stability classes at the boundary of wind speed and solar radiation. Let us take an example to explain the double class with wind speed in between 2 m/s and 3 m/s, and solar radiation greater than 50 langle/h, weather stability class can be A or weather class B as per the definition of weather stability class. This existing double class can be resolved using fuzzy logic based soft computing. For the demonstration purpose, wind speed(WS) and solar radiation during day(RD) are considered as imprecise variables and fuzzified them with triangular membership functions. Universes of discourse of wind speed (i.e. WS={Very low, low, Moderate, High, Very High}) and solar radiation during day(i.e. RD={Low, Moderate, High, Very High}) have been shown in the Figure 2 and Figure 3 respectively.

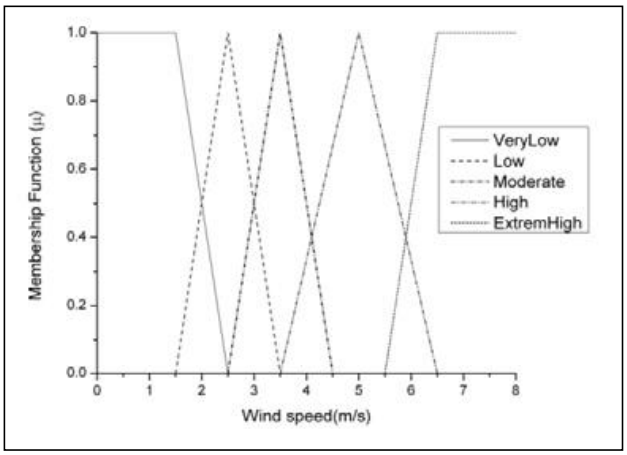

Figure 4 Universe of discourse of wind speed

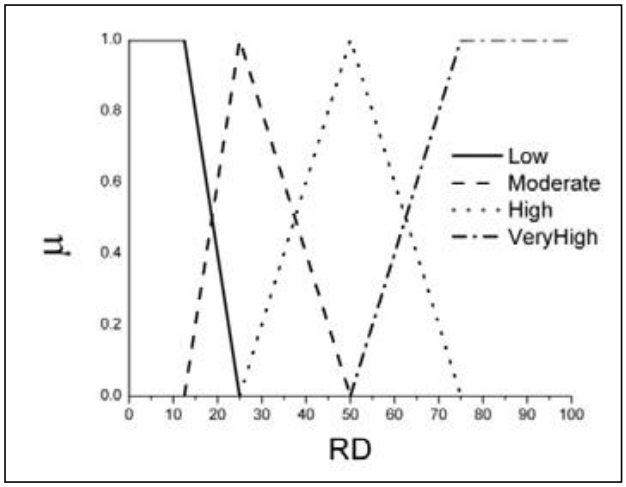

Figure 5 Universe of discourse of solar radiation during Day

To demonstrate the effect of weather stability class on the scale of 6, weather classes A to F have been assigned to integer numerical value from 1 to 6. The decimal weather stability class has been derived using fuzzy binary relationship based on the definition of weather stability class. For the case of double class definition, three cases are considered to derive decimal weather stability class. First case considers lower class among double class; second case considers average class of double class and third case considers higher class among double class. The following twenty rules are formed for first case.

IF(WS=Very low.and.RD=Very high)THEN WC=A

IF(WS=Low.and.RD=Very high)THEN WC=A

IF(WS=Moderate.and.RD=Very high)THEN WC=B

IF(WS=High.and.RD=Very high)THEN WC=C

IF(WS=Very high.and.RD=Very high)THEN WC=D

IF(WS=Very low.and.RD=High)THEN WC=A

IF(WS=Low.and.RD=High)THEN WC=B

IF(WS=Moderate.and.RD=High)THEN WC=B

IF(WS=High.and.RD=High)THEN WC=C

IF(WS=Very high.and.RD=High)THEN WC=D

IF(WS=Very low.and.RD=Moderate)THEN WC=B

IF(WS=Low.and.RD=Moderate)THEN WC=C

IF(WS=Moderate.and.RD=Moderate)THEN WC=C

IF(WS=High.and.RD=Moderate)THEN WC=D

IF(WS=Very high.and.RD=Moderate)THEN WC=D

IF(WS=Very low.and.RD=Low)THEN WC=D

IF(WS=Low.and.RD=Low)THEN WC=D

IF(WS=Moderate.and.RD=Low)THEN WC=D

IF(WS=High.and.RD=Low)THEN WC=D

IF(WS=Very High.and.RD=Low)THEN WC=D

The variation of decimal weather stability class with wind speed for six different solar radiations has been shown in the Figure 6. In the solar radiation during day range 25 langley/h to 50 lagley/h, six discrete points have been chosen to obtain variation of weather stability class. These points are 25 langley/h(i.e.SR25), 30 langley/h(i.e.SR30), 35 langley/h(i.e. SR35), 40 langley/h(i.e. SR40), 45 langley/h(i.e. SR45) and 50 langley/h(i.e. SR50). From the Figure 6, it is found that weather class with SR25 is highest among other solar radiation for all wind speed variation. Weather class with SR50 is found to be lowest among all other solar radiation. It is also found that with decreasing solar radiation, weather stability class increases. It is noted that weather class merges at a value of four at the higher wind speed irrespective of solar radiation, which is expected from the definition of weather stability class. As fuzzy binary relationship is with lower class among double class, decimal weather class shows class 1.0 for SR50 and class 2.0 for SR25 at wind speed less than 2.0 m/s.

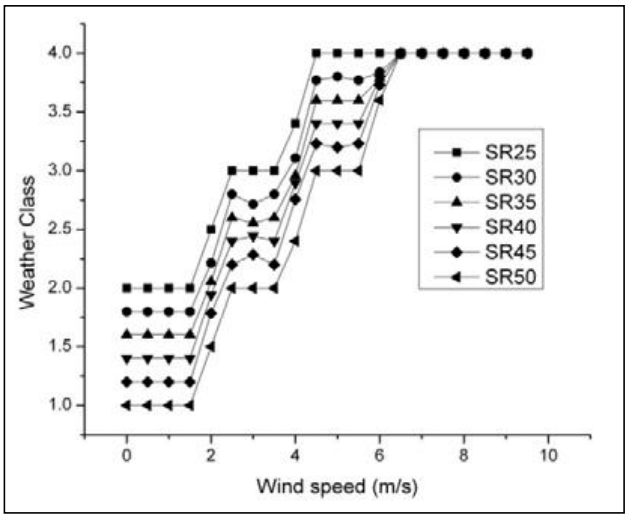

Figure 6 Decimal weather stability class for first case

Similarly, decimal weather class has been calculated for second case and third case for same solar radiation variations. The variation of decimal weather stability class with wind speed for different solar radiation for second case and third case has been shown in the Figure 7 and Figure 8, respectively. The nature of variation of decimal weather stability class is similar to that of first case.

From the Figure 7, it is found that the variation of decimal weather stability class with solar radiation is less comapared to the first case. It is happed due to the fuzzy interface rule with average value of double

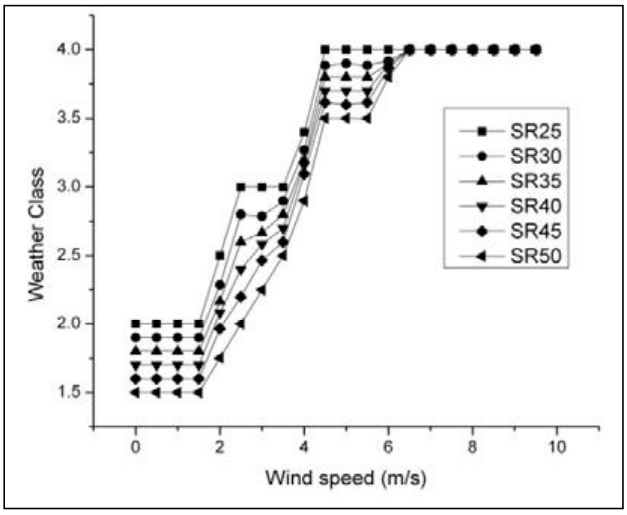

Figure 7 Decimal weather stability class for second case

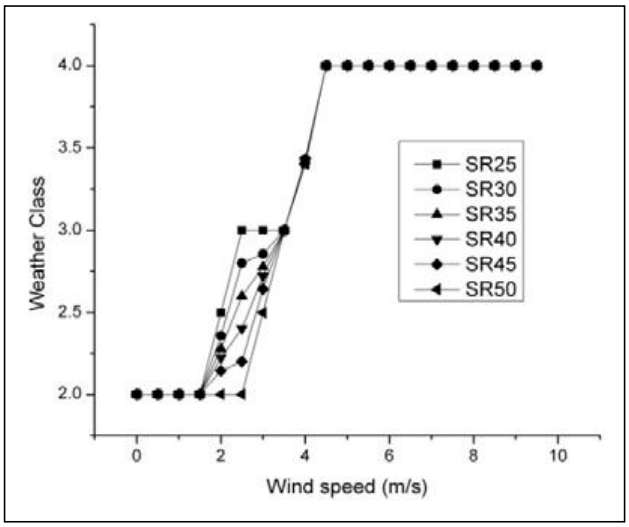

Figure 8 Decimal weather stability class for third case

class. That is why the weather stability class is 1.5 for SR50 at wind speed less than 2.0 m/s.

From the Figure 8, it is found that the variation of decimal weather stability class with solar radiation is collapsed. Hence selection of fuzzy rule base has strong influence on decimal weather stability class.

Mixure of weather class:

In the decimal weather stability class, fractional class is composed with more than one basic weather class (i.e A, B, C, D, E and F). In this exercise, wind speed is varied from 0 to 10 m/s and solar radiation is varied from 25 langley/h to 50 langley/h. Composite weather class for the variation of wind speed and solar radiation has been shown in the Table 3.

In the Table 3, weight fraction of composite weather class is given in the bracket. Using the

Table 3 Composite weather class for solar radiation during day in the range of 25 to 50 langley/h

wspeed	SR25	SR30	SR35	SR40	SR45	SR50
0	B	A(0.2) B(0.8)	A(0.4) B(0.6)	A(0.6) B(0.4)	A(0.8) B(0.2)	A
0.5	B	A(0.2) B(0.8)	A(0.4) B(0.6)	A(0.6) B(0.4)	A(0.8) B(0.2)	A
1	B	A(0.2) B(0.8)	A(0.4) B(0.6)	A(0.6) B(0.4)	A(0.8) B(0.2)	A
1.5	B	A(0.2) B(0.8)	A(0.4) B(0.6)	A(0.6) B(0.4)	A(0.8) B(0.2)	A
2	B(0.5) (0.5)	A(0.1429) B(0.5) C(0.3571)	A(0.2222) B(0.5) C(0.2778)	A(0.2778) B(0.5) C(0.2222)	A(0.3571) B(0.5) C(0.1429)	A(0.5) B(0.5)
2.5	C	B(0.2) C(0.8)	B(0.4) C(0.6)	B(0.6) C(0.4)	B(0.8) C(0.2)	B
3	C	B(0.2858) C(0.7142)	B(0.4444) C(0.5556)	B(0.5556) C(0.4444)	B(0.7142) C(0.2858)	B
3.5	C	B(0.2) C(0.8)	B(0.4) C(0.6)	B(0.6) C(0.4)	B(0.8) C(0.2)	B
4	C(0.6) D(0.4)	B(0.1622) C(0.5676) D(0.2703)	B(0.2553) C(0.5319) D(0.2128)	B(0.3191) C(0.4681) D(0.2128)	B(0.7054) C(0.4325) D(0.1622)	B(0.6) C(0.4)
4.5	D	C(0.2308) (0.7692)	C(0.4) D(0.6)	C(0.6) D(0.4)	C(0.7692) D(0.2308)	C
5	D	C(0.2) D(0.8)	C(0.4) D(0.6)	C(0.6) D(0.4)	C(0.8) D(0.2)	C
5.5	D	C(0.2308) D(0.7692)	C(0.4) D(0.6)	C(0.6) D(0.4)	C(0.7692) D(0.2308)	C
6	D	C(0.1622) D(0.8379)	C(0.2128) D(0.7872)	C(0.2128) D(0.7872)	C(0.2703) D(0.7298)	C(0.4) D(0.6)
6.5	D	D	D	D	D	D
7	D	D	D	D	D	D
7.5	D	D	D	D	D	D
8	D	D	D	D	D	D
8.5	D	D	D	D	D	D
9	D	D	D	D	D	D
9.5	D	D	D	D	D	D

concept of composite weather class, the empirical formula for atmospheric dispersion coefficients has been derived.

Empirical formulation for atmospheric dispersivity coefficients for composite weather classification

$$\sigma_y^{ABCDEF}(x) = \sum\nolimits_{i=A,B,C,D,E,F} w_i \sigma_y^i(x)$$

Let us take an example, to formulate dispersion coefficient in transverse and vertical direction with downwind distance for wind speed 2 m/s and solar insolation during day is 35 lagley/h. From the Table 3, the weighting factors for weather class A, B and C are 0.2222, 0.5 and 0.2778 respectively for the specified wind speed and solar insolation.

$$\sigma_y^{ABC}(x) = w_A \sigma_y^A(x) + w_B \sigma_y^B(x) + w_C \sigma_y^C(x)$$

Here, W_A is 0.2222; W_B is 0.5 and W_C is 0.2778. Empirical formula for individual weather class is calculated from equation (2). And coefficients used in the dispersivity formulation are given in the Table 1. Wind speed is considered as 2.0 m/s for the formulation of dispersion coefficient. The variation of dispersion coefficient for transverse wind direction with downwind distance (upto 10.0 km) has been shown and compared with class A class-B, SR25(i.e. classB(0.5) and Class-C(0.5)), SR30(i.e. Class-A(0.1429), Class-B(0.5) and class-C(0.3571)), SR35(i.e. Class-A(0.2222), Class-B(0.5) and Class-C(0.2778)),

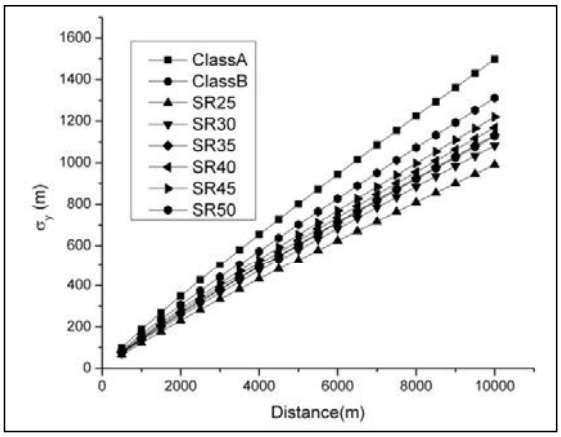

Figure 9 variation of SigmaY with distance for various composite weather class

SR40(i.e. Class-A(0.2778), Class-B(0.5) and class-C(0.2222)) SR45(i.e. Class-A(0.3571), Class-B(0.5), Class-C(0.1429)) and SR50(Class-A(0.5) and Class-B(0.5)) in the Figure 9.

From the slope of the dispersion coefficient with distance is minimum for SR25(Class-B(0.5) and Class-C(0.5)) case. It is increasing with solar radiation. It attains maximum value for Class-A. The variation of dispersion coefficient in vertical direction with downwind distance (upto 10.0 km) has been shown in the Figure 10. Here, wind speed is kept at 2.0 m/s. Effect of various composite weather classes on dispersion coefficient has been compared in Figure 10. It is found that slope of the dispersion coefficient is minimum for SR25 (class-B(0.5) and class-C(0.5)) case. Slope is increasing with solar radiation (SR30, SR35, SR40, SR45 and SR50). It attains maximum value for weather stability class A. It is found that the coefficient of dispersivity along vertical direction is more sensitive to composite weather stability class. The variation of coefficient of dispersion along vertical direction is comparatively very high than transverse direction. The effect of composite weather stability class on concentration reduction factor at various downwind distance has been estimated in the following section.

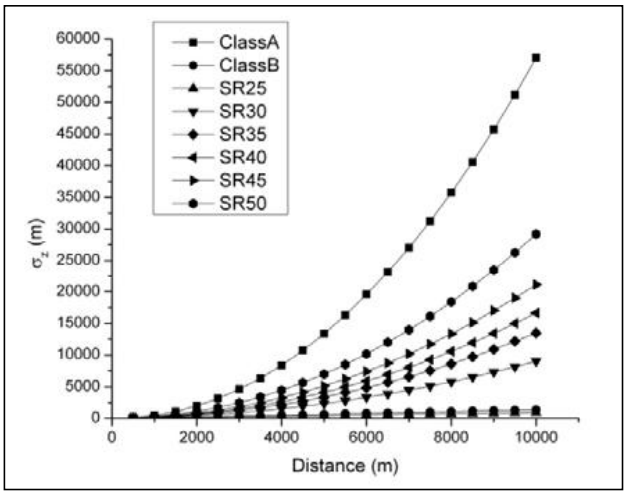

Figure 10 Variation of SigmaZ with distance for various composite weather classes

Estimation of concentration reduction factor:

In this section, different fuzzy interval arithmetic operations are used to get the concentration reduction factor through evaluation of Gaussian plume model. Finally, the effect of composite weather stability class on the estimation of concentration reduction factor has been demonstrated.

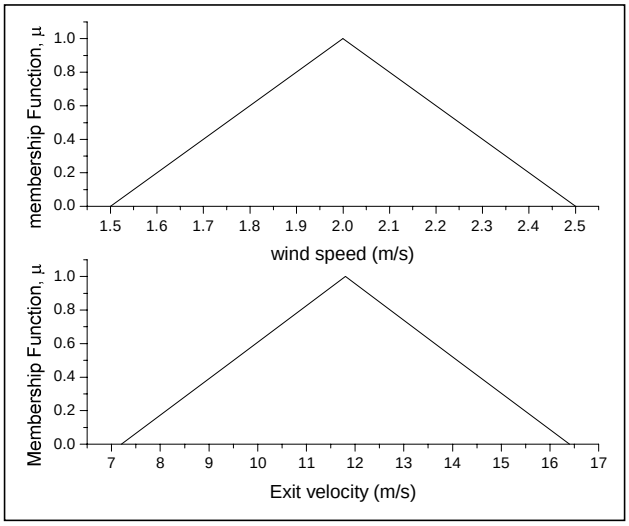

Figure 11 Fuzzy representation of wind speed and exit velocity

For concentration reduction factor estimation two imprecise variables have been considered with triangular membership function. These variables are wind speed (u) and plume exit velocity (W). The fuzzification of these variables has been done using triangular membership function and shown in the Figure 11.

Various fuzzy arithmetic operations such as division, multiplication, additions and subtraction, exponential to evaluate the Gaussian plume function. The transformation of fuzzy membership functions of derived parameters such as plume rise, effective stack height and concentration reduction factor has been demonstrated in Figure 12.

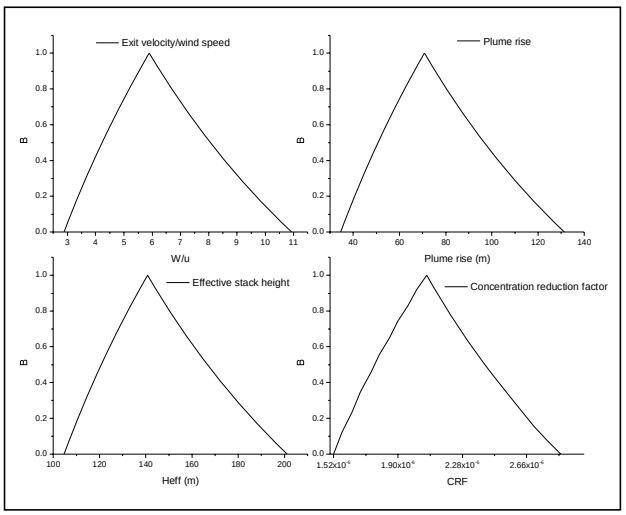

Figure 12 Various derived parameters arisen in fuzzy arithmetic operations

In the Figure 12, there are four graphs. Transformation of membership function for derived parameter plume exit velocity divided by wind speed has been shown in the top left graph. Similarly, transformation of membership function for plume rise, effective stack height and concentration reduction factor has been shown in the top right, bottom left and bottom right graphs respectively. It is found that support of the derived fuzzy variables is changing with fuzzy arithmetic operation. It is also found that crisp value of the derived variables is shifting from the interval midpoint.

Now let us concentrate on the meaning of fuzzy membership function of concentration reduction factor. Fuzzy membership function for concentration reduction factor at a downwind distance 1.5 km with coefficient of dispersion of SR35(i.e. Class-A(0.2222), Class-B(0.5) and Class-C(0.2778)) has been shown in the Figure 13.

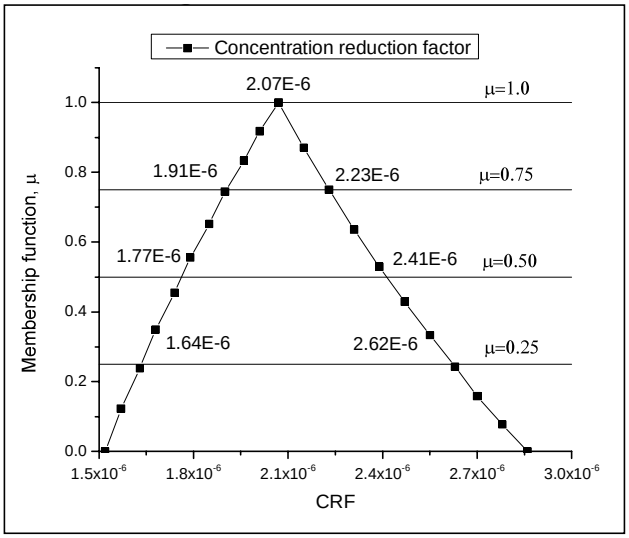

Figure 13 Membership function of concentration reduction factor at a distance 1.5 km.

From Figure 13, the range of concentration reduction factor for a specific alpha-cut value can be derived by drawing horizontal line with μ=α. This horizontal line will cut the membership function at two points. Concentration reduction factor at these points decides the range or uncertainty of the concentration reduction factor with degree of impreciseness denoted by alpha. It is found that α=1.0 the range becomes a single point corresponding concentration reduction factor is known as crisp value, which is considered as a precise value. The crisp value and various quartile ranges are given in the table 4.

Table 4 Various levels of uncertainty of CRF

Parameter	α-cut value	Range
Crisp	1.00	3.31E-7
Upper Quartile	0.75	2.24E-7 to 9.23E-7
Middle Quartile	0.50	1.43E-7 to 1.64E-6
Lower Quartile	0.25	6.24E-8 to 2.56E-6

The variation of concentration reduction factor with downwind distance has been shown in the Figure 14 for various weather classes. Apart from basic weather class A and Class B, six composite classes are considered. These are SR25, SR30, SR35, SR40, SR45 and SR50. With fraction of these composite weather classes are given in the previous section.

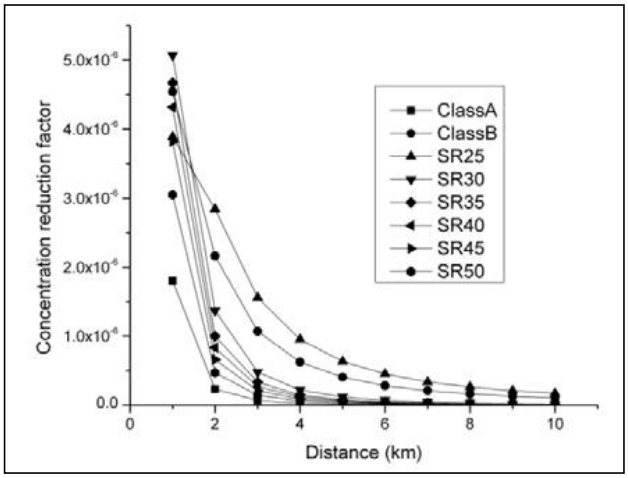

Figure 14 CRF with variation of downwind distance

From the Figure 14, it is found that concentration reduction factor is decreasing with downwind distance. Highest concentration reduction factor is found for SR25 and lowest for Class-A. The variation of concentration reduction factor for other composite classes is found to be in between the Calss-A and SR25. This is happed due to the variation of coefficient of dispersion with weather class. It is found that higher the coefficient of dispersion yields lower concentration reduction factor. It is found that composite weather class has an important role on concentration reduction factor.

6 Conclusions

Atmospheric dispersion analyses need to deal with imprecise definition of various input parameters, imprecise model for weather stability class. Fuzzy logic based soft computing has been used to demonstrate the decimal weather stability class, which is mixture of Pasquill-Gifford weather stability class. During development of decimal weather stability class,

various methodologies such as fuzzification, fuzzy interface rule base and defuzzification have been used. Composite weather stability class has been demonstrated for entire range of wind speed and solar radiation varied from 25 langey/h to 50 langley/h. In the decimal weather stability class, the weight fraction of composite weather stability class has been estimated. Based on the weight fraction of composite weather class, new empirical formulae for coefficient of dispersion along transverse and vertical direction have been derived. The effect of composite weather stability class on concentration reduction factors at various downwind distances have been estimated through evaluation of Gaussian plume model. During evaluation of Gaussian plume model, various fuzzy arithmetic operations are used and corresponding transformation of membership function for various derived parameters have demonstrated. Decimal weather stability class improves the prediction of concentration reduction factor. Among the imprecise variables, sensitive variable is found to be wind speed based on Hartley like measure estimation.

References

1. Dhanesh B. Nagrale, S. Bera, A. K. Deo, R. S. Rao, A. J. Gaikwad, "A Report on Decision Support System: Important Consideration for Acceptance", AERB Report, AERB/NSAD/TR/2012/03 (2012)
2. AERB Safety Guide, "Atmospheris dispersion and Modelling", AERB/NF/SG/S-1 (2008)
3. Timothy J. Ross, "Fuzzy Logic with Engineering Applications", 3rd Edition, John Wiley & Sons Publication, (2010)
4. M. Saeedi, H. Fakhraee and M. R. Sadrabadi, "A Fuzzy Modified Gaussian Air pollution dispersion model",Res. J. Environ Sci., 2(3):156-169(2008)
5. Subrata Bera, D. Datta, Avinash J. Gaikwad, "Role of fuzzy set theory in air pollution estimation", International Conference on Advanced Engineering Optimization Through Intelligent Techniques (AEOTIT), S. V. National Institute of Technology, Surat-395007, Gujrat, India, July 01-03, 2013
6. Rituparna Chutia, Supahi Mahanta, D. Datta, "Non-probabilistic sensitivity and uncertainty analysis of atmospheric dispersion", Annals of Fuzzy Mathamatics and Informatics, Vol. 5, No. 1.pp 213-228, (2013)
7. Guanrong Chen, Trung Tat Pham, "Introduction to fuzzy sets, fuzzy logic and fuzzy control system", CRC Press, (2001)
8. F. martin McNeil, Ellen Thro, "fuzzy logic A practicle approach", AP Professional, (1994)
9. Li-xin Wang "A course in Fuzzy systems and control", Prentice hall international, Inc (1997)
10. Palash Dutta, Hrishikesh Boruah, Tazid Ali,"Fuzzy Arithmetic with and without using α-cut method: A Comparative Study", International Journal of Latest Trends in Computing, Vol. 2, Issue 1 (2011)

Life Cycle Reliability and Safety Engineering
Vol.5 Issue 3 (2016) 41-48

Aircraft Air-intake Icing on the Ground as a Mechanism of the Motion in Mirce Mechanics

Dr Jezdimir Knezevic

MIRCE Akademy, Woodbury Park, Exeter, EX5 1JJ, UK

Abstract

Mirce Mechanics is a scientific theory of the motion of functionable systems through Mirce Spacetime resulting from any actions whatsoever and the actions required to produce any motion accurately proposed and demonstrated. Hence, the main purpose of this paper is to address the air-intake icing as a mechanism of the motion in Mirce Mechanics that causes the transition from the positive to the negative in-service state of an aircraft. To address this mechanism the Loganair scheduled cargo flight for the Royal Mail, from Edinburgh-Turnhouse Airport, Scotland to Belfast International Airport, has be selected for the analysis. The flight took place on 27th February 2001, with 17.10 take off and ditching into water several minutes later, killing both crew members A few other examples, where this mechanism caused the transition to the negative state, with similar consequences, are also mentioned in the paper.

1. Introduction

"*Everything that the human race has done and thought is concerned with the satisfaction of felt needs*". Albert Einstein

Human needs for transportation, ventilation, communication, refrigeration, information, computation and many other functions are continuously satisfied through human created and managed entities, commonly known as systems. Their design-in performance, in terms of speed, capacity, frequency, power and similar physically measurable quantities, can be accurately predicted during the design process and tested at the delivery, as they are functioning in accordance to well understood laws of natural sciences, such as: Newton's laws of motion, Maxwell's law of electrodynamics, Coulomb's law of solid friction, Hook's law of stress and strain Boltzmann's law of thermodynamics, to name a few, which are characterised by certainty, reversibility and independence of time, location and humans.

Experience teaches us that due to internal and external interactions, variety of mechanical, electrical, chemical, thermal, radiant and other physical events are generated, some of which cause the loss of the ability of systems to function. To maintain functionability[1], actions like servicing, repairs, inspections, replacements and similar, are undertaken by humans. Thus, the motion of functionability through time, which is physically manifested by the sequential transitions of functionable systems[2] through positive and negative functionability states, resulting from the complex interactions between atomic, environmental and human actions, is a key determinant of the in-service performance of systems. Unlike accurate quantitative information regarding the design-in functionality performance of systems that is available on the delivery day, the in-service performance is not. Instead, years later the statistics for various functionability measures become available. The reason for this is the fact that they are characterised by uncertainty, discontinuity, irreversibility, inseparability, and dependence of time, location and humans, and as such non predictable by existing laws of science. [1]

To rationally address questions of the accurate predictions of in-service performance of systems Dr Knezevic has established the MIRCE Akademy at Woodbury Park, Exeter, UK, in 1999. Staff, Fellows, Members and students of the Akademy have endeavoured to subject in-service behaviour of systems to the laws of science and mathematics to:

- Determine the trajectory of the motion of functionability of in-service systems through

[1] *Functionability, n. ability to deliver at least one measurable function, Reliability, Maintainability and Supportability – A probabilistic Approach, Text and Software package, pp. 291, Knezevic, J., McGraw Hill, London 1993. ISBN 0-07-707691-5*

[2] *In Mirce Mechanics a functionable system is defined as any collection of entities that enables the flow of functionability through time.*

time, which uniquely define the sequence of occurrences of positive and negative events, together with the statistics of the work done by the systems and on the system[3]

- Understand mechanisms that lead to the occurrence of in-service events like fatigue, operator errors, corrosion, creep, foreign object damage, a faulty weld, carburettor icing, shelf life, perished rubber, to name just, within physical scale (10^{-10} to 10^{10} metre).
- Define a mathematical scheme for predicting expected in-service behaviour of systems for a given operational scenario, maintenance policies and support strategy, which is vital for the calculation of the work done by the systems and on the system.

While in classical mechanics a force is said to do work if, when acting on a body, there is a displacement of the point of application in the direction of the force, in Mirce Mechanics a given system is said to do work, if there is a provision of a measurable function in the direction of time, named as functionability in motion.

In summary, the body of knowledge comprising of axioms, mathematical equations and methods that enable prediction of the motion of functionability through time to be made, for all possible combinations of design-in and in-service alternatives, based on the scientific understanding of the mechanisms that cause occurrences of observable positive and negative events through the life of in-service systems constitutes Mirce Mechanics.

The main purpose of this paper is to address air-intake icing as a physical process that could potentially cause the motion of an aircraft from positive to negative in-service states and thus have significant impact on the passengers and cargo.

The main example of this mechanism, analysed in this paper, is related to the Loganair Flight 670A on 27th February 2001 that lost all power on both engines soon after takeoff from Edinburgh. An attempt to ditch in the Firth or Forth in rough seas resulted in the break up and sinking of the aircraft and neither pilot survived. The loss of power was attributed to the release of previously accumulated frozen deposits into the engine core when the engine anti icing systems were selected ON, whilst climbing through 2200 feet. These frozen deposits were considered to have accumulated whilst the aircraft had been parked prior to flight without engine intake blanks fitted.

2. Aircraft Ground Air-intake Icing Phenomena

Within the aviation community the effects of airframe contamination and the potential consequences of failure to properly de-ice prior to takeoff are well documented and are generally well understood. However, the concepts and liabilities of jet engine contamination, inclusive of engine core and fan blade icing, have not had the same degree of exposure and are less well understood.

Blowing snow, precipitation, freezing fog, slush and other ground contaminants or airport snow removal operations can all result in the contamination of jet engine intakes and components. The area of the engine that will be affected is dependent upon the origin and type of contaminant, and whether or not the engines are running at the time of exposure. The potential for damage due to ice ingestion is significant but the more subtle effects of airflow disruption due to ice accretion on compressor and fan blades can also result in loss of thrust, engine damage or flameout.

The engine anti-ice system, as installed on most types, serves solely to prevent ice build up on the air intake opening of the engine nacelle. It does not prevent ice build up in the primary stages of the engine core (compressor) or on the fan blades. Jet engines are most susceptible to the build up of blade ice in conditions of freezing fog or freezing precipitation while the engine is at or near its minimum rotation speed (ground idle). Compressor and fan blades are aerofoils and, due to the affect that they have on the airflow across them, any ice accretion will normally be found on the back side of the blade. This makes the ice difficult to see during a preflight inspection and also inhibits its removal.

3. Loganair Flight 670A on 27th February 2001

For the purpose of this paper the Loganair scheduled cargo flight for the Royal Mail, from

[3]*Boeing 747, registration number N747PA, been air born 80,000 flying hours, transported 4,000,000 passengers, burned 271,000,000 gallons of fuel while receiving 806,000 maintenance man-hours and consuming: 2,100 tyres, 350 brake systems, 125 engines, among other parts, during the 22 years of in-service life , at Pan Am airlines.*

Edinburgh-Turnhouse Airport, Scotland to Belfast International Airport, has be selected for the analysis, as an illustration of the air-intake icing as a Mechanism of the Motion in Mirce Mechanics

3.1 The Aircraft

The aircraft considered was a Short 360-100, a turboprop airliner manufactured by Short Brothers Limited in 1987, constructor's serial number SH 3723 and registered G-BMNT. It is powered by two Pratt & Whitney Canada PT6A-67R engines.

For the Royal Mail flights the passenger seats had been removed for use as a freighter and its Certificate of Airworthiness was valid until 15 October 2001. The aircraft was loaded with 1,360 kg of fuel and carried 1,040 kg of cargo with a total weight at takeoff of 10,149 kg (maximum certified takeoff weight is 12,292 kg).

3.2 The Crew

The crew consisted of a 58 year old male holding a valid Airline Transport Pilot's license and with 13,569 hours' flying experience, as the pilot in command. [The co-pilot was a 29 year old male, also with a valid license and 438 total flight hours.

The report said that nothing is known of the crew's activities at the aircraft.

"It is probable that by the time the accident crew arrived, any accumulation of snow or slush on the airframe had been blown away or melted," the report said. "In the absence of any other information it is assumed that the crew carried out normal pre-flight procedures and checks." [2]

3.3 Environmental Conditions

Weather reported at the Edinburgh Airport, just before the accident, was as follows:

- Air temperature of +2°C,
- dew point of -3°C,
- Visibility of more then 10km, broken clouds at 4500 ft and cover at 8000 ft.

3.4 The Takeoff

Loganair Royal Mail charter flight 670A to Belfast was given a clearance at 15:03. Two minutes later, the crew advised Air Traffic Controller that they aborting the flight due to a technical problem.

The crew then advised their company that a generator would not come on line. An avionics technician carried out diagnosis during which both engines were ground-run twice. No fault was found and the flight crew requested taxi clearance at 17:10.

3.5 The Accident

A normal takeoff took place at 17:10, whit the pilot flying. It was followed by a normal reduction in power at 1200 feet above mean sea level. At 2200 feet, while the pilot was changing the radio frequency, the co-pilot selected the anti-icing systems. However, only 3.9 seconds later the torque indicators for both engines rapidly fell to zero, causing a complete loss of propeller thrust. In response, the first officer radioed a Mayday call on the Air traffic control frequency; the pilot initiated a descent with a reduced airspeed of 110 kt while turning right towards the coast. Realising that they could not reach shore the crew prepared for ditching. At airspeed of 86 knots, with a 6.8 degree nose up, and 3.6 degree left wing down attitude the aircraft thatched the water.

At the final stop, the aircraft was 65 metres off shore in a 45 degree nose down attitude, with the forward half of the fuselage submerged in a water depth of approximately 6 metres. As the results of the impact with water the flight deck was almost completely destroyed, with a fuselage firmly embedded in the sand. The empennage had separated and was found floating 100 metres to the east of the main wreckage.

Both crew members were drowned, although both crew seats remained attached to the flight deck floor with no failure of the safety harnesses. The cockpit voice recorder (CVR) and flight data recorder (FDR) were both recovered intact. The aircraft was eventually salvaged, dismantled and transported to UK Air Accidents Investigation Branch (AAIB) headquarters at Farnborough for a detailed examination.

3.6 Actions that Caused Occurrence of Negative In-service Event

Upon investigation completion it was concluded that the snow accumulated overnight changed the engine intake air flow, causing both engines to flame out after both engines' anti-ice vanes were simultaneously opened as per the standard operating procedure.

The aircraft concerned was parked overnight, heading directly into moderate to strong surface winds for approximately 17 hours. As no protecting plugs were put inside the engine intakes by the flight crew, against established practical procedure for flights

in adverse weather conditions, the wind drove a significant amount of snow into the intakes.

The reason for that was the fact that the intake plugs were not carried, as part of the aircraft's onboard equipment. Even further, they were not available at Edinburgh Airport. Finally, information concerning freezing weather conditions in the aircraft manufacturer's maintenance manual had not been including in the Loganair Operations Manual for Short 360, which meant not complied with.

The AAIB, in the final report, stated that the large volumes of snow or slush could have accumulated where it would not have been readily visible to the crew during a pre-flight inspection, as the engine intakes on this type of aircraft are about 2.8 m above the ground. [2]

4. Other Occurrences of Aircraft Ground Air-intake Icing Phenomena

A few examples of the aircraft ground air-intake icing occurrences are briefly describes here, as a further evidence of the nature of this phenomena and the manner of its manifestations.

- During the course of the investigation of the loss of G-BNMT, a report was received that there had been a previous occurrence, on an SD3-60 aircraft operated by a different company in the UK, of a double engine power anomaly as a result of accumulated ice or snow arising from pre-flight conditions. The power interruption occurred while the aircraft was on its take-off run. The event, that took place around 1992, had not been reported at the time through the established mandatory reporting system. However, both crew members and the station engineer concerned were located and spoken to, but the intervening period had resulted in considerable differences of recollection of the precise circumstances.
- The AAIB reported in the Bulletin 1/2002 on an accident which occurred on 20 March 2001 in which a DHC-8 aircraft experienced and undetected build up of slush in the engine intake and plenum areas. The aircraft was fitted with PW127 engines, a type with an intake system very different in concept from that on the PT6A-67, but which as similarly located and configured intakes in the engine nacelles. This accumulation had occurred while the aircraft was parked facing into wind in falling snow and resulted in both engines flaming out during the subsequent taxi for takeoff.
- On 13 January 1982, an Air Florida Boeing 737-200 took off in daylight from runway 36 at Washington National in moderate snow but then stalled before hitting a bridge and vehicles and continuing into the river below after just one minute of flight killing The aircraft was destroyed by impact forces and 69 of the 74 occupants and 4 people on the ground were killed and 4 more on the ground were injured. The accident was attributed entirely to a combination of the actions and inactions of the crew in relation to the prevailing adverse weather conditions and, crucially, to the failure to select engine anti ice on which led to over reading of actual engine thrust. [3]
- On 25 November 2004, a Mytravel Airways UK Airbus A320 departed the side of the runway at Harstad, Norway at a low speed after loss of directional control when thrust was applied for a night take off from surface-contaminated runway 35 in normal visibility and the aircraft departed the left side of the runway. The aircraft stopped short distance off the paved surface and the occupants were subsequently evacuated from the rear of the aircraft using normal aircraft steps before being taken back to the terminal by bus. Damage to the aircraft was minor and confined to the NLG. It was found that the crew had failed to follow an SOP designed to ensure that any accumulated fan ice was shed prior to take off and also failed to apply take off thrust as prescribed, thus delaying their appreciation of the uneven thrust produced. [5]
- On 20 March 2001, aircraft DHC-8-311, G-JEDD, with 2 Pratt & Whitney PW-123 turboprop engines landed at Bristol at 1314 hrs. At that time, the weather produced a surface wind from 080° at 25 gusting 36 kt, visibility 2,000 metres in light snow, scattered cloud base 500 feet, temperature 0°C. The aircraft parked normally on stand 5, heading east (into wind). After the passengers had deplaned, the crew went into the airport

terminal, as the next planned departure was at 1510 hrs. The crew did not fit the engine intake blanking plugs during the turnaround. During the intervening period, the weather conditions worsened. The snow fall became heavier with a progressive deterioration in visibility and the strong, gusty easterly wind continued. During its time on the ground, the aircraft began to accumulate a covering of snow. When the crew returned to the aircraft in time to prepare for the next planned departure, the commander arranged for the aircraft to be de-iced using heated type II fluid. After this was carried out and the commander completed a pre-flight external inspection, which included a visual inspection from the ground of each engine intake lip and a tactile inspection of the rear of each intake through the open bypass doors. The commander assessed that there was no build up of snow or slush in these areas and considered that the engine intakes were clear of ice and snow. Once the runway had re-opened, the crew performed a normal engine start and the aircraft began to taxi out for departure at 1535 hrs. On reaching the holding point for Runway 09, ATC requested that the aircraft hold position in order to allow a stream of inbound aircraft to land. While waiting with the aircraft's tail into wind, the right engine suddenly stopped, for no apparent reason. The crew carried out the Engine Failure procedure from the aircraft's Quick Reference Handbook (QRH), without selecting Ignition to Manual (ON) for the left engine. About 2.25 minutes after that the left engine also flameout. The commander informed ATC and requested a bus to deplane the passengers and a tug and tow bar to move the aircraft to the parking ramp. While passengers were leaving the aircraft the left propeller was still wind milling quite fast close to the forward exit door. The aircraft was then towed to a parking stand. On arrival, the aircraft was quarantined and the engine intake blanks were fitted. [6]

These few examples, like thousands of other incidents, are recorded in different aviation data bases, form the statistics of the past performances. However, as statistics does not study causes of statistical behaviour and is mainly used by statisticians and government organisations, rather than by design, operation and maintenance engineers, many of the future accidents end up as the statistics. As indicated in the introduction of the paper one of the main objectives of Mirce Mechanics is the scientific understanding of the mechanisms that drive in-service processes like fatigue, operator errors, corrosion, creep, foreign object damage, a faulty weld, carburettor icing, shelf life, perished rubber, to name just, which cause occurrences of negative events.

5. Functionability Analysis of the Air intake Icing Event

Mirce Mechanics is a a scientific theory of the motion of functionable systems through Mirce Spacetime resulting from any actions whatsoever and the actions required to produce any motion accurately proposed and demonstrated. Hence, the main objective of this paper is to present an example of t the functionability analysis as a consistent part of the Mirce Mechanics through analysis of the actions that caused the accident of the flight 670A to Belfast. The data provided in the Air Accident Report 2/2003 [2] is the main source of information used to conduct the functionability analysis considered.

5.1 Sequence of Pre-flight Events

The aircraft considered landed at Edinburgh Airport from its previous flight at 0003 hrs on 27th February 2001. The weather conditions, recorded in the weather report, were as follows: surface wind 040 ^{0}/22 gusting 36kt, visibility 5,000 metres, light ice pellets, scattered cloud at 900 feet, broken cloud at 1,200 feet, temperature + 1 ^{0} C, dewpoint 0 ^{0}C and barometric pressure adjusted to the sea level was 992 mb.

The aircraft was taxied to and parked on Stand 31, with a heading of 035 ^{0} M. The inbound crew reported that there were no abnormalities observed or technical defects on the aircraft. As the Loganair does not use this airport as operating base, flight crews were responsible for normal aircraft turnaround procedures. Hence, they supervised the refuelling of the aircraft to a final load of 360 kg before leaving.

The aircraft was scheduled to depart Edinburgh at 0040 hrs with a different operating crew, which arrived at the aircraft at about 0030 hrs. Due to existing weather conditions the crew required de-icing before departure but they were advised that there would be a delay of several hours before equipment would be available. In the interim they returned to

the crew room. At 0210 hrs the airport closed as a result of the severe weather. At 0600 hrs this second crew were advised that the airport was not likely to reopen for several hours and so they returned to the aircraft to ensure it was secure before going off duty. At this time they fitted propeller straps to each engine and also put on the pitot head covers. Engine air intake blanks were not available for the crew to fit to the aircraft. The aircraft had not been de-iced.

The overnight weather conditions comprised a sustained strong north easterly wind, with a maximum recorded speed of 43 kt. Light or moderate snow fall occurred until 0952 hrs. There was no further snowfall after this time and by 1500 hrs the weather conditions were: surface wind 030 ^{0} / 15km, visibility 10 km, scattered cloud at 4,000 feet, broken cloud at 7,000 feet, temperature + 2 ^{0} C, dewpoint –3 ^{0}C.

5.2 The Accident Flight

To commence a planned flight to Islay departing at 0910 hrs, the pilots that were aboard the aircraft on the accident flight reported for duty at Glasgow Airport at 0810 hrs on 27th February 2001. As a result of adverse weather conditions, that flight was cancelled and they were rescheduled to carry out the single sector flight delayed from 0040 hrs from Edinburgh to Belfast. Surface travel from Glasgow to Edinburgh was impossible due to adverse road conditions, so as soon as Edinburgh Airport re-opened at 11.30 hrs, the crew were positioned to Edinburgh as passengers on another company aircraft.

On their arrival at Edinburgh the crew went out to the aircraft. There was no record of their activities there, but at 1503 hrs they requested clearance to start engines. Start clearance was obtained and then, at 1512 hrs, the crew advised Air Traffic Control, ATC, they were shutting down due to a technical problem. During this period the right engine had been observed to start and stop several times.

The crew returned to the terminal and contacted their company at Glasgow to ask for engineering assistance. They indicated that the right engine driven generator would not come on line. A company avionics/instrument engineer was in transit through Edinburgh Airport. He was contacted by the Line Maintenance Controller at Glasgow and asked to assist the crew. He carried out trouble shooting with advice from the Maintenance Controller. This action involved transposing the connections to the Generator Control Protection Units and required the crew to start and run both engines for approximately 15 minutes. The connections were then returned to their original positions. Thereafter, the crew carried out a second engine run of similar duration, again at the engineer's request. The original fault could not be reproduced. A ground power unit was not available, so the engine starts were carried out using aircraft battery power.

The commander then requested that the engineer check the engine oil contents. He also asked him to confirm that the upper surfaces of the aircraft were free from ice and snow. The engineer noted that the oil levels were such that replenishment was not required and the only airframe contamination was a small slush deposit on the windscreen. This was cleared by the engineer. Both engines were then restarted after which the aircraft remained on stand with the engines running for about another 20 minutes.

At 1710 hrs the first officer requested taxi clearance. After a short delay the aircraft powered back off stand and taxied to depart from Runway 06. While taxiing, as part of the first flight of the day engine checks, the crew carried out an Auto feather test, during the automatic operation of the engine anti-icing vanes to fully deploy and return was also observed. The commander briefed the first officer that after takeoff they would recycle the landing gear once to ensure that it was free of snow and slush.

The aircraft was cleared for a flight to Talla (TLA). The commander was the designated handling pilot. He carried out a normal takeoff which was followed by the landing gear being cycled up and down once, before its final retraction. A reduction to climb power was made at 1,200 feet above mean sea level, amsl. The commander then called for the after take-off checks to be completed. When the 'Stall Warning Heaters' item was reached, he requested that the first officer put on all the anti-icing systems. At this time the aircraft was handed over from Edinburgh Tower to Scottish ATCC, which was acknowledged by the first officer. With the aircraft at 2,200 feet amsl, the first officer then selected the anti-icing systems 'ON' while the commander selected the new radio frequency. Four seconds after the selection of each anti-icing vane switch, the torque on the corresponding engine reduced rapidly to zero. The commander quickly observed that the aircraft had suffered a double engine failure and advised the first officer who immediately broadcasted a MAYDAY call. In response the ATC passed the crew position and heading information.

The commander continued to fly the aircraft, initiating a descent while allowing the airspeed to

reduce to 110 kt and turning the aircraft to the right towards the coastline. The rate of descent stabilised at 2,800 feet per minute and he realised that the aircraft would have to be ditched in the water. The first officer attempted to make a further call to ATC advising that the aircraft was ditching, but this was not received. As the aircraft descended close to the water surface, the commander gradually increased the pitch attitude of the aircraft and correspondingly reduced the speed.

The aircraft impacted the water in a 6.8^0 nose up attitude at airspeed of 86 kt on a heading of 109^0M. It came to rest on the sea bottom in a nose down attitude with the forward section of the fuselage submerged, 65 metres offshore, in a water depth of about six metres.

5.3 Operating Procedures

Aircraft operating procedures for flight crew were laid out in the Operations Manual. Emergency and Abnormal checklist Documents were derived from information contained in the Short Brothers Ltd, SD3-60 Aircraft Flight Manual (AFM), and approved by the UK Civil Aviation Authority (CAA).

The company's operations manual required ice-protection systems for the airframe, engines, propellers, windshield, pitot-static system and stall-warning system to be engaged before the aircraft enters visible moisture at an outside air temperature at or below 6 degrees C.

5.4 Ground Handling Procedures

In the Operations Manual Part 1, clearly specifies, that after flight, captain is responsible for safe guarding the aircraft if it is to be left unattended for any length of time, such during a split duty or an overnight stop. It specifies that:

" The aircraft is to be secured in such a manner that it is protected from adverse weather Conditions, actual or forecast, and is to be parked or hangared in a secure place or area. Control locks and, where applicable, propeller restraint straps and pogo sticks are to be used whenever aircraft are parked. Should an aircraft be left for any length of time then engine blanks, pitot covers and chocks must be in position.'

According [2] the Operations Manual Part 9 (Flying – Shorts SD3-60) in particular specifies that, even for short term parking, 'propeller ties should be fitted', in order to prevent undesired rotation of the propellers on the ground.

For the engine air intakes, that are located some 2.8 metres above the ground, the manufacturer supplied air intake blanks as original equipment, which were designed to be fitted in the engine intakes to prevent debris, dust or snow from entering the engine intake area. Although supplied originally by the manufacturer with the new aircraft, these intake blanks were not routinely carried on the operator's SD3-60 aircraft.

The Maintenance Manual and the Operations Manual both contained a requirement for intake blanks to be fitted prior to the aircraft being de-iced. The Operations Manual also specified that, when ground de-icing of aircraft was to be carried out, then this should be under the supervision of a company engineer.

It was the operator's standard practice to keep intake blanks only at its main operating bases, namely Glasgow, Kirkwall and Inverness, where they were invariably fitted only by engineers to the night-stopping aircraft. Hence, no engineering personnel and no engine intake blanks were provided overnight at Edinburgh to support this operation. No intake blanks were therefore readily available to the crew, so they were unable to meet the stated responsibilities with regard to the safeguarding of the aircraft.

Even further, the crew would have needed a stepladder to visually inspect the engine intakes. Steps were not available at the aircraft, and a visual inspection inside the intakes was not specifically part of the pre-flight procedure. However, if the air intakes had been closely examined, it is possible that, some deposits of snow may have been visible within the intake cowl area.

5. Results of the Functionability Analysis of the Air intake Icing Event

Based on the information presented in [2] and the analysis performed above it is possible to draw the following conclusions:

- The airline did not have an established practical procedure for flight crews to fit engine intake blanks in adverse weather conditions. This meant that the advice contained in the aircraft manufacturer's Maintenance Manual 'Freezing weather – precautions' was not compiled with. Furthermore intake blanks were not provided on the aircraft nor were any readily available at Edinburgh Airport. However, even if they could have be found at the airport it would not

be possible to install them without a ladders of a significant height.

- Resulting from the aircraft overnight parking position that exposed it directly into strong surface winds, during the conditions of light to moderate snowfalls, almost certainly a significant amount of snow entered into the engine intakes.
- The flow characteristics of the engine intake system most probably allowed large volumes of snow, ice or slush to accumulate in areas where it would not have been readily visible to the crew during a normal pre-flight inspection without making use of ladders, which were not readily available.
- The deposits of snow, ice or slush almost certainly migrated from the plenum chambers down to the region of the intake anti-ice vanes, at some stage (probably after engine ground running began).
- According to investigators [2] the conditions in the intakes prior to takeoff are considered to have caused re-freezing of the contaminant, allowing a significant proportion to remain in a state which precluded its ingestion into the engines during taxi, takeoff and initial climb.
- Movement of the intake anti-icing vanes, acting in conjunction with the presence of snow, ice or slush in the intake systems, altered the engine intake air flow conditions and resulted in the near simultaneous flameout of both engines.
- The standard operating procedure, approved by the operator, of selectingboth intake anti-ice vane switches simultaneously enabled a simultaneous double engine flameout.

7. Conclusions

Mirce Mechanics analysis of the factual results available [2] regarding the Loganair Flight 670A on 27th February 2001 that lost all power on both engines soon after take off from Edinburgh and ditched into water several minutes later was presented in this paper. The action that caused this fatal event was the release of previously accumulated frozen deposits that were considered to have been accumulated whilst the aircraft had been parked overnight without engine intake blanks fitted.

Hence, this is another confirmation of the validity of the Mirce Mechanics Axiom which states that "*The probability of a human error in the execution of any functionability action is greater than zero*" [7]. Even further, it is also confirmed that causes of in-service failures are not always due to the malfunctioning of internal components of a system, but also from environmental impacts and humans actions.

In summary this paper provides further confirmation that in-service reliability and safety considerations of a large number of modern functionable systems are complex properties whose full understanding requires scientific approach towards understanding intricate mechanisms that lead to the occurrence of in-service failures, starting from atomic structure that drives the behaviour of matter, up to the solar system that drives the energy conversions (a physical scale ranging from 10^{-10} to 10^{10} metre). Then and only then, can accurate and meaningful reliability and safety predictions become possible, enabling the ultimate goal of reducing the probability of the occurrence of functionability events (in-service failures) during the life of functionable systems.

References

1. Knezevic, J., Functionability in Motion, Proceedings of 1st DQM International Conference on Life Cycle Engineering and Management, pp. 10-25, Belgrade, 2010.
2. Aircraft Accident Report 2/2003, Air Accident Investigation Branch, Report on the Accident to Shorts SD3-60, G-BMNT near Edinburgh Airport on 27 February 2001, pp 52, Department for Transport, UK, March 2003.
3. NTSB/AAR-82-08, Air Florida, Inc., Boeing 737-222, N62AF, Collision with 14th Street Bridge, near Washington Nat'l Airport, Washington, DC, January 13, 1982.
4. Engine-intake Icing Sets Stage for Ditching of Shorts 360 During Cargo Flight, Flight safety Foundation, Accident Prevention, Vol 60, No 9, September 2003, UK
5. http://www.skybrary.aero/index.php/A320,_Harstad/Narvik_Norway_2004_(RE_GND) (29.07.2015)
6. Air Accident Investigation Branch Bulletin No: 1/2002 Ref: EW/C2001/3/4 Category: 1.1, Department for Transport, UK, 2002.
7. Knezevic, J., "Quality of Maintenance – Mirce Mechanics Axiom", Journal of Quality in Maintenance Engineering, Vol. 18, No 2, 2012, pp 216-226, Emerald Group Publishing Ltd. UK.

SRESA JOURNAL SUBSCRIPTION FORM

Subscriber Information (Individual)

Title	First Name	Middle Name	Last Name

Street Address Line 1

Street Address line 2

City	State/Province	Postal Code	Country

Work Phone	Home Phone	E-mail address

Subscriber Information (Institution)

Name of Institution/ Library _____

Name and Designation of Authority for Correspondence _____

Address of the Institution/Library _____

Subscription Rates

	Subscription Quantity	Rate	Total
Annual Subscription (in India)	_____	Rs. 15, 000	_____
(Abroad)	_____	$ 500	_____
	_____		_____
	_____		_____

Payment mode (please mark)

Cheque ☐ Credit Card ☐ Master Card ☐ Visa ☐ Online Banking ☐ Cash ☐ De mand Draft ☐

Credit card Number _____

Credit Card Holders Name _____

Credit Card Holde _____

Guidelines for Preparing the Manuscript

A softcopy of the complete manuscript should be sent to the Chief-Editors by email at the address: editor@sresa.org.in. The manuscript should be prepared using 'Times New Roman' 12 font size in double spacing, on an A-4 size paper. The illustrations and tables should not be embedded in the text. Only the location of the illustrations and tables should be indicated in the text by giving the illustration / table number and caption.

The broad structure of the paper should be as follows: a) Title of the paper – preferably crisp and such that it can be accommodated in one or maximum two lines with font size of 14 b) Name and affiliation of the author(s), an abstract of the paper in ~ 100 words giving brief overview of the paper and d) Five key words which indicates broad subject category of the paper. The second page of the paper should start with the title followed by the Introduction

A complete postal address should be given for all the authors along with their email addresses. By default the first author will be assumed to be the corresponding author. However, if the first author is not the corresponding author it will be indicated specifically by putting a star superscript at the end of surname of the author.

The authors should note that the final manuscript will be having double column formatting, hence, the size of the illustration, mathematical equations and figures should be prepared accordingly.

All the figures and tables should be supplied in separate files along with the manuscript giving the figure / table captions. The figure and table should be legible and should have minimum formatting. The text used in the figures and tables should be such that after 30% reduction also it should be legible and should not reduced to less than font 9.

Last section of the paper should be on list of references. The reference should be quoted in the text using square bracket like '[1]' in a chronological order. The reference style should be as follow:

1. Pecht M., Das D, and Varde P.V., "Physics-of-Failure Method for Reliability Prediction of Electronic Components", Reliability Engineering and System Safety, Vol 35, No. 2, pp. 232- 234, 2011.

After submitting the manuscript, it is expected that reviews will take about three months; hence, no communication is necessary to check the status of the manuscript during this period. Once, the review work is completed, comments, will be communicated to the author.

After receipt of the revised manuscript the author will be communicated of the final decision regarding final acceptance. For the accepted manuscript the author will be required to fill the copy right form. The copy right form and other support documents can be down loaded from the SRESA website: http://www.sresa.org.in

Authors interested in submitting the manuscript for publication in the journal may send their manuscripts to the following address:

Society for Reliability and Safety
RN 68, Dhruva Complex
Bhabha Atomic Research Centre,
Mumbai – 400 085 (India)
e-mail : editor@sresa.org.in

The Journal is published on quarterly basis, i.e. Four Issues per annum. Annual Institutional Subscription Rate for SAARC countries is Indian Rupees Ten Thousand (Rs. 10,000/-) inclusive of all taxes. Price includes postage and insurance and subject to change without notice. For All other countries the annual subscription rate is US dollar 500 ($500). This includes all taxes, insurance and postage.

Subscription Request can be sent to SRESA Secretariat (please visit the SRESA website for details)

SRESA's International Journal of

Life Cycle Reliability and Safety Engineering

Contents

Vol. 5 Issue No.3 July-September 2016 ISSN – 2250 0820